

NOV 30 1964

UCRL-7777

MASTER

University of California
Ernest O. Lawrence
Radiation Laboratory

This paper was submitted for publication in the open literature at least 6 months prior to the issuance date of this Microcard. Since the U.S.A.E.C. has no evidence that it has been published, the paper is being distributed in Microcard form as a preprint.

THE HYDRODYNAMIC BEHAVIOR
OF SUPERNOVAE EXPLOSIONS

RELEASED FOR ANNOUNCEMENT
IN NUCLEAR SCIENCE ABSTRACTS

Livermore, California

DISCLAIMER

This report was prepared as an account of work sponsored by an agency of the United States Government. Neither the United States Government nor any agency Thereof, nor any of their employees, makes any warranty, express or implied, or assumes any legal liability or responsibility for the accuracy, completeness, or usefulness of any information, apparatus, product, or process disclosed, or represents that its use would not infringe privately owned rights. Reference herein to any specific commercial product, process, or service by trade name, trademark, manufacturer, or otherwise does not necessarily constitute or imply its endorsement, recommendation, or favoring by the United States Government or any agency thereof. The views and opinions of authors expressed herein do not necessarily state or reflect those of the United States Government or any agency thereof.

DISCLAIMER

Portions of this document may be illegible in electronic image products. Images are produced from the best available original document.

UNIVERSITY OF CALIFORNIA
Lawrence Radiation Laboratory
Livermore, California

Contract No. W-7405-eng-48

THE HYDRODYNAMIC BEHAVIOR OF SUPERNOVAE EXPLOSIONS

Stirling A. Colgate

Richard H. White

July 1964

LEGAL NOTICE

This report was prepared as an account of Government sponsored work. Neither the United States, nor the Commission, nor any person acting on behalf of the Commission:

A. Makes any warranty or representation, expressed or implied, with respect to the accuracy, completeness, or usefulness of the information contained in this report, or that the use of any information, apparatus, method, or process disclosed in this report may not infringe privately owned rights; or

B. Assumes any liabilities with respect to the use of, or for damages resulting from the use of any information, apparatus, method, or process disclosed in this report.

As used in the above, "person acting on behalf of the Commission" includes any employee or contractor of the Commission, or employee of such contractor, to the extent that such employee or contractor of the Commission, or employee of such contractor prepares, disseminates, or provides access to, any information pursuant to his employment or contract with the Commission, or his employment with such contractor.

The Hydrodynamic Behavior Of Supernovae Explosions *

Stirling A. Colgate and Richard H. White

Lawrence Radiation Laboratory, University of California
Livermore, California

July 1964

I. INTRODUCTION

We regard the release of gravitational energy attending a dynamic change in configuration to be the primary energy source in supernovae explosions. Although we were initially inspired by and agree in detail with the mechanism for initiating gravitational instability proposed by Burbidge, Burbidge, Fowler, and Hoyle (1957) (hereafter referred to as " B^2FH "), we find that the dynamical implosion is so violent that an energy many times greater than the available thermonuclear energy is released from the star's core and transferred to the star's mantle in a supernova explosion. The energy released corresponds to the change in gravitational potential of the unstable imploding core; the transfer of energy takes place by the emission and deposition of neutrinos associated with nucleon beta decay transitions.

The original concept of B^2FH for the explosion of a supernova depended upon the ingenious observation that the matter of a massive star ($M \gtrsim 10 M_{\odot}$) at the end point of its evolution is gravitationally unstable and necessarily initiates a dynamical implosion. It was suggested in B^2FH and later discussed in detail by Hoyle and Fowler (1960) that the rapid compression of the implosion triggers a thermonuclear explosion in the envelope which then leads to a major mass ejection from the star. Recently, Ono and co-workers (1960, 1961) and Ohyaama (1963) have contributed to this concept by calculating analytically the behavior of a thermonuclear detonation shock wave in a stellar envelope.

In the ensuing calculations we will demonstrate that this concept neglects the important dynamical effect of the rarefaction wave created by the implosion itself. This wave completely attenuates the effect of the thermonuclear explosion. A rapid thermonuclear release of energy undoubtedly occurs, but in our view it is too small to significantly effect the subsequent dynamical history of the star. The reason for the dominance of the rarefaction is that the implosion occurs at a velocity greater than the speed of sound in the material undergoing thermonuclear detonation and, as a consequence, any thermonuclear detonation expands predominantly inward.

In Fig. 1 we have synthesized from Minkowsky's recent comprehensive review (to be published) an average Type I and Type II supernova light curve. Table I lists average properties of the two types.

The assignment of the probable mass of the presupernova star is in qualitative agreement with Hoyle and Fowler (1960) who point out that the minimum presupernova mass $M \geq M_{cr} = 1.16 M_{\odot}$ is that mass that can be stably supported by cold electron degeneracy pressure alone (Chandrasekhar 1939). Below this critical mass, evolution to a stable white dwarf can take place with no mass loss but a star more massive than M_{cr} must somehow lose mass before terminating its evolution in a stable "cold" state. As pointed out by Hoyle and Fowler (1960), smaller mass corresponds to longer evolution time and hence the stars of mass only slightly greater than M_{cr} are naturally associated with old stars (population II). This assumes necessarily no large fractional quasi-static mass loss during the late, red giant, stage of evolution. However, Hoyle and Fowler (1960) evoke just such a mass loss to exclude stars of mass $10 M_{\odot} \geq M \geq 1.5 M_{\odot}$ from the probable initial presupernova masses. On the other hand, recent measurements by Deutsch (1963) indicate that quasistatic mass loss may not account for all mass loss of stars of $M \geq 1.5 M_{\odot}$,

and so a continuous range of presupernovae masses must be considered. The very large stars $M \geq 10 M_{\odot}$, as a consequence of rapid evolution, naturally fall into the young population I stars with large envelopes of unburned hydrogen, while the old stars of small mass and depleted hydrogen are naturally associated with the Type I supernova.

These general considerations have an obliging consistency, but the invariance of the total emitted light despite the large differences in the observed ejected kinetic energy can only be understood from the hydrodynamics of the explosion itself.

II. SUMMARY

The results of the hydrodynamic calculations can be summarized as follows: If the mass of the evolved Fe core of the star, M_{core} , is $\geq 5 M_{\odot}$, the core may be unstable to the Fe-He transition and initiate a dynamical implosion starting at a density of 10^7 to 10^8 g/cm³. A somewhat smaller core will evolve quasistatically (stably) to a density of 10^{11} g/cm³ and then become unstable. Regardless of the prior evolutionary history, once $M_{\text{core}} \geq M_{\text{cr}}$ and $\rho \geq 10^{11}$ g/cm³ there occurs a dynamic implosion that proceeds independently of the evolution prior to this state. The instability occurs because neutrino emission by inverse beta decay to neutron-rich matter removes heat (and hence pressure) faster than quasistatic contraction can supply it. The resulting implosion continues in approximate free fall until the neutron Fermi pressure in the core becomes high enough to stop the radial velocity. This occurs only when the equation of state of the core matter becomes "stiff" enough to counterbalance the gravitational force. The requisite restriction in the degrees of freedom of matter occurs only in the limit of "unbound" nucleons where the density is therefore at least an order of magnitude greater than nuclear and the com-

position almost entirely neutrons ($\rho \simeq 5 \times 10^{14} \text{ g/cm}^3$). A very small fraction ($\approx 5\%$) of the neutron core forms adiabatically and cold. The outer layers of matter fall onto this core and accumulate as a shock wave. The heat generated behind this shock will necessarily be emitted in neutrinos but, because of the high shock temperature and high local density, the neutrino mean free path is small and a diffusion wave of neutrinos deposits the energy throughout the rest of the star. Since this energy is of the order of the gravitational potential of the neutron core, it is independent of the initiating instability and it is more than adequate to eject a much larger mass (the stellar envelope) from its lesser gravitational potential.

The deposition of neutrino energy gives rise to a radially outgoing shock which traverses the envelope of the star giving each radial region a different velocity and internal energy. In general, the velocity and internal energy increase toward the surface, becoming relativistic for a small fraction of the envelope ($\approx 10^{-5} M$), and thus leading to cosmic rays (Colgate and Johnson 1960). The peak of the optical light corresponds to the time when, following expansion, radiation can diffuse from the major fraction of the mass of the star. The adiabatic expansion of the shock-deposited internal energy cools the major fraction of the matter below 5×10^3 deg before radiation can take place and only a small mass fraction arrives at the "surface" with sufficient temperature to radiate in the visible spectrum. With the possible exception of the red giant structure, the shock-deposited internal energy is inadequate to explain the observed luminosity. On the other hand, if so much as 1 M_{\odot} of matter of atomic weight greater than that of helium is ejected, then the radioactive energy of beta decay of neutron-rich nuclei or thermal spallation fragment nuclei inject sufficient energy late in time (≈ 1 week) to give rise to the observed peak luminosity.

As a consequence, the expansion mechanism is the same for both small and large stars and the observed differences depend upon the particular history of that fraction of the exploding matter that is dominantly luminous.

III. NUMERICAL HYDRODYNAMICS

The detailed calculations of the stellar hydrodynamics have been performed using a finite difference approximation to the differential equations.

Spherical symmetry has been assumed on the basis that magnetic fields and angular momentum are small and that the symmetrizing effect of the gravitational field ensures a high degree of azimuthal symmetry during the quasi-static phase of the star's evolution. The magnitude of nonspherically symmetric perturbations will be estimated following a discussion of the results of the numerical calculations. The gravitational field is introduced as a radius-dependent potential and an arbitrary "sink" or "source" is used to simulate energy emission or deposition by neutrinos. The radiation transport or electron thermal conduction of energy is assumed negligible during the time scale of the phenomena.

Following is a description of the finite difference equations used in our calculations:

A. Definition of Variables

The variables used in these equations are defined as follows:

- t = time,
- r = distance from star's center,
- u = fluid velocity,
- ρ = mass density,
- v = specific volume ($1/\rho$),
- ϵ = specific internal energy,

$P(\epsilon, v)$ = pressure,

Q = von Neumann-Richtmyer artificial viscosity,¹

G = universal gravitational constant,

m = mass per steradian = $\int \rho r^2 dr$, and

\dot{s} = energy source rate (energy input per unit time per unit mass).

B. Differential Equations

For spherically symmetric radial flow we write the equations in the Lagrangian coordinate frame; the mass m is taken as the Lagrangian coordinate and $r(m, t)$ is related to u by $u = (\partial r / \partial t)_m$.

Mass Conservation:

$$m(r, t) = m(r_0, 0) \quad (1)$$

Momentum Conservation:

$$\frac{\partial u}{\partial t} = - r^2 \frac{\partial}{\partial m} (P + Q) - \frac{4\pi m G}{r^2} \quad (2)$$

Energy Conservation:

$$\frac{\partial \epsilon}{\partial t} = - (P + Q) \frac{\partial v}{\partial t} + \dot{s} \quad (3)$$

Here \dot{s} is used to simulate sinks and sources due to neutrino emission and deposition.

C. Zoning

The star is divided into concentric spherical shells having boundaries numbered 0, 1, 2, . . . , J from center outward. Quantities associated with zone (shell) boundaries are subscripted j ; quantities associated with zone centers are subscripted $j + 1/2$:

$$r_j, u_j$$

$$P_{j+1/2}, Q_{j+1/2}, \rho_{j+1/2}, v_{j+1/2}, \epsilon_{j+1/2}, \text{ etc.}$$

D. The Difference Equations

Time centering is indicated by a superscript n or $n + 1/2$. The initial configuration is defined by input:

$$\begin{array}{ll} r_j^0 & j = 0, J \\ u_j^0 & j = 0, J \\ \epsilon_{j+1/2}^0 & j = 0, J - 1 \\ \rho_{j+1/2}^0 & j = 0, J - 1 \end{array}$$

Then

$$\Delta m_{j+1/2}^0 = \frac{1}{3} \left[(r_{j+1}^0)^3 - (r_j^0)^3 \right] \rho_{j+1/2}^0,$$

$$\Delta m_j^0 = \frac{1}{2} \left[\Delta m_{j+1/2}^0 + \Delta m_{j-1/2}^0 \right],$$

$$m_j^0 = \sum_{k=0}^{j-1} \Delta m_{k+1/2}^0.$$

Mass Conservation:

$$\Delta m_{j+1/2}^n = \Delta m_{j+1/2}^{n+1/2} = \Delta m_{j+1/2}^0$$

$$\Delta m_j^n = \Delta m_j^{n+1/2} = \Delta m_j^0$$

(1a)

$$m_j^n = m_j^0$$

The initial zone masses are carried in memory and hence no calculations are required to conserve mass.

Momentum Conservation:

$$u_j^{n+1/2} = u_j^{n-1/2} - (r_j^n)^2 \left[P_{j+1/2}^n - P_{j-1/2}^n + Q_{j+1/2}^{n-1/2} - Q_{j-1/2}^{n-1/2} \right] \times \frac{\Delta t^n}{\Delta m_j} - \frac{4\pi m_j G}{(r_j^n)^2} \Delta t^n \quad (2a)$$

This calculation is followed by updating of the quantities:

$$r_j^{n+1} = r_j^n + u_j^{n+1/2} \Delta t^{n+1/2},$$

$$v_{j+1/2}^{n+1} = \frac{1}{3} \frac{(r_{j+1}^{n+1})^3 - (r_j^{n+1})^3}{\Delta m_{j+1/2}},$$

$$v_{j+1/2}^{n+1/2} = \frac{1}{2} (v_{j+1/2}^{n+1} + v_{j+1/2}^n),$$

$$\tilde{\epsilon}_{j+1/2}^{n+1/2} = \epsilon_{j+1/2}^n + \frac{1}{2} \frac{\Delta t^{n+1/2}}{\Delta t^{n-1/2}} (\epsilon_{j+1/2}^n - \epsilon_{j+1/2}^{n-1}),$$

$$\tilde{P}_{j+1/2}^{n+1/2} = P(\tilde{\epsilon}_{j+1/2}^{n+1/2}, v_{j+1/2}^{n+1/2}),$$

$$Q_{j+1/2}^{n+1/2} = \begin{cases} 2 \left(u_{j+1}^{n+1/2} - u_j^{n+1/2} \right)^2 / v_{j+1/2}^{n+1/2} & \text{if } v_{j+1/2}^{n+1} < v_{j+1/2}^n \\ & \text{and } u_{j+1}^{n+1/2} < u_j^{n+1/2}, \\ 0 & \text{if } v_{j+1/2}^{n+1} \geq v_{j+1/2}^n \\ & \text{or } u_{j+1}^{n+1/2} \geq u_j^{n+1/2}. \end{cases}$$

Energy Conservation:

$$\epsilon_{j+1/2}^{n+1} = \epsilon_{j+1/2}^n - \left(\tilde{P}_{j+1/2}^{n+1/2} + Q_{j+1/2}^{n+1/2} \right), \left(v_{j+1/2}^{n+1} - v_{j+1/2}^n \right) + s_{j+1/2}^{n+1/2} \Delta t^{n+1/2}$$

(3a)

E. Temperature

Temperatures can be determined by introducing an equation of state

$$T = T(\epsilon, v)$$

or by modifying Eq. (3):

$$\left(\frac{\partial \epsilon}{\partial T}\right)_v \left(\frac{\partial T}{\partial t}\right) = - \left[P + Q + \left(\frac{\partial \epsilon}{\partial v}\right) \right] \frac{\partial v}{\partial t} + \dot{s}; \quad P = P(T, v), \epsilon = \epsilon(T, v). \quad (4)$$

And correspondingly (3a) is modified to read:

$$T_{j+1/2}^{n+1} = T_{j+1/2}^n + \frac{1}{(\tilde{\epsilon}_T)_{j+1/2}^{n+1/2}} \left[-(\tilde{P}_{j+1/2}^{n+1/2} + Q_{j+1/2}^{n+1/2} + (\tilde{\epsilon}_v)_{j+1/2}^{n+1/2}) (v_{j+1/2}^{n+1} - v_{j+1/2}^n) + \dot{s}_{j+1/2}^{n+1/2} \Delta t^{n+1/2} \right]$$

where

$$\tilde{P}_{j+1/2}^{n+1/2} = P\left(\tilde{T}_{j+1/2}^{n+1/2}, v_{j+1/2}^{n+1/2}\right),$$

$$(\tilde{\epsilon}_v)_{j+1/2}^{n+1/2} = \left(\frac{\partial \epsilon}{\partial v}\right)_T \Big|_{T_{j+1/2}^{n+1/2}, v_{j+1/2}^{n+1/2}}$$

$$(\tilde{\epsilon}_T)_{j+1/2}^{n+1/2} = \left(\frac{\partial \epsilon}{\partial T}\right)_v \Big|_{T_{j+1/2}^{n+1/2}, v_{j+1/2}^{n+1/2}}$$

and

$$\tilde{T}_{j+1/2}^{n+1/2} = T_{j+1/2}^n + \frac{1}{2} \frac{\Delta t^{n+1}}{\Delta t^n} (T_{j+1/2}^n - T_{j+1/2}^{n-1}).$$

The energy conservation equation can be iterated by recomputing $\tilde{P}_{j+1/2}^{n+1/2}$, $(\tilde{\epsilon}_v)_{j+1/2}^{n+1/2}$ and $(\tilde{\epsilon}_T)_{j+1/2}^{n+1/2}$ from a revised $\tilde{T}_{j+1/2}^{n+1/2}$ defined:

$$\tilde{T}_{j+1/2}^{n+1/2} = \frac{1}{2} (T_{j+1/2}^{n+1} + T_{j+1/2}^n).$$

This procedure is rarely necessary.

F. Time Steps

Stability of the explicitly differenced momentum conservation equation in the absence of gravitational fields requires $\Delta t \leq \Delta r/c$ where Δr is the zone thickness ($r_{j+1} - r_j$) and c is the sound speed. The presence of a Q places a more severe restriction on the time step but for practical purposes it has been found quite adequate to pick $\Delta t = 0.2 \Delta r/c$.

Additional time step controls are imposed to inhibit the volume or internal energy of any zone from changing by more than 2% per cycle.

$$\Delta t^{-1/2} = \Delta t^{1/2}$$

are input and then

$$\Delta t^n = \frac{1}{2} (\Delta t^{n+1/2} + \Delta t^{n-1/2})$$

and

$$\Delta t^{n+3/2} = \text{infinum} \left(0.2 \frac{r_{j+1}^n - r_j^n}{c_{j+1/2}^n}, \frac{0.02 v_{j+1/2}^n \Delta t^{n+1/2}}{v_{j+1/2}^n - v_{j+1/2}^{n-1}}, \frac{0.02 \epsilon_{j+1/2}^n \Delta t^{n+1/2}}{\epsilon_{j+1/2}^n - \epsilon_{j+1/2}^{n-1}} \right)$$

The sound speed, c , can be obtained from

$$c^2 = \left(\frac{\partial p}{\partial \rho} \right)_s = \frac{1}{\rho^2} \left(\frac{\partial p}{\partial T} \right)_\rho \left(\frac{\partial \epsilon}{\partial T} \right)_\rho^{-1} \left[p + \left(\frac{\partial \epsilon}{\partial v} \right)_T \right] + \left(\frac{\partial p}{\partial \rho} \right)_T$$

The pragmatic test of a numerical calculation code is its ability to integrate equations having known solutions. Four types of problems of importance in stellar hydrodynamics are equilibrium, adiabatic flow, free fall, and shock propagation. We have endeavored to subject our code to tests in each of these categories.

The ability of the code to correctly calculate equilibrium configurations is demonstrated by the stellar calculations themselves; each problem is started

from a stable polytropic configuration; our model oscillates around the equilibrium with an amplitude that corresponds to "round-off" errors in the input data. These oscillations damp with time.

Similarly the ability of the code to follow an adiabatic expansion is illustrated by the explosion phase of the star where the mantle of the star expands adiabatically following the analytic solution for a 10^{20} change in density. This will be discussed in the section on optical emission.

The ability of the code to correctly follow free fall in a gravitational field has been checked by comparison with the following analytic solution: With $P = 0$, the momentum conservation equation becomes

$$\left(\frac{\partial^2 r}{\partial t^2} \right)_m = - 4\pi G \frac{m}{r^2} .$$

Regarding $u = \left(\frac{\partial r}{\partial t} \right)_m$ as a function of m and r the above can be written

$$\frac{1}{2} \left(\frac{\partial u^2}{\partial r} \right)_m = - 4\pi G \frac{m}{r^2} ,$$

which has the solution

$$\frac{1}{2} \left[u^2 - u_0^2(m) \right] = 4\pi Gm \left[\frac{1}{r} - \frac{1}{r_0(m)} \right]$$

where u_0 and r_0 may be taken to be the velocities and positions corresponding to m at $t = 0$. Regarding u as a function of m and t and taking $u_0(m) = 0$ then

$$\left(\frac{\partial r}{\partial t} \right)_m = u = (8\pi Gm)^{1/2} \left(\frac{1}{r} - \frac{1}{r_0} \right)^{1/2} .$$

This equation can be integrated analytically:

$$(8\pi Gm/r_0)^{1/2} = (r_0 - r)^{1/2} r^{1/2} + r_0 \sin^{-1} \left(\frac{r_0 - r}{r_0} \right)^{1/2} .$$

With an initially uniform density ρ_0 , $m = r_0^3 \rho_0 / 3$ and

$$\left(\frac{8\pi G}{3} \rho_0\right)^{1/2} t = \left(1 - \frac{r}{r_0}\right)^{1/2} \left(\frac{r}{r_0}\right)^{1/2} + \sin^{-1} \left(1 - \frac{r}{r_0}\right)^{1/2}. \quad (5)$$

Figure 2 shows an r/r_0 versus t plot for several zones of a 100-zone problem. Q as well as P was set to zero so the compression is strictly adiabatic (as was assumed in the above analytic solution). The analytic solution is also shown (solid line) in Fig. 2. Figure 3 shows $\log \rho$ versus $\log r$ for the same problem as well as the expected solution.

Finally, the test of shock wave propagation has been made for many simple analytic cases, but the peculiar circumstances of shock propagation in stellar envelopes requires a more sophisticated test. In particular, we would like to be assured that a shock wave propagates correctly not only in a uniformly dense medium but also into a density gradient. The predicted increase in speed as the shock traverses the decreasing density of the stellar mantle is a determining feature in much of the explosion phenomena. Fortunately, a similarity solution of a shock in a power-law density gradient pointed out to us by Burgers (1949) permitted verification of the shock behavior. One assumes a plane strong shock propagating through an ideal gas with ratio of specific heats $\gamma = 5/3$.

If the original density of the medium is

$$\rho = \rho_0 \left(\frac{x_0}{x}\right)^{7/4}$$

and the pressure driving the shock is

$$p_s = p_0 \left(\frac{t_0}{t}\right)^{5/3}$$

(note the absence of any dependence of p_s on x)

then the position of the shock front is

$$x_s = x_0 \left(\frac{t}{t_0} \right)^{4/3}$$

and the velocity of the shock is

$$v_s = v_{s0} \left(\frac{x_s}{x_0} \right)^{1/4} = \left(\frac{4}{3} \frac{p_0}{\rho_0} \right)^{1/2} \left(\frac{x_s}{x_0} \right)^{1/4} \quad (6)$$

Using the density gradient and zoning shown in Fig. 4, the shock behavior of Figs. 5 through 7 verified the ability of the code to reproduce the analytic solution. In general if approximately 10 or more zones are used per decade change in density, the shock pressure should be accurate to within $\approx 10\%$. Too few zones inhibit the velocity increase of the shock in a decreasing density gradient.

IV. EQUATION OF STATE

Equation of state information is introduced into the code either in tabular or analytic form as $p(\epsilon, v)$ or as $[p(T, v), \epsilon(T, v)]$.

The first dynamical problem considered in detail was the quasistatic evolution of a star into the predicted iron-helium gravitational instability. As a consequence, considerable effort was made to tabulate an equation of state in the temperature-density region leading up to and following this transformation, so that once the principal features of the hydrodynamics became recognized, the results of a simplified equation of state could be compared to the more accurate problem. The task of assembling this equation of state was performed as a separate problem by Grasberger (1961) and Grasberger and Yeaton (1961).

A. Basic Assumptions

Our stellar mixture is taken to consist of Fe^{56} nuclei, alpha particles, protons, neutrons, and electrons at a temperature T and density ρ .² The mixture is assumed to represent matter undergoing transmutation during the

evolution of a supernova. At an earlier stage and lower temperature the mixture is assumed to be pure iron with 26 electrons per nucleus. The electrons are conserved through the evolution, but the iron nuclei transform into 13 alpha particles plus 4 neutrons, according to the considerations of B²FH. Furthermore, at still higher temperatures the alpha particles decompose into two protons and two neutrons. We assume that these two stages are sufficiently decoupled that we may neglect decomposition of alpha particles until the iron nuclei are nearly all transformed.

The heavy particles are nondegenerate for the temperatures and densities considered here. We assume they obey a classical perfect-gas law. However, the electrons are partially degenerate, and at these high temperatures relativistic modifications must be also included. We assume that the electrons obey a partially degenerate, relativistic, perfect-gas relation. Thus we have for the pressure and total energy

$$P = P_n + P_e + P_r, \quad (7)$$

$$\epsilon = \epsilon_n + \epsilon_e + \epsilon_r + S,$$

where the subscripts n, e, and r refer to the nuclei, electrons, and radiation field, respectively, and S is the energy of transmutation due to conversion of iron into helium, and of helium into protons and neutrons. We have

$$P_n = \frac{\rho kT}{H\bar{\mu}_n}; \quad \epsilon_n = \frac{3}{2} \frac{kT}{H\bar{\mu}_n}, \quad (8)$$

where $\bar{\mu}_n$ is the mean molecular weight per nucleus and H is the mass of a hydrogen nucleus. We define the ratios of the partially degenerate, relativistic electron-gas pressure and kinetic energies to their classical perfect-gas counterparts as π and χ , respectively. Thus

$$P_e = \pi N_e kT; \quad \epsilon_e = \frac{3}{2} \chi N_e kT/\rho, \quad (9)$$

where N_e is the number of electrons per cubic centimeter. The radiation field is assumed to be in thermodynamic equilibrium so that

$$P_r = \frac{a}{3} T^4; \quad \epsilon_r = aT^4/\rho, \quad (10)$$

where a is the radiation-density constant.

The quantities π and χ are functions of ϕ and β , where

$$\phi = \frac{3h^3}{8\pi m^3 c^3} N_e, \quad (11)$$

$$\beta = kT/mc^2. \quad (12)$$

These functions have been tabulated elsewhere by Grasberger (1961). An IBM-7090 machine program code has been used to obtain their values for the pairs of T and ρ given here, using the quantum theory of an ideal electron gas as discussed by Chandrasekhar (1939).

B. Case of Iron-Helium Mixture

Let U be the fraction by weight of the mixture consisting of helium plus neutrons. We assume that each iron nucleus may transform into 13 helium nuclei plus 4 neutrons. Therefore, $1 - U$ is the fraction by weight of iron nuclei.

Statistical equations yield the following relation between the number per cubic centimeter of He^4 and Fe^{56} :

$$N(56, 26) = \omega(56, 26) N(4, 2)^{13} N(1, 0)^4 \frac{(56)^{3/2}}{2^{43}} \left(\frac{2\pi\hbar}{M_0 kT} \right)^{24} \exp Q/kT, \quad (13)$$

where $\omega(56, 26)$ is the statistical weight of iron which we take to be 1.4, Q is the energy of dissociation and is equal to 123.8 MeV, and $N(1, 0)$ is the number of neutrons per cubic centimeter. Expressing the numerical densities in terms of U and the material density, and assuming that the number of neutrons is equal to 4/13 times the number of alpha particles, Eq. (8) may be written in the form

$$\log U - \frac{1}{17} \log (1 - U) = 0.3955 - 0.9412 \log \rho_8 + 1.4118 \log T_{\text{keV}} - \frac{3163}{T_{\text{keV}}}, \quad (14)$$

where ρ_8 is in units of 10^8 g/cm^3 , the temperature is in keV, and the logarithms are to the base ten.

The energy needed to convert 1 g of iron into helium plus neutrons is 2.136×10^{18} ergs. Therefore, the energy of transmutation in ergs/g used in Eq. (2) for this stage is

$$S_0 = 2.136 \times 10^{18} \text{ U}. \quad (15)$$

C. Case of Helium-Neutron-Proton Mixture

After complete decomposition of iron into helium and neutrons, we have a mixture of 92.8% by weight of He^4 and the rest neutrons. The helium will further decompose into two neutrons and two protons. Let Y be the fraction by weight of the mixture consisting of He^4 .

In statistical equilibrium we have

$$N(4, 2) = \frac{1}{2} \omega(4, 2) N(1, 1)^2 N(1, 0)^2 \left(\frac{2\pi\hbar}{M_0 kT} \right)^{9/2} \exp Q'/kT, \quad (16)$$

where $\omega(4, 2)$ is the statistical weight for helium which we take equal to unity, and Q' is the energy of dissociation and is equal to 28.21 MeV. We may express Eq. (16) in the form

$$\log Y - 2 \log (0.24869 - 0.5Y + 0.25Y^2) = 3.0140 + 3 \log_{10} \rho_8 - 4.5 \log_{10} T_{\text{keV}} + 12,252/T_{\text{keV}}. \quad (17)$$

The energy needed to convert 1 g of helium into neutrons plus protons is 6.327×10^{18} ergs. The energy of transmutation in ergs/g used in Eq. (2) for this stage is

$$S_1 = [2.136 + 6.818 (0.928 - Y)] \times 10^{18}. \quad (18)$$

D. Numerical Results

For convenience we express densities in units of 10^8 g/cm^3 , temperatures in kV, pressures in units of 10^{16} dyn/cm^2 , and energies in units of 10^{16} ergs/g .

Equations (3), (4), (5) become

$$P_n = 9.6517 \times 10^6 \rho_8 T_{\text{keV}} / \bar{\mu}_n; \epsilon_n = 0.14478 T_{\text{keV}} / \bar{\mu}_n. \quad (19)$$

$$P_e = 4.4848 \times 10^6 \rho_8 T_{\text{keV}} \pi; \epsilon_e = 0.067272 T_{\text{keV}} \chi. \quad (20)$$

$$P_r = 0.0045681 T_{\text{keV}}^4; \epsilon_r = 1.3704 \times 10^{-10} T_{\text{keV}}^4 / \rho_8. \quad (21)$$

The quantities N_e , ϕ , and β become

$$N_e = 2.7998 \times 10^{31} \rho_8; \quad (22)$$

$$\phi = 47.729 \rho_8; \beta = 0.00195706 T_{\text{keV}}. \quad (23)$$

For the iron-helium case we have

$$(\bar{\mu}_n)^{-1} = 0.28526 U + 0.01787. \quad (24)$$

For the helium-neutron-proton case we have

$$(\bar{\mu}_n)^{-1} = 0.99150 - 0.74177 Y \quad (Y \leq 0.928). \quad (25)$$

The gas pressure and gas energy are

$$P_{\text{gas}} = P_n + P_e; \epsilon_{\text{gas}} = \epsilon_n + \epsilon_e + S. \quad (26)$$

The total pressure and energy are

$$P = P_{\text{gas}} + P_r; \epsilon = \epsilon_{\text{gas}} + \epsilon_r \quad (27)$$

The tabular forms³ give the quantities U , π , χ , P_{gas}/P , P_{gas} , P , ϵ_{gas} , and ϵ as functions of ρ_8 and T_{keV} for the iron-helium stage, and the quantities Y , π , χ , P_{gas}/P , P_{gas} , P , ϵ_{gas} , and ϵ for the helium-neutron-proton stage.

Figures 8 and 9 summarize the tabular material by giving the pressure and $p/\rho\epsilon$ as functions of density and temperature. Later the adiabatic γ will be related to gravitational stability, where

$$\frac{P}{\rho\epsilon} = \gamma - 1. \quad (28)$$

V. CALCULATION OF GRAVITATIONAL INSTABILITY

Figure 10 shows the assumed initial stellar structure, a 10 M \odot polytrope of index 3. The central density of 1.13×10^7 g/cm³ and central temperature of 509 keV were chosen to be just prior to the Fe-He transformation. From the plot of the stellar mass distribution on the $p/\rho\epsilon$ representation of the equation of state (Fig. 9), we can see that the major fraction of the star has $\gamma > 4/3$ and so we expect stability. (Section VI gives details of the above argument.) Figure 11 shows the radial oscillations for a small fractional time of the equilibrium calculation of the star. The comparison of the energy in these oscillations to the internal energy of the gas gives a measure of the round-off errors associated with the input initial conditions and/or errors in the calculational procedure.

$$\frac{\Delta W}{W} \sim \frac{\left\langle \frac{1}{2} u^2 \right\rangle \text{time average}}{KT} \sim 5 \times 10^{-5}. \quad (29)$$

The smallness of the above result gives confidence that the equilibrium polytropic solution and hydrodynamical computation are self-consistent. The different frequencies correspond to the different radial modes of oscillation of the system. The boundedness of these oscillations is shown for the first 40 sec of Fig. 12 during which the calculation proceeded unchanged. Having demonstrated stable equilibrium, an energy sink term was introduced to simulate evolution of the star. Since it is believed that the evolution of a star at this stage is governed by photo neutrino loss, (Chiu and Stabler 1961) and pair-annihilation neutrinos (Chiu and Morrison 1960; Chiu 1961) then because of

the semi-infinite neutrino mean free path the energy loss is local rather than a transport process. Further, it is expected that only a small fractional energy loss is required to initiate the dynamical instability and so the resulting change in structure from a polytrope of index 3 is negligible. Therefore, if the energy is removed predominantly from the center of the star, the details of the energy loss mechanism are unimportant provided only that the sink is slow enough so that the star evolves quasistatically into instability. The sink rate introduced at 50 sec time in Fig. 12 removed 2-1/2% of the internal energy of the star from the inner 50% of the mass during the following 40 sec. The inner core (9% of the total mass) made approximately 500 periods of oscillations during this time and the fundamental mode approximately 2 periods. The condition of quasi-static evolution is therefore well satisfied and the resulting instability is independent, to first order, of sink rate or distribution. Of course, the evolution of the star up to the point of instability is highly dependent upon the energy loss mechanism but assuming a polytrope of index 3 immediately prior to instability prejudices the structure. This assumption will be examined in greater detail in the final discussion.

The onset of instability shown in Fig. 12 is expanded in Fig. 13 and then was calculated in greater detail by increasing the number of zones in the problem from 16 to 100 (Fig. 14). The solid lines of Fig. 14 show the radial position versus time of the collapse of the 10 M_{\odot} star with the Grasberger-Yeaton equation of state. The inner zones fall in first and the calculation was terminated when the central density reached 3×10^{11} g/cm³ which was already outside the region of validity of the tabulated equation of state. At this point the inner zones are essentially in free fall, i. e., $\partial p / \partial r \ll \rho MG / r^2$ and, in addition, no compression waves or shocks have formed. As a consequence, all zones are following an adiabatic compression. Since the initial state of polytropic index 3 corresponds to $T \propto \rho^{1/3}$

and the equation of state corresponds to $\gamma \simeq 4/3$, all zones initially are on the same adiabat and so all zones in the subsequent compression pass through the same set of states. This is illustrated in Fig. 15 in which the same path is followed in temperature and density by the zones corresponding to 10%, 20%, and 50% mass fraction. A further confirmation of the adiabaticity of the free fall was demonstrated by setting the artificial viscosity, Q , equal to zero and observing a duplicate result.

The free fall at high density and lack of reflected energy (bounce) is to be expected (see Sec. VI) and so — to confirm our understanding of the requirement for a new equilibrium, or bounce — the equation of state was modified to include a small fraction of initial pressure (10^{-3}) of a hypothetical gas of $\gamma = 2$. The dashed curves (Fig. 14) show the resulting bounce at the expected 1000- fold compression and the heavy dots show the reflected shock wave. This shock wave is probably strong enough to eject 10% of the mass of the star although a detailed calculation was not completed.

VI. STELLAR STABILITY

For equilibrium, the equation of motion can be set equal to zero so that

$$\frac{\partial^2 r}{\partial t^2} = -4\pi r^2 \frac{\partial p}{\partial M_r} - \frac{GM_r}{r^2} = 0.$$

Multiplying by r and using

$$M_r = \int_0^r 4\pi r^2 \rho \, dr$$

gives

$$\frac{3p}{\rho} - \frac{GM_r}{r} - \frac{\partial}{\partial M_r} (4\pi r^3 p) = 0;$$

and integrating gives (Edington 1926)

$$\int_0^M \frac{3p}{\rho} dM_r + \Omega = 0 \quad (30)$$

where

$$\Omega = - \int_0^M \frac{GM_r dM_r}{r} \quad (31)$$

The total internal energy U is

$$U = \int_0^M \epsilon dM_r \quad (32)$$

where ϵ is the specific internal energy given by

$$\epsilon = \frac{p}{(\gamma - 1)\rho}$$

so that the total energy of binding E of a star becomes

$$E = U + \Omega, \quad (33)$$

which must be negative for the star to be bound. Clearly a star whose total energy is positive can approach a lower energy state by expansion, so that by Eqs. (30) and (32), the mass average of γ ,

$$\langle \gamma \rangle_m \cong 4/3 \quad (34)$$

for stable equilibrium.

In the special case $\gamma = 4/3$, the total energy is zero so that a homologous change in radius can take place with no change in total energy. As a consequence, the pressure associated with such a homologous deformation becomes a lower bound for equilibrium support of the star. If a star has neutral equilibrium for a pressure following a given adiabat, less pressure will cause collapse and more will cause expansion. The solid curve of Fig. 16 shows the pressure during the Fe-He transformation of unstable collapse. If instead the γ of the stellar gas had been held fixed at $\gamma = 4/3$, the dashed straight line lying above and at higher pressure gives the extrapolated pressure for neutral stability. The pressure

defect for equilibrium support of the whole star corresponds to the difference between these two curves and it can be seen that the real pressure ($10^{10} \leq \rho \leq 10^{11} \text{ g/cm}^3$) is approximately one-fourth that required for support. As a consequence, the matter of the star is close to free fall. The artificial hard core ($\gamma = 2, E_{hc}/E_{total} = 10^{-3}$ initial) "bounces" when the pressure due to the hard core returns to the neutral stability ($\gamma = 4/3$) value. The neutral stability pressure will, of course, depend upon the mass to be supported and so in the implosion of Fig. 14, it is evident that the initial "bounce" will involve only a fraction of the total mass, dependent upon the details of the hydrodynamics.

If we characterize a neutral stability pressure curve for each mass by $p/\rho^{4/3}$, then on the basis of constant structure (polytrope of index 3) and Eq. (30)

$$\frac{3p}{\rho} M \propto \frac{M^2 G}{R}$$

and

$$p/\rho^{4/3} \propto M^{2/3}. \quad (35)$$

Figure 17 shows the quantity $p/\rho^{4/3}$ for the explosion history of all problems. The initial equilibrium values follow the scaling in mass of Eq. (35) and the cores form at pressures corresponding to the mass and momentum involved.

A. The Formation of the Core

The formation of a core or "bounce" following an unstable stellar implosion requires that the reduced pressure $p/\rho^{4/3}$ reach a value significantly higher than the minimum required for support of whatever central stellar fraction falls as a unit. From the solution of Eq. (5) we know that free fall of a uniform-density, zero-pressure core will remain adiabatic; however, finite pressure causes a pressure gradient and hence a velocity gradient during implosion. If the adiabatic γ is increasing with density, the central mass fraction will reach an equilibrium

support pressure before the outer zones so that a core will first form adiabatically with the outer zones then falling onto the core as a shock wave. The Grasberger-Yeaton equation of state depends, among many assumptions, upon the constancy of the electron-neutron ratio. For the dynamical collapse time of 0.1 to 0.01 sec of Fig. 14 this is amply justified in terms of beta decay equilibrium times which are long for a density less than 10^{10} g/cm³. However, above this density this assumption is no longer valid and as we will show, the time required to achieve nuclear equilibrium through beta decay becomes shorter than the adiabatic dynamical compression time. As a consequence, not only will the electron fraction change drastically, and hence the dominant degeneracy pressure, but also the thermal content of the matter will be radiated away by the neutrino flux. The lower bound on the pressure curve then becomes that corresponding to cold equilibrium matter. Figure 18 shows this equation of state as first derived by Cameron (1959) and Salpeter (1960), and recently more accurately by Wheeler (1964), as well as our approximate analytic fit for the following hydrodynamic calculations. Below 10^{11} g/cm³ the pressure is due to degenerate electrons for which $\gamma = 4/3$ (Chandrasekhar 1939). The slight curvature of the Wheeler solution in this region is due to the shift in beta decay stability of the minimum energy nucleus. Above 2×10^{11} g/cm³ the Fermi energy of the degenerate electrons becomes greater than the n-p mass difference referred to the binding in helium ($E_p = 32 mc^2$). As a consequence, electrons combine with protons and a large pressure defect occurs. The fact that the Salpeter pressure lies so far below the Wheeler curve (in the region $2 \times 10^{11} \leq \rho \leq 2 \times 10^{12}$ g/cm³) is due to different estimates of nuclear binding. However, both pressures are so far below the neutral stability value that the difference in the free fall trajectory is negligible. The increase in pressure in the region above 2×10^{12} g/cm³ density is primarily due to the free nucleon Fermi potential

(nucleon degeneracy); but in the Salpeter case it is additionally dependent upon the assumption of the nucleon repulsive hard core potential. The existence of this potential at high energy (> 300 MeV) may be of some doubt (Salpeter 1964); however, the fractional energy of the hard core potential invoked is small (50 MeV out of 300 MeV total) so that the final core size and stability will be only modestly affected. Since the cold-matter pressure curve reaches the $10 M_{\odot}$ neutral stability line for $\rho \approx 10^{15}$ g/cm³, this becomes the expected density for total star bounce assuming complete neutrino cooling. Both general relativity and the smaller mass fraction reaching the core simultaneously will modify this expected density.

B. Magnetic Field and Rotation

For a new equilibrium to exist for our imploding star at a density significantly less than predicted above, there must exist either an exothermic reaction, leading to a lower energy state of matter than the presently known nuclear binding or a restriction in the degrees of freedom of the system. The possibility of a lower energy state of matter below that explored for nuclear interactions is indeed remote. A restriction in the degrees of freedom of the system requires a conservation law that restricts an energy component from sharing its energy with the other degrees of freedom of the system. The only known possible restrictions are angular momentum and magnetic field.

Consider first a three-dimensional compression of a magnetic field. The dominant effect of a rapid compression will be the increase in magnetic intensity at any fluid element. To compute the magnitude of this increase, we choose a set of fluid particles lying on a surface ds_0 bounded by a closed curve c_0 and follow their motion. At some later time these particles will define a surface ds bounded by a closed curve c . To a first approximation, the magnetic flux

will be conserved so that the field intensity will increase in the ratio ds_0/ds and since $ds_0/ds \propto (r_0/r)^2$ (where r is the distance of the fluid particles from the star's center), we have

$$B \propto 1/r^2 \propto (\rho^{1/3})^2. \quad (36)$$

The pressure associated with the magnetic field is proportional to B^2 so that

$$P \propto \rho^{4/3}. \quad (37)$$

This corresponds to $\gamma = 4/3$ for a spherical compression of a magnetic field, and, as a consequence, magnetic field pressure in a star has a neutral effect upon gravitational stability.

The conservation of angular momentum requires

$$mr\omega^2 = \text{constant}$$

(r perpendicular to the axis of rotation).

The energy density of rotation at constant angular momentum becomes

$$W_\omega = \rho \epsilon_\omega = \rho u^2/2 = \rho_0 \left(\frac{r_0}{r}\right)^2 = \rho_0 \frac{u_0^2}{2} \left(\frac{r_0}{r}\right)^5 \quad (38)$$

or

$$W_\omega \propto \rho^{5/3}$$

so that the effective γ is $5/3$ and rotation is a stabilizing effect upon gravitational instability.

The ratio of rotational energy to gravitational energy for a homologous compression becomes

$$\frac{E_\omega}{\Omega} = \frac{\int \epsilon_\omega dM}{\int \frac{MG}{r} dM} \propto r^{-1}. \quad (39)$$

We now make the following assumptions:

1. The star rotates with angular velocity ω , which, due to the effect of a very small magnetic field, and/or convective mixing, is initially independent of r .

2. The core of the star is approximately 10% of the total mass at 10% of the outer radius. By "core" we mean that fraction of the star which falls as a unit during the instability. The 10% figures are verified by subsequent calculation.

Then from Eqs. (31) and (38) the ratio of E_ω/Ω for the core before collapse and at constant angular momentum becomes

$$\left(\frac{E_\omega}{\Omega}\right)_{\text{core}} = \frac{r_{\text{max}}}{r_{\text{core}}} \frac{M_{\text{star}}}{M_{\text{core}}} \left(\frac{E_\omega}{\Omega}\right)_{\text{star}} \quad (40)$$

Since for rotational stability prior to collapse

$$\left(\frac{E_\omega}{\Omega}\right)_{\text{star}} \leq 1,$$

then

$$\left(\frac{E_\omega}{\Omega}\right)_{\text{core}} \leq 10^2.$$

Therefore, from Eq. (39) the core can collapse to 1% of its original radius and the density increase from ρ_c to at least $10^6 \rho_c$ before rotation can distort the spherical symmetry. This compression is large enough that the neutrino emission and deposition process can take place in spite of the most extreme assumption of initial rotation. A prior small surface mass loss, and/or a red giant envelope, would ensure negligible rotational effect.

C. Neutrino Emission

The initial assumption of our numerical hydrodynamics is that energy remains local to the fluid within the time of dynamical change of configuration.

This assumption is thoroughly justified for electron thermal conduction and radiation diffusion where the scattering mean free paths are infinitesimal compared to the dimensions of the star. This is not the case for neutrino processes for which, in most instances, the emitted energy leaves the star with no interaction. The criterion for relative importance of neutrino energy emission versus hydrodynamic changes of energy becomes the ratio of the time for emission of the thermal energy to the time of compression in free fall. To be neglected an emission process must satisfy the condition

$$\left(\frac{1}{\epsilon} \frac{d\epsilon_{\nu}}{dt}\right) \ll \left(\frac{1}{\rho} \frac{d\rho}{dt}\right)_{\text{free fall}} \quad (41)$$

where $d\epsilon_{\nu}/dt$ is the neutrino energy emission rate and ϵ is the specific internal energy.

In order to evaluate this condition we prejudge our final calculations by stating that approximately 1 M_{\odot} is involved in the core formation. Observing that this mass falls maintaining nearly uniform density, and equating the kinetic energy to the change in potential

$$(\dot{r})^2 M/2 \cong M^2 G \left(\frac{1}{r} - \frac{1}{r_0}\right) \cong \frac{M^2 G}{r}$$

or

$$\dot{r} = \left(\frac{2MG}{r}\right)^{1/2}$$

and therefore

$$\frac{1}{\rho} \frac{d\rho}{dt} = \left(\frac{18MG}{r^3}\right)^{1/2} = 2.2 \times 10^2 \rho_{10}^{1/2} \text{ sec}^{-1}. \quad (42)$$

where ρ_{10} is the density expressed in units of 10^{10} g/cm³. The neutrino emission rates have recently been reviewed exhaustively by Fowler and Hoyle (1964) for massive stars and the early phase of supernova collapse. Massive stars necessarily imply no electron degeneracy, and Fowler and Hoyle reach the conclusion that no neutrino processes significantly compete with the mech-

anism of Fe-He transformation for initiation of gravitational collapse. However, here we are concerned with such a comparison in the advanced stages of dynamic collapse where the structural changes and the resulting electron degeneracy are considered. In Fig. 15 we see that the thermodynamic state history of the imploding core of the $10 M_{\odot}$ star tends to "skirt" the boundary in temperature-density space of the Fe-He transformation. In other words the large endothermic energy of the Fe-He phase change acts as a buffer preventing an increase in temperature despite the adiabatic increase in density and, as a consequence, the core is cooler at a given density than it would be following a $\gamma = 4/3$ adiabat. The cooling is sufficient so that in the case of the $10 M_{\odot}$ implosion the core becomes partially degenerate at $\rho = 10^{10} \text{ g/cm}^3$ and $T = 11.8 \times 10^9 \text{ deg}$ (see Fig. 15). Since the phase change of Fe \rightarrow He is essentially completed here we find $\gamma \cong 4/3$. Then

$$T_9 = 11.8 (\rho_{10})^{1/3} \text{ deg} \quad (43)$$

where T_9 is the temperature expressed in units of 10^9 degrees Kelvin.

D. Pair Annihilation Neutrinos

If we use the pair annihilation neutrino cross section (Levin 1963; Chiu and Stabler 1961) assuming no suppression of the positron density due to degeneracy, we have an upper limit to the universal Fermi interaction energy loss rate. Then from Chiu (1961)

$$\frac{d\epsilon_{\nu}}{dt} = 4.3 \times 10^{15} \rho^{-1} T_9^9 \text{ ergs/g cm}^3 \text{ sec},$$

approximating the results of Fig. 8

$$\epsilon = 0.83 \times 10^{17} T_9 + 7.5 \times 10^{21} T_9^4 \rho^{-1} \text{ ergs/g cm}^3 \text{ sec}.$$

And by using Eq. (43)

$$\epsilon \approx 1.1 \times 10^{18} \rho_{10}^{1/3} \text{ ergs/g cm}^3 \text{ sec.}$$

$$\begin{aligned} \therefore \left. \frac{1}{\epsilon} \frac{d\epsilon}{dt} \right)_{\text{core}} &= \frac{1.9 \times 10^{15} \rho_{10}^3}{1.1 \times 10^{18} \rho_{10}^{1/3}} \\ &= 1.7 \times 10^{-3} \rho_{10}^{8/3} \text{ sec}^{-1} \end{aligned} \quad (44)$$

so that for $\rho \leq 2 \times 10^{11} \text{ g/cm}^3$ the neutrino pair emission rate will be considerably less than the hydrodynamic compression rate.

E. Beta Decay Neutrinos

The dominant energy loss is a modified Urca process and occurs due to inverse beta decay



at a temperature where there is a partial He thermal decomposition to ($\approx 1\%$) free protons, and a density high enough so that the electron Fermi energy enhances the above reaction.

In the density range $2 \times 10^{10} < \rho < 2 \times 10^{11} \text{ g/cm}^3$, E_F , the electron Fermi energy, is less than the n-p mass difference so that only the thermally decomposed protons or proton-rich nuclei will contribute to the inverse beta decay process. Even if there are no thermal free protons, the matter is proton rich at $2 \times 10^{11} \text{ g/cm}^3$ provided no beta decay has taken place. A measure of this proton richness is expressed as the ratio of mean atomic number to mean atomic weight — which for cold Fe is 0.465 and decreases to 0.35 at $\rho = 2 \times 10^{11} \text{ g/cm}^3$ (Salpeter 1960; Wheeler 1964). Consequently, the lightest thermally-formed, proton-rich fragments will give the maximum contribution to inverse beta decay.

The beta decay rate becomes

$$\dot{\beta} = \int_0^{\infty} N_p N_e(E) \sigma(E) v(E) dE \quad (45)$$

where we assume (1) the proton thermal energy makes a negligible contribution to the center-of-mass energy and the proton number density N_p is a small fraction f of the total electron number density N_e . Then the differential electron density $N_e(E)dE$ becomes

$$(2) N_e(E) dE = \frac{3N_e}{E_F^3} E^2 dE, \quad (46)$$

and for extreme relativistic degeneracy, where $E_F = 6 \times 10^{-3} \rho^{1/3} mc^2$ (ρ in g/cm^3),

$$(3) \sigma(E) \simeq \sigma_0 \left(\frac{E}{mc^2} \right)^2, \quad E \gg mc^2 \quad (47)$$

where $\sigma_0 = 1.7 \times 10^{-44} cm^2$ from the Reines-Cowan (1959) experiment and

$$(4) v(E) = c.$$

Therefore,

$$\begin{aligned} \dot{\beta} &= \frac{3fN_e^2 \sigma_0 c}{E_F^3} \int_0^{E_F} E^4 dE \\ &= 3.6 f \times 10^9 \rho^{8/3} sec^{-1} cm^{-3} \end{aligned} \quad (48)$$

where ρ is given in g/cm^3 .

The neutrinos will be emitted with a spectrum up to E in energy that will depend upon the nucleus from which they came.

Since

$$kT \leq E_\nu \leq E_F \leq E_{z \rightarrow z-1},$$

then choosing the smallest of these limits, for the mean neutrino energy

$$\frac{d\epsilon_{\nu}}{dt} \geq 4 \times 10^2 f \rho^{5/3} T_9 \text{ ergs/g sec} \quad (49)$$

and the characteristic thermal emission rate becomes

$$\frac{1}{\epsilon} \frac{d\epsilon_{\nu}}{dt} \geq 0.2 \times 10^2 f \rho_{10}^{5/3} \text{ sec}^{-1}. \quad (50)$$

For $f = 0.03$ which is characteristic of the $10 M_{\odot}$ core in the density range $2 \times 10^{10} \leq \rho \leq 2 \times 10^{11}$,

$$\frac{1}{\epsilon} \frac{d\epsilon_{\nu}}{dt} = \left(\frac{1}{\rho} \frac{d\rho}{dt} \right)_{\text{free fall}}$$

when $\rho = 5 \times 10^{10} \text{ g/cm}^3$.

Thus, regardless of the Fe-He transformation, inverse beta decay neutrino emission ensures a sufficient reduction in pressure to result in free fall. The temperature is reduced to the point where the proton fraction f becomes vanishingly small; however, since an f value of 0.03 already assures free fall, a lower temperature will not significantly alter the hydrodynamics.

Once $\rho \geq 2 \times 10^{11} \text{ g/cm}^3$, the Fermi energy E_F becomes greater than the neutron binding energy ($32 mc^2$ referred to He) and inverse beta decay proceeds where $f = 1/2$, $\sigma = \sigma_0 (E_F/mc^2 - 32)^2$. A slight increase in E_F above $32 mc^2$, $\rho > 2 \times 10^{11}$, results in a transformation to equilibrium cold neutron matter and the corresponding cold neutron star equation of state becomes applicable.

VII. HYDRODYNAMIC CALCULATIONS WITH NEUTRINO EMISSION

An equation of state was synthesized from the cold matter approximation shown in Fig. 18. Although the pressure defect (from equilibrium) is much larger in both this and the Salpeter equation of state than in the Wheeler one, the difference to the hydrodynamics is negligible because the matter is close to free fall in either case.

For the pressure we have

$$p = 10^{16} \times \left[0.032\rho T + 0.004567T^4 + \left\{ \begin{array}{ll} 0.04\rho^{4/3} & \rho < 2 \times 10^{11} \\ 4.67 \times 10^{13} & 2 \times 10^{11} < \rho < 2 \times 10^{12} \\ 23 + 121.9 \times 10^{-22} \rho^{2.6} & \rho > 2 \times 10^{12} \end{array} \right\} \right] \text{ dyn/cm}^2 \quad (51)$$

where ρ is in g/cm^3 and T in keV. And for the internal energy we have

$$\epsilon = 10^{16} \times \left[\epsilon_0 + \frac{0.0137T^4}{\rho} + \left\{ \begin{array}{ll} 0.12\rho^{1/3} & \rho < 2 \times 10^{11} \\ 933.5 - 4.67 \times 10^{13} \rho^{-1} & 2 \times 10^{11} < \rho < 2 \times 10^{12} \\ 23 \ln \rho + 0.76 \times 10^{-20} \rho^{1.6} & \rho > 2 \times 10^{12} \end{array} \right\} \right] \text{ ergs/g} \quad (52)$$

where

$$\epsilon_0 = \begin{cases} 0.096T & T < 509 \text{ keV,} \\ 0.267T - 87 & T > 509 \text{ keV.} \end{cases}$$

For T less than 509 keV, the coefficient ϵ_0 represents an equivalent specific heat ratio $\gamma = 4/3$ and above 509 keV, a specific heat ratio $\gamma = 1.12$ corresponding to the thermal decomposition of iron and then helium as determined earlier in more exact calculations (Fig. 9). The remaining terms correspond

to radiation energy and cold neutron matter. (The electron-positron pair energy is strongly suppressed due to the high matter density.) A time-dependent energy loss term was included with an assumed $f = 0.03$ with kT emitted per neutrino. Equation (49) becomes

$$\dot{s} = \frac{d\epsilon_\nu}{dt} = - 0.1 \rho^{5/3} T \text{ ergs/g-sec} \quad (53)$$

where ρ is in g/cm^3 and T in keV.

Figure 19 shows the equilibrium and unstable collapse of the $10 M_\odot$ star as before, except in this case the calculation was continued until a core was formed. Matter continues to fall in on the core but no shock wave is reflected outwards because the rapid neutrino energy loss completely dissipates any thermal energy generated. As more matter accumulates on the core ($> 2 M_\odot$) the general and special relativistic effects become large enough to represent a major error in the calculation. As a measure of the size of this correction, the equilibrium condition for the static solution becomes (Oppenheimer and Volkoff 1939)

$$\frac{dp(r)}{dr} = - \frac{[\rho(r) + c^{-2}p] G [M(r) + 4\pi c^{-2}p(r)r^3]}{r [r - 2c^{-2}GM(r)]} \quad (54)$$

The factor enhancing the nonrelativistic pressure gradient is shown in Fig. 19 as a function of various stages of core collapse and suggests the impossibility of any sizable reflected energy. However, aside from the extreme dubiousness of extrapolating general relativistic static solutions to the dynamic case, a more detailed account of the neutrino energy flux offers the possibility of exploding the star before general relativistic effects become of overwhelming importance.

The temperature versus density for $10 M_\odot$ is shown in Fig. 20 for several representative zones. Initially all zones of the star are on the same $\gamma = 4/3$

adiabat and evolve to the Fe-He transformation at $T = 509$ keV on the same adiabat. Throughout the transition they follow the $\gamma = 1.12$ adiabat, but above $\rho \approx 10^{10}$ g/cm³ the neutrino energy sink removes energy fast enough so that the temperature of various zones depends upon their compression rates. The peak in temperature at $\rho \approx 10^{14}$ g/cm³ corresponds to a shock of width Δr formed as the matter "falls" onto the stationary core. The magnitude of this peak depends upon the compression rate of any given zone, namely

$$\frac{1}{\rho} \frac{d\rho}{dt} = \frac{1}{\Delta r} \frac{dr}{dt} \quad (55)$$

where Δr is the width of the zone and so as $\Delta r \rightarrow 0$, the compression rate becomes infinite. The calculational limit is the finite number of zones required for the stellar approximation; but physically the limit in Δr is the collisional mean free path which determines the thickness of the shock. The value of the temperature peak as additional matter falls on the equilibrium core is then a calculational limit and does not reflect physical reality. Figure 21 shows the results of the same calculation with the exception that $d\epsilon_{\nu}/dt = 0$. The shock temperature of 80 MeV is artificially high due to the neglect of electron-positron and neutrino-antineutrino pairs in the equation of state. However, the core shock wave is demonstrated and the high temperature focuses attention upon the approximation of stellar neutrino transparency. Figures 22 and 23 show the same general behavior for a 100 M \odot star with the neutrino energy sink, namely, the formation of a "cold" neutron core with no reflected shock wave.

A. Neutrino Deposition During Adiabatic Free Fall

From Fig. 20 and Eq. (50) the major fraction of the internal energy of the adiabatic compression during free fall is emitted for $10^{10} \leq \rho \leq 10^{11}$ g/cm³ with a neutrino energy ($E_F + kT$) less than the n-p mass difference of 20.3 MeV in He. Therefore, as these neutrinos (actually antineutrinos) traverse the exte-

rior matter of the star they can interact only by inverse beta decay on free neutrons, or by electron antineutrino scattering.

At the mean density for adiabatic core neutrino emission $\langle \rho \rangle \approx 5 \times 10^{10}$ g/cm³ [Eq. (50)]; the maximum energy neutrino becomes $E_F + kT \approx 11$ MeV and the mean free path by inverse beta decay on the neutrons from thermally decomposed Fe, i. e., $^{56}\text{Fe} \rightarrow ^{56}\text{Ni} + 4n$ becomes

$$\lambda_{\beta} = \frac{1}{N_n \sigma} = \frac{1}{6 \times 10^{23} \frac{4}{56} \sigma_0 (E_F)^2} = 3 \times 10^{18} \text{ g/cm}^2. \quad (56)$$

The integral density of the stellar region external to $\rho = 5 \times 10^{10}$ g/cm³ where there are free neutrons is

$$\int_{\rho = 5 \times 10^{10}}^{\rho = 10^{10}} \rho \, dr \approx 5 \times 10^{17} \text{ g/cm}^2.$$

Consequently, 10% of the adiabatic core neutrinos will be absorbed if all are emitted at E_F . Because of the low free-proton density and availability of other partially proton-rich fragments it is probable that the majority of adiabatic core neutrinos will have energy less than E_F and the reabsorption will be small.

The antineutrino electron (at rest) scattering has been calculated (but not measured) first by Feynman and Gell-Mann (1958) and later with a factor of 2 correction by Heller (1963) and Azinov and Shekhter (1961, 1962).

If the thermal motion as well as degeneracy energy of the relativistic electron gas is included, (Bahcall 1964) has demonstrated that for nondegeneracy

$$\sigma_{ve} \approx \frac{\sigma_0}{2} \left(\frac{kT}{mc^2} \right) \left(\frac{E_{\bar{\nu}}}{mc^2} \right) \quad (kT \gg mc^2) \quad (57)$$

and for degeneracy with Fermi level E_F

$$\sigma_{ve} = \frac{\sigma_0}{6} \left(\frac{E_{\bar{\nu}}}{mc^2} \right)^2 \frac{E_{\bar{\nu}}}{E_F}. \quad (58)$$

For $kT \ll E_{\bar{\nu}}$, the mean energy deposited becomes $E_{\bar{\nu}}/2$ so that for the stellar conditions during adiabatic compression $kT \ll E_{\bar{\nu}} \approx E_F$ and $n_N/n_e \approx 1/7$, the scattering becomes less than 5/8 of the absorption and so can also be neglected.

B. Neutrino Deposition from Core Shock Wave

The temperature immediately behind the core shock wave can be calculated from the Hugoniot conditions (Courant and Fredericks 1948). Prior to the shock transition, the pressure is sufficiently low that the matter is in free fall and, as a consequence, the kinetic energy equals the change in potential.

$$\frac{(\dot{r})^2}{2} = MG \left(\frac{1}{r_{\text{core}}} - \frac{1}{r_i} \right) \quad (59)$$

Regardless of the instability initiating either the Fe-He transition or inverse beta decay at $\rho > 2 \times 10^{11} \text{ g/cm}^3$, the subsequent change in radius from the initial radius r_i to the final core radius r_{core} at $\rho \approx 10^{15} \text{ g/cm}^3$ is large enough such that the final potential depends only upon r_{core} and therefore upon the equation of state at the new equilibrium. For a 1 M_{\odot} core

$$\frac{(\dot{r})^2}{2} = 1.67 \times 10^{20} \text{ ergs/g}$$

when $r_{\text{core}} = 8 \times 10^5 \text{ cm}$ and $\bar{\rho} = 10^{15} \text{ g/cm}^3$. Since for a strong shock the internal energy behind the shock equals the change in fluid kinetic energy across the shock, then

$$\rho_i \left(\frac{\dot{r}}{2} \right)^2 = \frac{\rho_s kT}{\gamma - 1} + \Gamma \sigma T^4 \quad (60)$$

where $k/(\gamma - 1)$ is an effective specific heat of the baryon-plus-meson gas and Γ includes the relativistic leptonic as well as photon contribution to the energy density. ρ_i and ρ_s are the respective incident and shock densities. An exact

detailed calculation of the equation of state for these conditions is beyond the scope of this paper but it is necessary to demonstrate that $T \geq 30$ MeV in order to substantiate the process of explosion by neutrino thermal conduction.

We first estimate ρ_i from the hydrodynamic calculations and then calculate the temperature assuming all the internal energy is in the lepton and photon gas. The respective baryon and Fermi pressures are then compared to the relativistic gas as a correction.

In Fig. 19 a solar mass of matter is accumulated "on" the core of 1 M \odot and radius 8×10^5 cm in a time τ approximately 3×10^{-3} sec. This time corresponds to the traversal time of sound through the core at the density corresponding to the initial adiabatic neutrino emission. Assuming free fall and the conditions of Eq. (59) then

$$4\pi r^2 \dot{r} \rho_i \tau = 2 \times 10^{33} \text{ g} \quad (61)$$

and

$$\rho_i \simeq 5 \times 10^{12} \text{ g/cm}^3.$$

Using this density, assuming all the shocked gas pressure resides in the relativistic component, and equating pressure to the time rate of change of momentum we have

$$\rho_i (\dot{r})^2 = p = E/3 = \Gamma \sigma T^{4/3} \quad (62)$$

To calculate Γ we assume (to be confirmed later) that the electron pair component of the relativistic gas will be suppressed due to a high electron Fermi potential (Landau and Lifshitz 1958). However, because the neutrino opacity is great enough to give many mean free paths for scattering and absorption (to be discussed later) the energy of the thermal neutrino gas must be included. Integrating the Fermi gas distribution function over all energies at temperature T

one obtains for the Fermi gas alone $\Gamma_F = 7/8$ and including both neutrinos and antineutrinos $\Gamma_{\bar{\nu},\nu} = 7/4$. This assumes the neutrino chemical potential is small compared to kT giving the maximum possible value to Γ and hence minimum temperature. Then for the relativistic gas exclusive of electron pairs $\Gamma = 11/4$ and so for a minimum temperature (exclusive of baryon specific heat) we obtain from (62) $T = 60$ MeV. The density behind the shock is determined by the energy

$$\rho_s \frac{(\dot{r})^2}{2} = \Gamma \sigma T^4 = 3\rho_i (\dot{r})^2 \quad (63)$$

or

$$\rho_s = 6 \rho_i = 3 \times 10^{13} \text{ g/cm}^3$$

The electron Fermi level for $z/A = 1/2$ is $E_f \approx 100$ MeV and since the corresponding neutron Fermi level is only 13 MeV, due to the prior inverse beta decay (during adiabatic free fall), the nuclear composition will have been only slightly shifted to neutron-rich composition and the electron Fermi level will have been correspondingly reduced. The temperature of 60 MeV is too low to produce a significant number of mesons ($E_{\text{threshold}} = 140$ MeV) and so only the baryon component to the specific heat remains. The fractional nuclear binding at $T \approx 10$ MeV is negligible and so solving the pressure equation

$$\rho_i (\dot{r})^2 = 2\rho_s RT/3 + \Gamma \sigma T^4/3 \quad (64)$$

with $\rho_s = 6\rho_i$ and $\Gamma = 2.75$ gives $T = 55$ MeV.

Having estimated the temperature on the basis of neutrino thermal equilibrium, we must justify this by demonstrating that the stellar matter external to the shock is opaque to neutrinos and also that the neutrino emission rate is fast enough to reach equilibrium.

The thermal neutrino population can be created either by beta decay processes or directly by neutrino pair formation. In the beta decay process the electrons (or positrons) removed by absorption are replaced by electron-positron pair formation from the photons, so that either process can give rise to an arbitrary number of neutrinos.

For direct neutrino pair formation the time required to emit the shock energy [Eq. (59)] in neutrino pair energy [Eq. (44)] at a temperature of 55 MeV is $\tau_{\text{pair}} = 10^{-7}$ sec assuming equal positron-electron density. The corresponding time for inverse beta decay [Eq. (47)] and $\rho_s = 3 \times 10^{13}$ g/cm³ is $\tau_\beta \simeq 10^{-7}$ sec so that the distance behind the shock at which neutrino equilibrium should exist becomes

$$x_s = \dot{r} \left(\frac{1}{\tau_{\text{pair}}} + \frac{1}{\tau_\beta} \right)^{-1} = 150 \text{ cm.} \quad (65)$$

Similarly the combined mean free path for electron neutrino scattering and absorption becomes from Eqs. (47), (56), and (59), at $\rho_s = 3 \times 10^{13}$ g/cm³

$$\lambda_{55 \text{ MeV}} = \frac{1}{\rho_s (\sigma_s + \sigma_{\text{ab}})} = 450 \text{ cm.} \quad (66)$$

Both these distances are sufficiently smaller than the radius of the core ($r \simeq 8 \times 10^5$ cm) to ensure neutrino thermal equilibrium.

The neutrino energy density can therefore be treated as analogous to Planck radiation using the concepts of opacity, diffusion, and finally emission from a surface (Christy 1964). The surface temperature T_s at the radius of the core corresponding to the energy flux of the shock wave becomes

$$\frac{\rho_i(\dot{r})^3}{2} = \frac{c}{4} (\Gamma_{\nu\nu}) \sigma T_s^4, \quad (67)$$

giving $T_s = 41$ MeV. This is sufficiently high that the average mean free path in the imploding matter ρ_i is small, approximately one-tenth of the local scale

$$\text{height, } h = \left(\rho \frac{\partial \rho}{\partial r} \right)^{-1},$$

$$\lambda_{40 \text{ MeV}}(\rho_i) \approx 10^4 \text{ cm}$$

$$h \approx r/10 = 10^5 \text{ cm}$$

but because the neutrino opacity is a rapidly decreasing function of neutrino energy, the emitting surface will not be at a significantly larger radius than the shock. As a consequence, the irreversible thermal energy of the shock will be emitted as a neutrino flux from a surface slightly larger than the core radius. At an emission surface one-half the flux is absorbed in the matter external to the surface and it is the heat from this neutrino energy flux deposited in matter at a smaller gravitational potential which expels the external matter of the star.

Therefore, the larger the radius of the emitting surface, the less deposition required for explosion and so the assumption used for the time-dependent calculations that the emitting surface coincides with the shock surface is a conservative one. It is assumed that the time for mu-meson neutrino production is sufficiently longer than beta neutrino production that the major fraction of the shock energy will have been transferred before mu-meson neutrino emission.

C. Neutrino Deposition Calculation

To simulate the emission and deposition of neutrinos from the shock at the core, one half of the time-dependent energy sink was deposited in the matter external to the core shock. This deposition is initiated only when the core shock

is formed and is turned off when the rarefaction due to the expansion terminates the core shock. The integral sink in ergs/sec is

$$-\dot{S} = \int_0^M \left(\frac{d\epsilon}{dt} \nu \right) dM_{\text{emitted}} \quad (68)$$

The source deposition in ergs/g-sec becomes

$$\left(\frac{d\epsilon}{dt} \nu \right)_{\text{dep.}} = \frac{\dot{S}\kappa}{4\pi r^2} \exp \left[-\kappa \int_{r_{\text{shock}}}^r \rho dr \right], \quad r \geq r_{\text{shock}} \quad (69)$$

where $\kappa = \ln 2 / \int_{r_{\text{shock}}}^{\infty} \rho dr$. Figures 24 through 27 show the resulting explosion of a 10 M \odot polytrope 3 star. The initial equilibrium test (not shown) covered a real time of 30 sec and the instability was initiated by removing 1% of the internal energy. The core forms adiabatically and cold with 5% of the mass of the star. After "bounce" a shock forms and the deposition is initiated. Figure 27 shows the increasing temperature of the mantle material due to the time-dependent deposition. Although the core shock zone never reaches a temperature corresponding to the previously calculated 55 MeV, the energy sink and deposition transfer the available energy independent of peak temperature. This is because the sink term is so large it assures that all the internal energy is emitted. Since the artificial viscosity, Q , necessarily converts all the kinetic energy of free fall into internal energy, this same energy must appear as neutrino sink and later a fraction as deposition in the mantle. In this calculation 2 M \odot accumulated in the core before sufficient heat was deposited to reverse the implosion and create an explosion. This mass is larger than the general relativistic stable limit of ≈ 0.6 M \odot of Oppenheimer and Volkoff (1939), Cameron (1959), and Misner and Zepolsky (1964) and so would be unstable. However, the fractional mass in the core depends critically upon the stellar structure during implosion and how this is modified during the deposition process. Before the core approaches the general

relativistic limit the total energy available for deposition becomes the binding energy [Eq. (37)]

$$\left[1 - \frac{1}{3(\gamma - 1)} \right] \frac{M_{\text{core}}^2}{r}$$

In the general relativistic limit, Misner and Zapolsky (1964) have shown that the binding energy of a neutron star is limited to $0.05 M_{\text{core}}^2$ assuming no nucleon hard core potential so that if the fractional stellar mass intermediate in the implosion is small, due to stratification in the initial instability, then the deposition energy is sufficient to remove $0.05 M_{\text{core}} c^2 / \frac{M^2 G}{r}$ or ≈ 50 times the core mass from the initial stellar structure. This is large enough so that it is likely — but not proved — that a general relativistically stable core may remain following instability of even the most massive initial star.

The stratification, referred to above, in the implosion occurs due to the availability of thermonuclear energy from the outer layers of the star which have not yet evolved to Fe. This energy places these zones on a higher adiabat during implosion so that the pressure gradient leads to a slightly slower implosion and, consequently, an enhanced separation between core and mantle. Although this energy source has been considered as the primary energy source for Type I supernova (Fowler and Hoyle 1960) and Type II supernova (Ohyama 1963) we find that the rarefaction left by the imploding core is always sufficient to essentially "swallow" the thermonuclear explosion. This is because the sound speed in the unstable, imploding core is higher than in the external thermonuclearly exploded material. A simulated calculation of this effect is included in the appendix.

The explosion phase from neutrino deposition (Figs. 25 and 26) develops into a radially outgoing shock because the material closer to the core shock receives more neutrino deposited energy and has a higher temperature and

higher sound speed. The shock wave speeds up (becomes stronger) in the density gradient of the mantle (Colgate and Johnson 1960; Ono 1961) as can be seen by the curvature in Fig. 26. The radial matter velocity following expansion is shown in Fig. 28 as a function of external mass fraction F . The slope $\dot{r} \approx (F)^{-1/6}$ is in agreement with the similarity solution of Ono (1961) if the plane parallel mass element ρdr is replaced by the spherical element $4\pi r^2 \rho dr$ which, in an exponential atmosphere, is proportional to F .

In Fig. 27, the velocity of 2.6×10^{10} cm/sec for the 10^{-4} mass fraction corresponds to the special relativistic energy $2M_0 c^2$, i. e., the rest mass energy equals the kinetic energy and so matter ejected external to this radius we identify with cosmic rays. The hydrodynamic computing code will not yet perform special relativistic hydrodynamics, but similarity solutions of a quite general nature derived by Johnson (Colgate and Johnson 1960) lead to an energy spectrum of ejected matter that agrees, within rather narrow limits, with the observed cosmic ray spectrum. The total cosmic ray energy injected into the galaxy becomes $MF_{cr} c^2 = 2 \times 10^{51}$ ergs. For a cosmic ray energy density of 5×10^{-14} erg/cm³ in the galactic volume of 5×10^{68} cm³, and a lifetime of 2×10^8 years, one $10 M_{\odot}$ supernova would be required each 10^3 years (Colgate and White 1963).

D. Smaller Supernovae

Figures 29 through 36 show the corresponding hydrodynamic calculations for $2 M_{\odot}$ and $1.5 M_{\odot}$ supernovae. Both stars evolve on a low enough adiabat (high density, low temperature) such that subsequent compression does not cause the matter to pass through the Fe-He thermal decomposition and instability mechanism. Instead the stars evolve by pair neutrino emission and/or radiation until their central density is high enough (2×10^{10} to 2×10^{11} g/cm³) for inverse beta decay to become significant. The subsequent cooling and shifting

to the large pressure defect cold neutron matter equation of state causes a dynamical implosion, similar to the 10 M_{\odot} case with subsequent core formation, shock, neutrino emission and deposition, and finally explosion. The expansion velocities and residual core mass are lower, but without the inclusion of general relativity, a very exact equation of state including thermonuclear energy, and an accurate initial stellar structure, the residual core mass and explosion velocities should be considered accurate only to within a factor of 2.

The energy sink term was used as given in Eq. (53) which is unrealistic to the extent that the neutrino emission rate is calculated for 3% free protons. The hydrodynamics of the implosion are not dependent upon the initial energy loss rate, but upon the equation of state in the region of formation of neutron-rich matter. As long as the pressure falls below the neutral stability value as it does for $\rho \geq 2 \times 10^{11}$ g/cm³ (Fig. 16) a dynamical instability occurs. A calculation of the 1.5 M_{\odot} star with the sink term reduced to one-tenth the previous value gave essentially the same results.

To demonstrate the effect of stellar structure, a red giant envelope of 7.5 M_{\odot} was added to the 2 M_{\odot} (polytrope 3) star to match the structure in the carbon-burning stage calculated by Kippenham (1963) for a 7.5 M_{\odot} late evolution star. The assumption implied by the structure is that the core of the star evolves by neutrino loss to the conditions of instability before the low density mantle supported by thermonuclear energy can collapse. The true structure probably lies somewhere between the two extremes of red giant structure and polytrope of index 3 depending upon the mixing rate during late evolution (Hayashi 1962). Fortunately, however, the mechanism and resulting behavior of the explosion is only slightly modified for the two models. Figure 37 shows the comparison of the Kippenham model and the model constructed from the 2 M_{\odot} polytrope 3 core and the Kippenham envelope. Figures 38

and 39 show the radius time behavior with the slowing down of the explosion shock in the massive mantle and the subsequent increase in strength again at the surface. Figure 40 shows the temperature-density history of the envelope with the shock heating and subsequent adiabatic expansion.

VIII. OPTICAL EMISSION

The optical emission expected from a 10 M \odot supernova colliding with the optimum density (10^{-16} g/cm³) interstellar medium has been calculated previously by Colgate and Cameron (1963) and estimated to correspond to the total kinetic energy released of $\approx 10^{52}$ ergs. However, in the usual case of expansion into the near vacuum of the interstellar medium, the shock luminosity becomes negligible, and the radiation from the internal energy, as well as radioactive energy of the expanding stellar gases, becomes dominant. We will estimate these two effects separately and show that depending somewhat upon the initial stellar structure the maximum optical emission most probably arises from the energy of radioactive decay of the heavy nuclear matter. The shock-deposited internal energy in general becomes too small after adiabatic expansion to significantly contribute to the observed optical emission.

A. Light from Shock-Deposited Internal Energy

The outer layers of the stellar explosions are heated primarily by a shock wave. This is because the neutrino flux originates at the small radius of the core and is reduced by radial divergence at the stellar surface. Following the passage of the radially outgoing shock wave (Figs. 26, 31, and 35) and possibly including a few weak reflected shocks in the case of the red giant envelope (Fig. 39), the velocity distribution of the stellar matter is a monotonically increasing function of radius. As a consequence, each volume element undergoes a continuous expansion which, in the absence of heat flow or sources, is adiabatic.

We will then calculate the temperature and density time history of the expanding matter and from this a maximum possible luminosity based upon the assumptions that 1) there is no heat flow, and 2) we can "see" into the matter of maximum luminosity.

If matter initially $\rho_i T_i r_i$ expands adiabatically and spherically with a specific heat ratio γ and if $T \gg 10^4$ deg, the optical luminosity L in the visible spectrum $\Delta h\nu$ wide becomes

$$L = \frac{2\pi\nu^2 (\Delta h\nu)kT 4\pi r^2}{c^2} \quad (70)$$

but

$$T = T_i \left(\frac{\rho}{\rho_i} \right)^{\gamma-1} = T_i \left(\frac{r_i}{r} \right)^{3(\gamma-1)},$$

so that

$$L \simeq (r)^{-3(\gamma-1) + 2}.$$

If $\gamma = 5/3$ for a free-particle, nonrelativistic gas, L is independent of radius.

If $\gamma = 4/3$ for a relativistic or radiation dominated gas, $L \approx r$. This holds provided both $\gamma = 4/3$ and $T > 10^4$ deg. At 10^4 deg or less

$$L = c/4\sigma T^4 \approx (r)^{-12(\gamma-1) + 2} \quad (71)$$

and so regardless of γ the luminosity is a rapidly decreasing function of radius. Consequently, the maximum possible light due to internal energy occurs at that radius for which the temperature is 10^4 deg.

The stellar envelope is initially shocked to a temperature approximately equal to 5×10^9 deg, and where the ratio of internal energy in radiation to energy in particles is

$$\beta = \frac{aT^4}{\rho RT/(\gamma-1)} > 1.$$

As $\beta \rightarrow \infty$, the radiation dominates and the effective gamma is $4/3$ and so we must calculate the adiabatic law for a medium of two components of different γ .

$$pdV = - dE$$

$$p = R\rho T + \frac{a}{3} T^4$$

$$E = \frac{R\rho}{(\gamma - 1)} T + aT^4V$$

$$\therefore (R\rho + \frac{4}{3} aT^3) \frac{dV}{V} = -\left(\frac{R\rho}{\gamma - 1} + 4aT^3\right) \frac{dT}{T}. \quad (72)$$

With the above definition of β we recover the two limits of the adiabatic law;

as $\beta \rightarrow 0$

$$\ln V = -(\gamma - 1) \ln T,$$

and $\beta \rightarrow \infty$

$$\ln V = -\frac{1}{3} \ln T.$$

Substituting the definition of β into Eq. (72) and integrating we obtain

$$\ln \frac{V_0}{V} = \frac{4}{4 - 3\gamma} [\beta - \beta_0 + \ln \beta/\beta_0]. \quad (73)$$

Therefore, if the gas is initially shocked such that $\beta \gg 1$ where $\gamma_{\text{particles}} = 5/3$ then it expands initially with an effective $\gamma = 4/3$ during a volume change

$$\frac{V_0}{V} = 4 \beta_0 \exp [4(\beta_0 - 1)] \quad (74)$$

and

$$T_0/T = (4\beta_0)^{1/3} \exp [4/3(\beta_0 - 1)].$$

This implies that when the explosion shock reaches a low enough density and high enough strength in traversing the stellar envelope such that $\beta > 15$, then the subsequent expansion to 10^4 deg corresponds to $\gamma = 4/3$. Figure 41 shows the envelope expansion of the 10 M_{\odot} star and the agreement between the calculational code adiabat and the analytic solution for a 10^{20} change in density. The maximum radius at which 10^4 deg temperature occurs for the various explosions is shown in Fig. 42. This curve has a maximum corresponding to the two require-

ments of maximum initial temperature and $\beta \approx 15$. As the shock traverses the envelope, β increases and T decreases.

B. Radiation Flow

Figure 42 shows the integral density per unit area of the expanding matter at the location of the r_{\max} , $T = 10^4$ deg mass point. The question arises whether the internal energy associated with this temperature can diffuse from the stellar surface within the cooling time of further adiabatic expansion.

Let us approximate the density distribution by a series of steps of uniform density of width h where the original density distribution is given by

$$\rho = \rho_0 e^{-r/h}. \quad (75)$$

Provided $\beta > 1$, the characteristic time τ for radiant energy to diffuse into or out of a region of uniform density and initially uniform temperature of width h is

$$\tau = \frac{h^2}{D} \text{ sec} \quad (76)$$

where the diffusion coefficient D is given in terms of the Rosselin mean opacity \bar{k} as

$$D = \frac{c}{3} (\bar{k}\rho)^{-1}. \quad (77)$$

We observe that in the adiabatic expansion of the envelope (Figs. 24, 29, and 33) $h/r \approx 0.1$ so that an observer travelling with a "zone" of matter of width h sees a characteristic time for the release of radiant energy of

$$\tau = \frac{h^2}{D} = 3 \times 10^{-2} \frac{r^2 \bar{k}\rho}{c} \text{ sec.} \quad (78)$$

But again from Figs. 24, 29, and 33 we note that in the Lagrange frame (moving with the fluid) $\rho = \rho_1 (r_1/r)^3$, so that for matter designated by density ρ_1 at radius r_1

$$\tau = 3 \times 10^{-2} \frac{\bar{k}}{c} \rho_1 (r_1)^3 / r \text{ sec.} \quad (79)$$

The total emitted power from any given zone then becomes

$$L_{\text{Bol}} = \frac{4\pi r^2 h a T^4}{\tau} \text{ ergs/sec} \quad (80)$$

but for $\beta > 1$, $T = T_1 r_1/r$ so that

$$L_{\text{Bol}} = \frac{a T_1^4 c r_1}{3 \times 10^{-2} \bar{k} \rho_1} \text{ ergs/sec.} \quad (81)$$

To the extent that \bar{k} is a constant L_{Bol} is a constant for any zone and so the major contribution to the emitted energy occurs during the last doubling in radius where τ becomes equal to the expansion time. A further accentuation of the emission at the largest radius when T is lowest is due to the behavior of the opacity \bar{k} . In Fig. 41 showing temperature versus density for the envelope expansion a line is drawn separating the two regions of opacity, namely free electron scattering and bound-free or free-free transitions (Schwarzschild 1958). It is evident that the material of maximum luminosity lies well above this boundary so that \bar{k} becomes a constant, namely the Compton scattering cross section per free electron. Further expansion leads to still lower opacity (Allen 1963) because at the very low density the hydrogen negative ion content is sufficiently small that recombination leads to a direct reduction in opacity. Therefore, a "window" effectively opens at $T \simeq 10^4$ deg due to a reduction in opacity as well as the window in time due to expansion [Eq. (79)].

Using the criterion that the emission time must equal the expansion time at the 10^4 deg surface gives from Eq. (78)

$$3 \times 10^{-2} r^2 \bar{\kappa} \rho / c = \left(\frac{1}{r} \frac{dr}{dt} \right)^{-1}. \quad (82)$$

Taking $\bar{dr}/dt = 3 \times 10^9$ cm/sec and $\bar{\kappa} = 0.1$ g/cm² (50% ionized) the condition for the emitting region becomes

$$\rho r = 3 \times 10^3 \text{ g/cm}^2.$$

This condition is met by the maximum radius of the $T = 10^4$ deg matter for the polytrope 3 initial star (Fig. 42). For the red giant, this same density times thickness is reached at approximately $0.5 r_{\text{max}}$. Shown in Table II is the luminosity calculated from each of the envelope expansions by the relation

$$L_{\text{Bol}} = \frac{aT^4 V}{\tau} = 4aT^4 \pi r^2 \frac{dr}{dt}. \quad (83)$$

where V = volume and t = expansion. The luminosities calculated from the emission of the shock deposited internal energy are all at least an order of magnitude less than the observed ($\approx 10^{43}$ ergs/sec), and only in the case of the red giant structure is the time in approximate agreement ($\approx 10^6$ sec). Since these luminosities represent the maximum "uncovery" rate of internal energy and are based upon the smallest possible opacity, it seems unlikely that this energy source explains the usual supernova emission.

C. Luminosity from β Decay

In the typical explosion by neutrino deposition, roughly 1 M \odot of the matter ejected has undergone either compression to $\rho > 3 \times 10^{10}$ g/cm³ or been processed by a shock wave where $T_9 > 15$ deg. In the first case, the nuclei formed in the "r" process (B^2 FH) will be neutron rich, and in the second case light nuclear fragments will be formed far off the stability line, either proton or

neutron rich. In both cases the resulting nuclei will decay by beta emission and the initial presence of a stable nucleus will be the exception rather than the rule. This is because the beta-stable nuclei are far fewer than the bound ones.

An approximate estimate of the energy decay rate can be made by assuming; 1) all nuclei are radioactive with end point energies E , and 2) at least two decays are required to reach stability. From the Fermi theory of beta decay (Konopinski 1943) the mean decay time is proportional to E^{-5} for high energy decays where $E \gg mc^2$ so that the energy emission becomes

$$R = \int_0^{\infty} E f(E) \exp(-E^{-5}t/t_0) dE \quad (84)$$

Since all decay energies $E \leq E_0$ are approximately equally probable where E_0 is the upper limit of the distribution $f(E)$, then $f(E) \simeq f_0$ for $E < E_0$, and a change of variables gives

$$R = \frac{\beta_0}{t_0} \left(\frac{t}{t_0} \right)^{-1.4} \quad (85)$$

where the constants β_0 and t_0 are to be determined. For the distribution of neutron-rich fission fragments, $\beta_0 \simeq 5$ MeV, which is one-half the approximate energy difference between stability and the "neutron drip line," the remainder being carried off by neutrinos. The characteristic time t_0 is the decay period for a typical allowed transition of 10 MeV; $t_0 \simeq 1$ sec. For long times where $t/t_0 \gg 1$, the second decay in the nuclear chain to stability becomes important and $\beta_0 \rightarrow 10$ MeV, $t/t_0 \gg 1$. [With these constants Eq. (85) adequately describes measured fission fragment beta decay (Fermi 1949)]. The light spallation fragments will have a lower energy and slower average decay rate, $\beta_0 \simeq 2.5$ MeV, $t_0 \approx 30$ sec, and should therefore be expected to contribute more energy late in time, but since the spallation products have not been calculated in detail the more conservative "neutron-rich" decay constants will be used.

The luminosity of the beta active gas will be due both to the instantaneous beta decay rate when the gas becomes transparent as well as the release of internal energy from prior decay.

The trapped energy is determined by the balance between adiabatic cooling and beta decay injection. Let w = total internal energy. Then

$$(\gamma - 1) w \frac{1}{\rho} \frac{d\rho}{dt} = \frac{M\beta_0}{t_0} (t/t_0)^{-1.4} \text{ ergs/sec.} \quad (86)$$

Since the radiation internal energy will be large compared to the matter energy, $\gamma = 4/3$ and therefore for $r \gg r_{\text{initial}}$ and \dot{r} a constant

$$(\gamma - 1) (1/\rho) (d\rho/dt) = t^{-1}$$

and so

$$w = M\beta_0 (t/t_0)^{-0.4} \text{ ergs.} \quad (87)$$

The rate of release of internal energy becomes

$$\dot{w} = -w \frac{1}{\int \rho dr} \frac{d\left(\int \rho dr\right)}{dt} = \frac{2w}{t} = -\frac{2M\beta_0}{t_0} (t/t_0)^{-1.4}. \quad (88)$$

The luminosity becomes

$$L = \dot{w} + MR = \frac{3M\beta_0}{t_0} (t/t_0)^{-1.4} \text{ ergs/sec.} \quad (89)$$

Using the diffusive condition [Eqs. (78) and (82)] for determining the time of energy release from a mass M and noting that $M = 4\pi r^2 h\rho \simeq r^3$ and from Fig. 28 that $\dot{r} = 10^9 (M/M_0)^{-1/6}$

$$t = 10^{-11} M_0^{-1/2} M^{7/12} \text{ sec} \quad (90)$$

and

$$L = 8 \times 10^{15} \beta_0 f t_0^{0.4} F^{1/6} M_0^{0.30} \text{ ergs/sec} \quad (91)$$

where f = the heavy element fraction by weight and F = external mass fraction. Choosing $F = 1/2$, $M_0 = 2 M_\odot$, and assuming $\bar{A} = 50$ so that $\beta_0 = 2 \times 10^{17}$ ergs/g, $t_0 = 1$ sec for allowed transitions of $\bar{E} \approx 10$ MeV, then

$$L = 10^{43} f \text{ ergs/sec.} \quad (92)$$

It is therefore necessary to choose the heavy element fraction to be unity to achieve the observed luminosity. If supernova are the exceptional mass ejection mechanism then $f = 1$ for $1 M_\odot$ ejection is not an unreasonable estimate.

D. Surface Conditions

Independent of the energy source the radius of the surface where

$$\int_{r_s}^{\infty} \rho \bar{k} dr = 2/3$$

becomes

$$r_s = r + h \ln \frac{3}{2} h \rho_D \bar{k} \quad (93)$$

where $h \rho_D = 10^3 \text{ g/cm}^2$, or

$$r_s = 2.4 \times 10^{14} \text{ cm}$$

and the surface temperature becomes

$$T = \left(\frac{L}{c/4\sigma 4\pi r_s^2} \right)^{1/4} = 21,000^\circ \text{K.}$$

The mass average velocity of the colder gas external to the surface becomes

$$\bar{u} = \left(\int_{r_s}^{\infty} u \rho dr \right) / \left(\int_{r_s}^{\infty} \rho dr \right). \quad (94)$$

Since $u \approx F^{-1/6} \approx (h\rho)^{-1/6}$ (Fig. 26) then $\bar{u} \approx 7/6 u_s$ and the expected Doppler shift of any absorption lines should be, from Fig. 39,

$$7/6 u_s = 1.2 \times 10^4 F_s^{-1/6} \text{ km/sec.}$$

Doppler shifted absorption lines (Greenstein 1964) have been observed at a luminosity maximum with $\Delta u = 10^4$ km/sec. These results are also not inconsistent with the explanation of the long time optical luminosity exponential decay discussed by B^2FH due to spontaneous fission of Cf 254. The surprising uniformity of peak luminosity (Minkowsky, to be published) of Type I and II events is due to the approximate constancy of the mass ($\approx 1 M_{\odot}$) involved in the initial gravitational instability. As a consequence, the mass of the ejected radioactive material is similarly expected to be constant so that the energy source is of constant magnitude, but the surface composition and hence spectra should vary widely depending upon the initial envelope composition.

E. Reimplosion Luminosity

If low density matter falls back on the neutron star core, the kinetic energy will be converted to thermal energy which in turn can be radiated away. Although the resulting radiation temperature may be very high at the neutron star surface, the subsequent diffusion in the expanding low density matter would result in the same surface temperature as any of the previously considered energy sources of equal magnitude. The necessarily reimploded mass fraction to result in the observed peak luminosity for 10^6 sec is small because of the large gravitational potential of the neutron star surface.

$$\frac{FM^2G}{r} = L_{\text{Bol}} t = 10^{49} \text{ ergs} \quad (95)$$

and so for a core of one solar mass and radius 10 km the required reimplosion mass becomes $5 \times 10^{-5} M_{\odot}$. This is sufficiently small so that a careful hydrodynamical calculation would appear necessary. Fortunately, however, the required luminosity implies a pressure due to the energy flux greater than the gradient of the gravitational potential, and so can be excluded on very general grounds as a significant energy source.

In the presence of a luminous flux ϕ , the pressure gradient becomes

$$\nabla p = \nabla \left(NkT + \frac{a}{3} T^4 \right) + \phi \frac{\bar{k}\rho}{c}. \quad (96)$$

For the matter to reach the neutron star surface in free fall, this pressure gradient must be much less than the gradient of the gravitational potential. Therefore, the condition for maximum energy flux and free fall is $T \rightarrow 0$ and

$$\frac{\phi \bar{k}\rho}{c} \ll \frac{\rho MG}{r^2} \quad (97)$$

or

$$L_{\text{Bol}}(\text{Maximum}) \leq 4\pi r^2 \phi_{\text{max}} \leq 2.4 \times 10^{37} \text{ ergs/sec} \quad (98)$$

for $r = 10^{16}$, $M = 1 M_{\odot}$, and $\bar{k} = 0.2 \text{ g}^{-1} \text{ cm}^{-2}$. Therefore the gravitational energy source is too small to supply the observed luminosity.

We have therefore demonstrated that the dynamical collapse of a central portion of a highly evolved star results in sufficient gravitational energy that when conducted by neutrinos to the remaining nonimploded mass explodes this mass in a fashion consistent with observed supernova events.

ACKNOWLEDGMENTS

It is a pleasure to acknowledge the encouragement and tutelage of many people in the preparation of this work. Among these are Edward Teller, Montgomery Johnson, A. G. W. Cameron, Wm. Fowler, and Wm. Grasberger. Mr. Earl Tech has given major assistance with the computations.

APPENDIX A: THE THERMONUCLEAR PROCESS IN SUPERNOVA

The fundamental concept of this appendix is that a detonation is initiated solely by a "large" perturbation of the equilibrium state. Such a large perturbation occurs only when the star initiates a dynamical collapse due to the equation of state of the core. The relatively "soft," easily compressible imploding core then cannot support the additional pressure of the thermonuclear detonation so that no significant mass fraction is ejected solely due to the detonation. The initiation of detonation requires that an incremental increase in thermal energy will be regenerated by reactions before being relaxed by expansion. We are therefore concerned with an initial perturbation corresponding to a uniform compression of the fuel region and we wish to find the stellar conditions corresponding to the minimum expansion velocity or maximum relaxation time. The minimum initiating perturbation calculated for these conditions gives the absolute minimum perturbation for detonation. Assuming a lowest mode oscillation frequency σ_{osc} and a perturbation in thermal energy $\Delta\epsilon_{th}$ (ergs/g) gives rise to a perturbed reaction rate ΔR ergs/g-sec. The condition for detonation then becomes

$$\sigma_{osc} \Delta\epsilon_{th} \leq \Delta R \quad (A-1)$$

If the thermonuclear reaction rate R in ergs/g-sec has a temperature coefficient such that

$$\frac{\Delta R}{R} = \Gamma \frac{\Delta T}{T} \quad (A-2)$$

and noting that for partial degeneracy $\epsilon_{th} \approx T^2$ so that $\frac{\Delta R}{R} = (\Gamma/2) \Delta\epsilon_{th}/\epsilon_{th}$, then the condition for detonation becomes

$$\sigma_{osc} \leq \frac{\Gamma}{2} \frac{R}{\epsilon_{th}} \quad (A-3)$$

But R/ϵ_{th} corresponds to the evolution rate σ_{evol} . Therefore, for detonation

$$\sigma_{evol} \cong (2/\Gamma) \sigma_{osc} \quad (A-4)$$

Rosseland (1949) and Ledoux and Sauvenier-Goffin (1950) have shown that the lowest mode pulsation frequency is given by

$$\sigma_{osc}^2 = (3\gamma - 4) \frac{\Omega}{I} \quad (A-5)$$

where Ω is the gravitation energy [Eq. (31)] and I the moment of inertia. By Eqs. (32) and (33)

$$\sigma_{osc}^2 \cong \text{stellar binding energy}/R^2 \quad (A-6)$$

which for degeneracy increases only slowly with $1/R$. On the other hand, the evolution rate by neutrino emission is a rapidly increasing function of $1/R$, so that the most favorable conditions for detonation are small radius, high central density, and rapid evolution. Schatzman (1958) has estimated the fundamental oscillation frequency for degenerate white dwarfs and gives rates $1 < \sigma < 10$ per second for the density range $10^7 < \rho_c < 10^9$ g/cm³. Using the differential thermonuclear reaction rate given by Ohyama (1963) and Fowler and Hoyle (1960) of $\Gamma \cong 85$ for carbon burning, then for detonation the evolution time must be less than approximately 10 sec. This time is so short compared to the neutrino evolution time ($\tau_{pair} \cong 10^{10}$ sec, $\tau_{inverse \beta \text{ decay}} \cong 10^3$ sec) that only a dynamical collapse due to a change in equation of state by inverse beta decay could trigger a detonation.

Two thermonuclear test problems were calculated numerically using the above criteria for evolution time immediately prior to instability — namely the central density and temperature had to be such that $\Gamma < 4/3$ so that a dynamical collapse would be eminent. Under these conditions the thermonuclear energy of 5×10^{17} ergs/g represents a small perturbation to the initial energy content of the matter, so that the rarefaction wave originating at the core due to the pressure

defect in the equation of state "swallows" the thermonuclear explosion before any significant mass can be ejected.

Figure 43 shows the temperature versus time for the implosion of a $10 M_{\odot}$ star where $3 M_{\odot}$ were "detonated" in 0.1 sec by adding 5×10^{17} ergs/g to the matter in a temperature zone initially corresponding to $1 \leq T_9 \leq 3$ and at a time corresponding to 20% increase in temperature from the dynamical instability. The estimate of the thermonuclear zone is somewhat exaggerated, but the effect on the subsequent supernova history is negligible. Figure 44 shows the velocity history of the region just external to the detonation and how indeed the matter first expands, but then falls with the rest of the stellar collapse. The notation with the $9-1/2 M_{\odot}$ zone indicates that the peak expansion kinetic energy is one-fortieth of the gravitational potential so that it is evident that the detonation will implode "inward" unless the core remains rigid. In all subsequent effects the $10 M_{\odot}$ implosion behaved as the previous calculations without a thermonuclear detonation.

The small mass stars evolve with a low enough temperature so that they miss the Fe-He instability and only at a central density of 10^{11} g/cm³ do nuclear binding and inverse beta decay cause a decrease in the adiabatic γ below $4/3$. Figure 45 shows the temperature density history of a $1.5 M_{\odot}$ collapsing star where again 5×10^{17} ergs/g was introduced in 0.01 sec throughout the entire star when $\rho_c \simeq 2 \times 10^{11}$ g/cm³. Despite the exaggerated detonation energy, the calculation shows an entirely similar state history as the nonthermonuclear problem (Fig. 36), primarily because the subsequent neutrino deposition energy is so much greater than the thermonuclear. It is therefore our conclusion that a thermonuclear detonation in a star will occur only when initiated by a dynamical collapse, but that the conditions for the latter lead to a subsequent configuration explosion that completely dominates the thermonuclear phenomena.

FOOTNOTES AND REFERENCES

* Work performed under the auspices of the U. S. Atomic Energy Commission.

¹The artificial viscosity "Q" is used in numerical calculations to convert kinetic energy into internal energy and thereby simulate shock heating. A discussion of this method is given by Richtmyer in his Difference Methods for Initial Value Problems; Chapter X is devoted to fluid dynamics.

²The following four sections have been contributed by William H. Grasberger and appeared originally as part of University of California Radiation Laboratory Report UCRL-6465 (1961).

³These forms are available upon request in University of California Radiation Laboratory Reports UCRL-6465 and UCRL-6196.

Allen, C. W., 1963, Astrophysical Quantities (The Athlone Press, London).

Azinov, Ya. J., and Shekhter, V. M., Zh. Eksperim. i Teor. Fiz. 41, 592; 1962, JETP 14, 424.

Bahcall, J. N., 1964, "Neutrino Opacity I," "Orange Aid" preprint series, Calif. Inst. Tech., to be published in Physical Review.

Burbidge, E. M., Burbidge, G. R., Fowler, W. A., and Hoyle, F., 1957, Rev. Mod. Phys., 29, 547.

Burgers, J. M., and Robbertse, W. P., 1949, Proc. Koninkl. Ned. Akad. Wetenschap. 52, 958, 1067.

Cameron, A. G. W., 1959, Astrophys. J. 130, 884.

Chandrasekhar, S., 1939, An Introduction to the Study of Stellar Structure (The University of Chicago Press).

_____, 1957, (Dover Publication, New York).

Christy, R., 1964, private communication.

Chiu, H. Y., and Stabler, R. C., 1961, Phys. Rev. 122, 1317.

- Chiu, H. Y., and Morrison, P., 1960, Phys. Rev. Letters 5, 573.
- Chiu, H. Y., 1961, Phys. Rev. 123, 1040.
- Colgate, S. A., and Johnson, H. J., 1960, Phys. Rev. Letters 5, 235.
- Colgate, S. A., and White, R. H., "Cosmic Rays from Large Supernova," Intern. Conf. on Cosmic Rays, Jaipur, India, Dec. 1963, to be published.
- Colgate, S. A., and Cameron, A. G. W., 1963, Nature 200, 870.
- Courant, R., and Fredericks, K. O., 1948, Supersonic Flow and Shock Waves (Interscience, New York).
- Deutsch, A. J., "Mass Loss from Red Giants," The Stellar Evolution Conference, Nov. 13-15, 1963, NASA, New York, to be published.
- Eddington, A. S., 1926, The Internal Constitution of the Stars (Cambridge).
- Fermi, E., 1949, Nuclear Physics (University of Chicago Press).
- Feynman, R., and Gell-Mann, M., 1958, Phys. Rev. 109, 193.
- Fowler, W. A., and Hoyle, F., 1964, "Neutrino Processes and Pair Formation in Massive Stars and Supernova" Astrophys. J. Suppl. Series IX. No. 91.
- Grasberger, W. H., 1961, University of California Radiation Laboratory Rept. UCRL-6196.
- Grasberger, W. H., and Yeaton, J. N., 1961, University of California Radiation Laboratory Rept. UCRL-6465.
- Greenstein, J., 1964, private communication.
- Hayashi, C., Hoshi, R., and Sugimoto, D., 1962, Prog. Theo. Phys. 22.
- Heller, L., 1963, Los Alamos Rept. LAMS 3013.
- Hoyle, F., and Fowler, W. A., 1960, Astrophys. J. 132, 565.
- Kippenham, R., private communication and Conference on Stellar Evolution held at NASA Inst. for Space Studies, New York, Nov. 1963, to be published.
- Konopinski, E. J., 1943, Rev. Mod. Phys. 15, 209.
- Ledaux, P. J., and Sauvenier-Goffin, E., 1950, Astrophys. J. 111, 611.

Levin, M., 1963, Ph.D. thesis, California Institute Technology.

Minkowsky, R. L., to be published in Astron. Soc. Pacific.

Misner, C. W., and Zepolsky, H. S., 1964, Phys. Rev. Letters 12, 635.

Ohyama, N., 1963, Prog. Theoret. Phys., 30, 170.

Ono, Y., Sakashita, S., and Yawazaki, H., 1960, Prog. Theoret. Phys. 23, 294.

_____, 1960, Prog. Theoret. Phys. 24, 155.

Ono, Y., Sakashita, S., and Ohyama, N., 1961, Prog. Theoret. Phys. Suppl. No. 20, 85.

Oppenheimer, J. R., and Volkoff, G. M., 1939, Phys. Rev. 55, 374.

Reines, F., and Cowan, C. L., Jr., 1959, Phys. Rev. Vol. 113, 273.

Richtmyer, R. D., 1957, Difference Methods for Initial-Value Problems (Interscience Publishers, Inc., New York).

Rosseland, S., 1949, The Pulsation Theory of Variable Stars (Clarendon Press, Oxford).

Salpeter, E. E., 1960, Ann. Phys. 9, 11.

Salpeter, E. E., meeting on "Neutron Stars and Celestral X-Ray Sources" held at the NASA Inst. for Space Studies, New York, March 20, 1964, to be published.

Schatzman, E., 1958, White Dwarfs (North Holland Publishing Co., Amsterdam).

Schwarzschild, M., 1958, Structure and Evolution of the Stars (Princeton University Press).

Wheeler, J. A., Meeting on "Neutron Stars and Celestral X-Ray Sources" held at the NASA Inst. for Space Studies, New York, March 20, 1964, to be published.

_____, 1964, in Gravitation and Relativity, ed. by H. Chin and W. F. Hoffman (W. A. Benjamin, Inc., New York), Chap. 10.

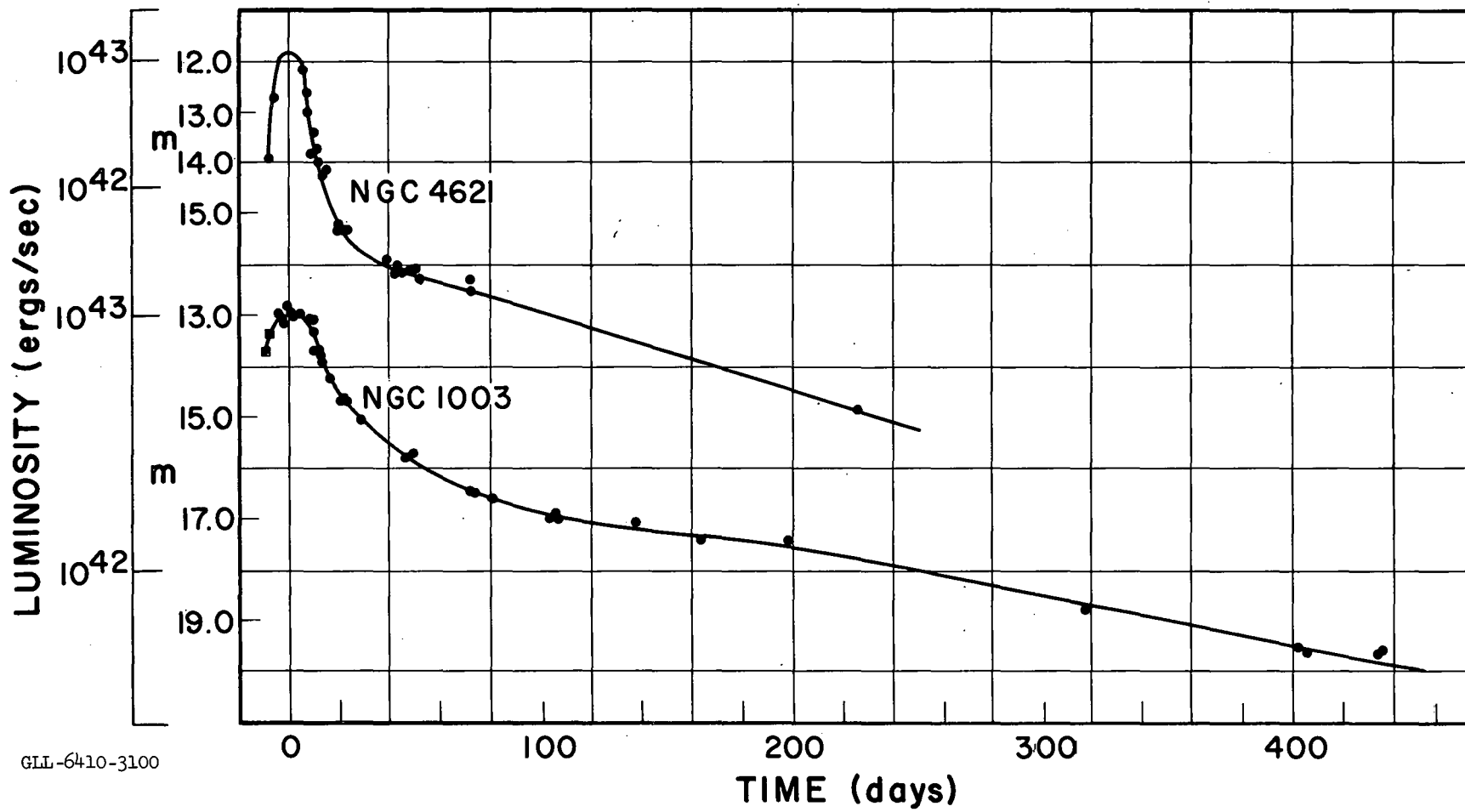
/sk

Table I. Properties of Type I and Type II supernovae.

	Total optical energy (ergs)	Peak luminosity (ergs/sec)	Ejected hydrogen	Typical ejected mass (M \odot)	Observed ejected kinetic energy (ergs)	Occurrence (stellar population)	Probable origin (M \odot)
Type I	4×10^{49}	10^{43}	No	0.1-1	$4 \times 10^{48-49}$	Old stars	1.16-2
Type II	2×10^{49}	10^{43}	Yes	1-10	$4 \times 10^{50-51}$	Young stars	>2

Table II. Luminosity calculated for each of the envelope expansions.

Stellar Mass	Bolometric luminosity (ergs/sec)	Time to peak (sec)
1.5 M \odot	3.3×10^{38}	3.1×10^4
2 M \odot	4×10^{39}	3.6×10^4
10 M \odot	10^{41}	1.4×10^5
Red giant	3×10^{41}	1.6×10^6



GLL-6410-3100

Fig. 1. Two typical supernova light curves are shown giving a peak luminosity of 10^{43} ergs/sec at a time ≥ 5 days (courtesy Minkowsky, to be published).

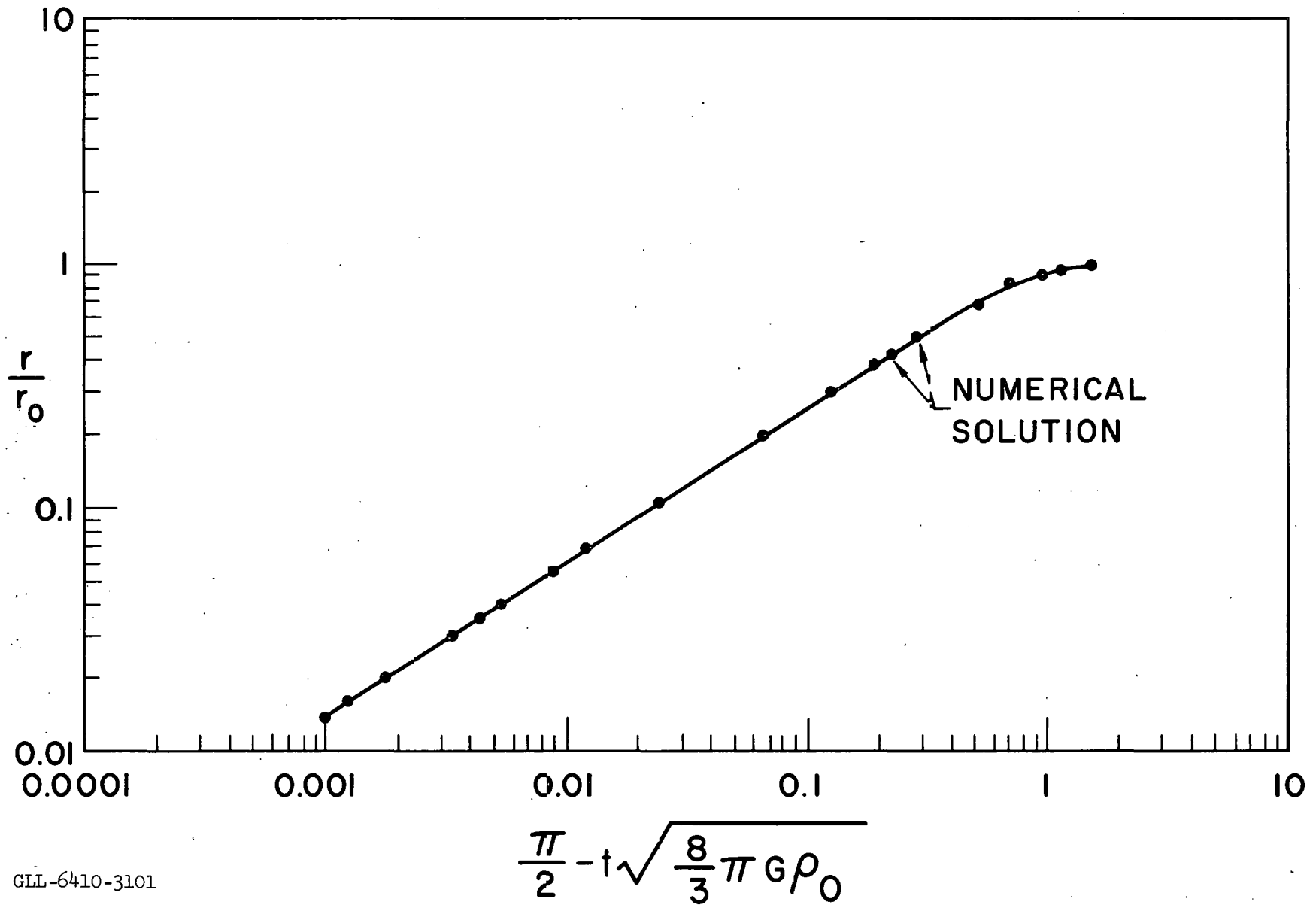
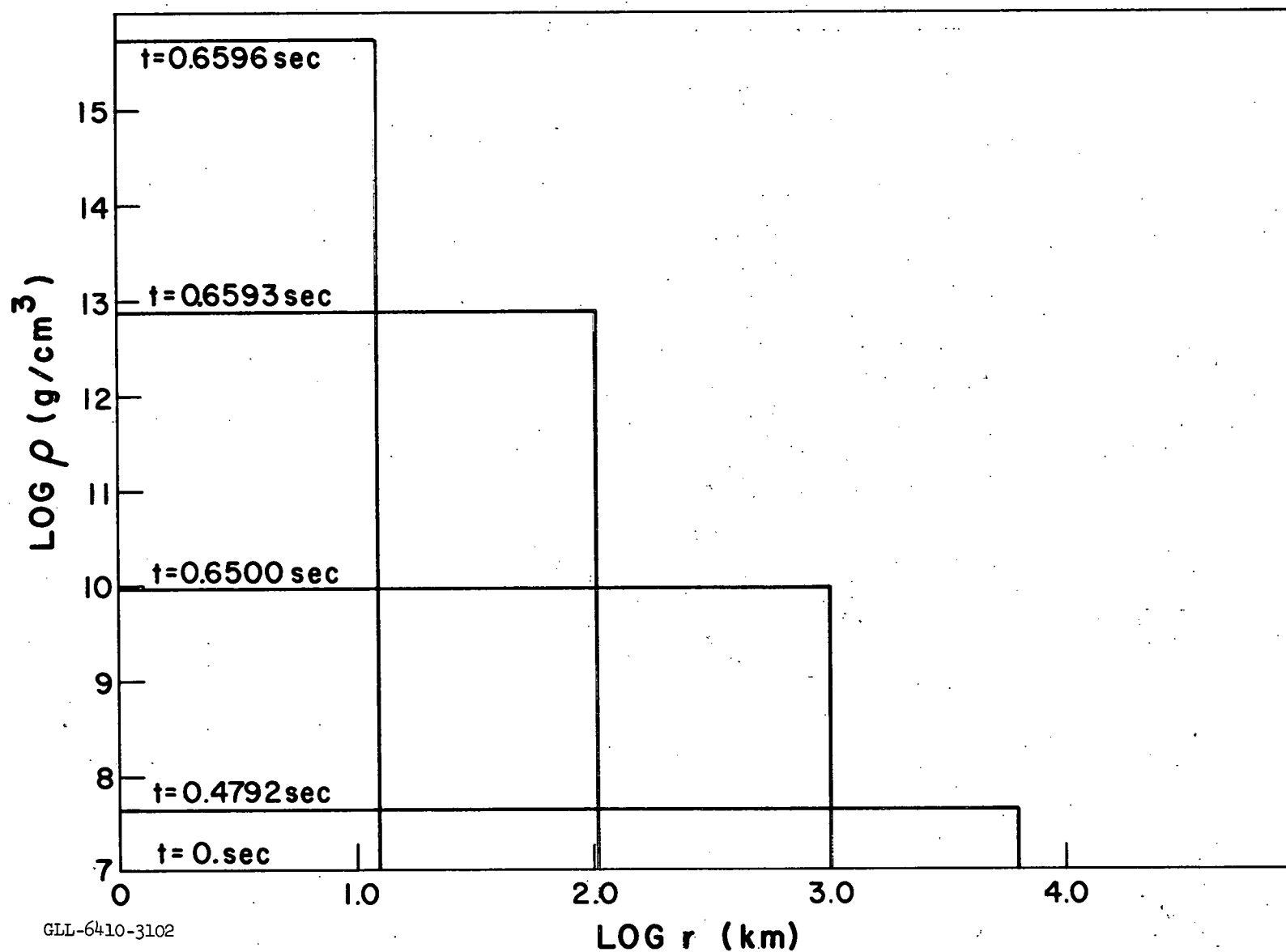


Fig. 2. Radius vs time for the numerical calculation of the uniform-density, free-fall test problem.



GLL-6410-3102

Fig. 3. Log density vs log radius for the uniform-density, free-fall test problem. The relative error in uniformity of numerically computed density was less than 10^{-3} .

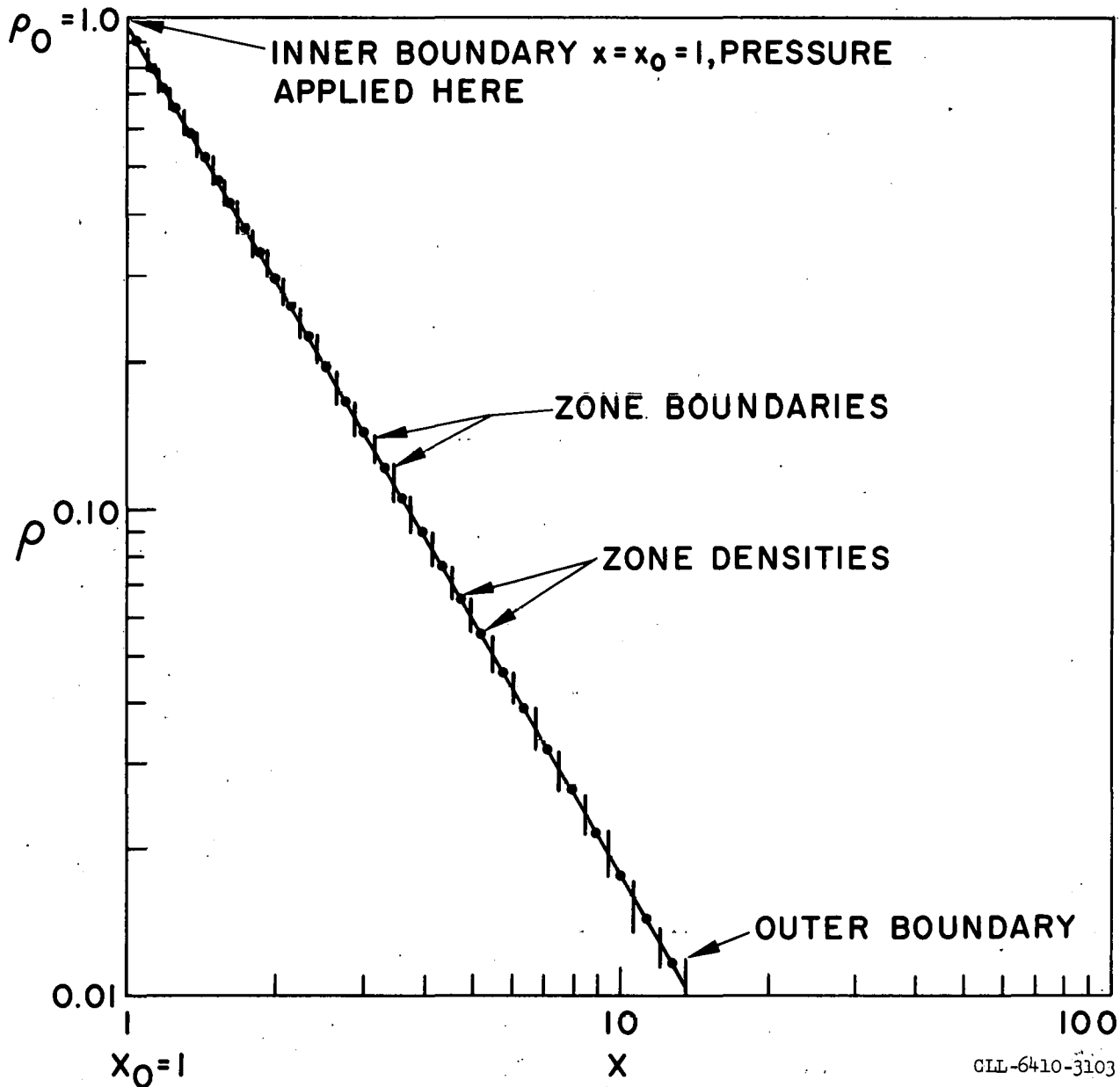


Fig. 4. Density vs radius for initial conditions of similarity solution of a shock in a density gradient. The vertical bars represent the initial zoning for the numerical calculation; the dots correspond to the density.

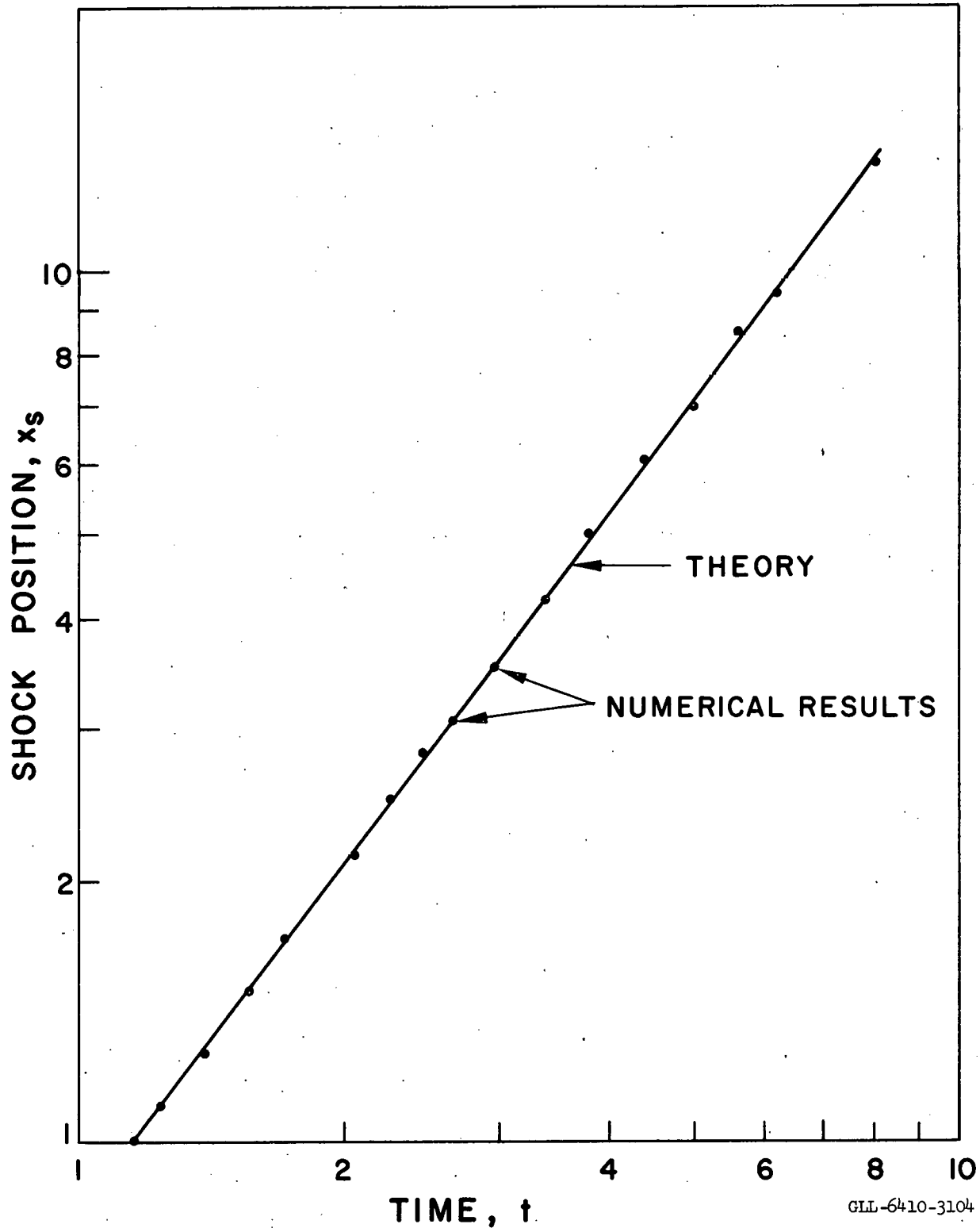


Fig. 5. Shock position vs time for shock similarity test problem.

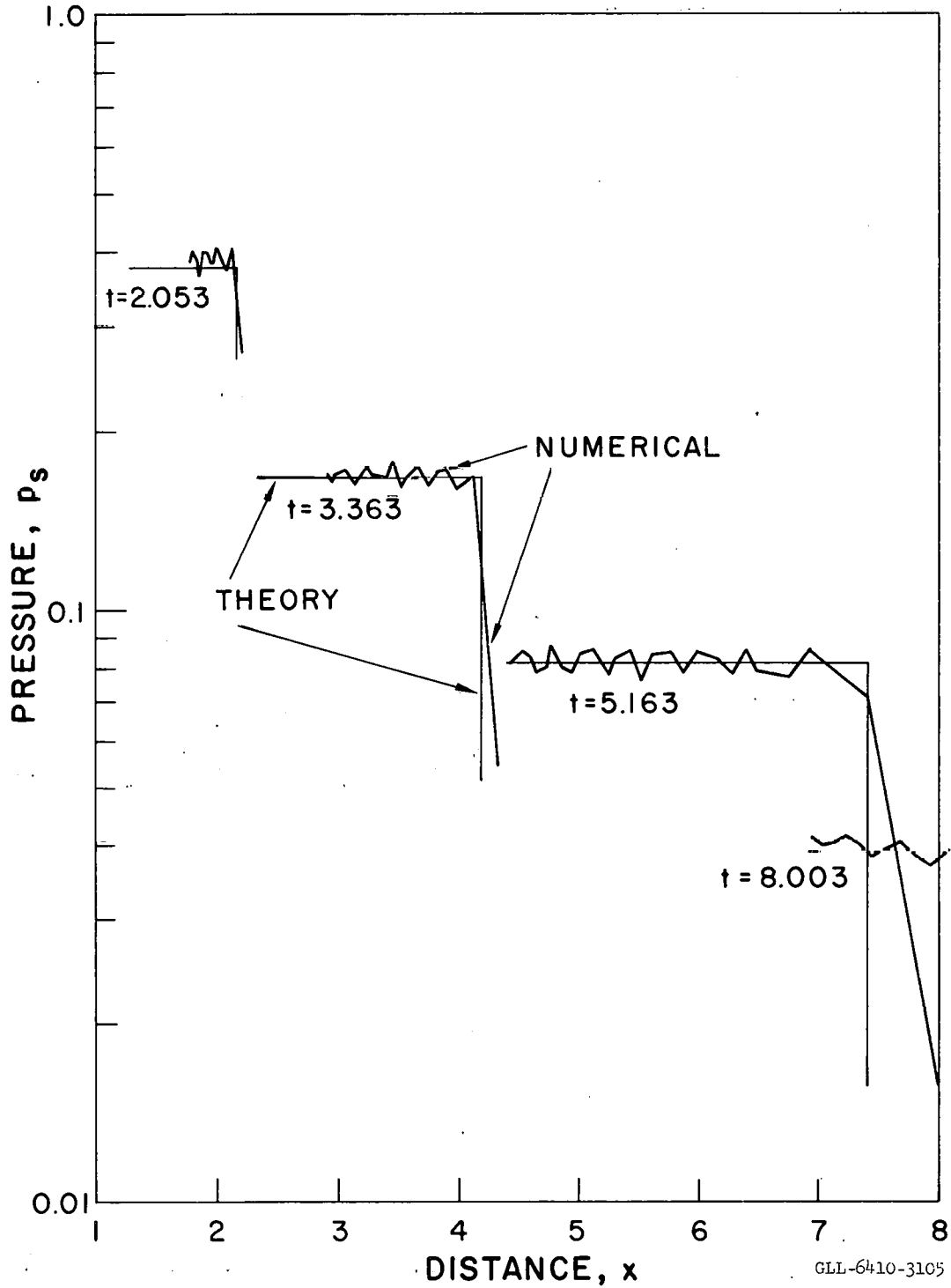


Fig. 6. Pressure vs distance for shock test problems. The uniformity of pressure behind the shock is the characteristic feature of the similarity solution and is verified by the numerical calculation.

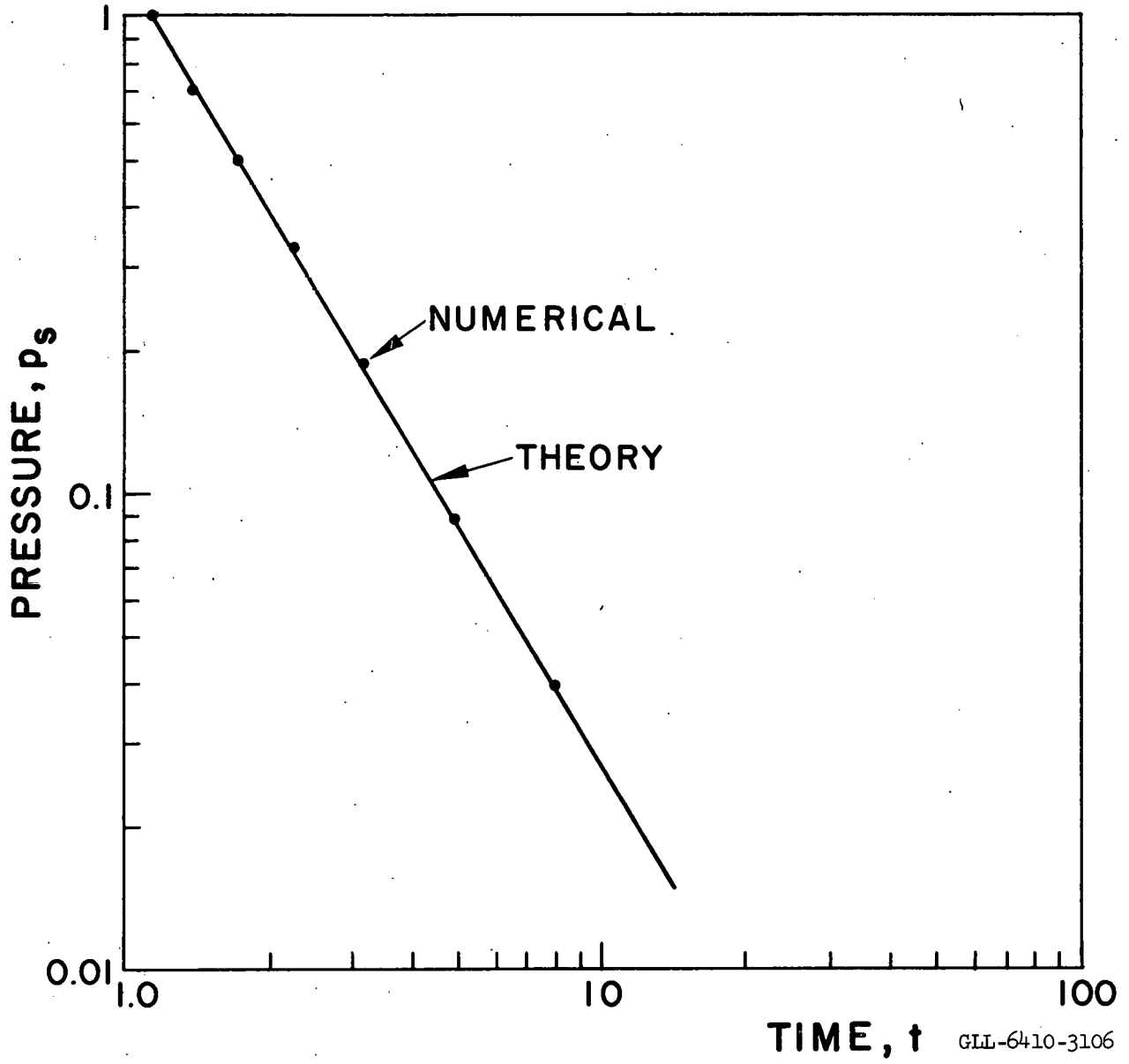


Fig. 7. Pressure vs time for shock test problem.

GLL-6410-3106

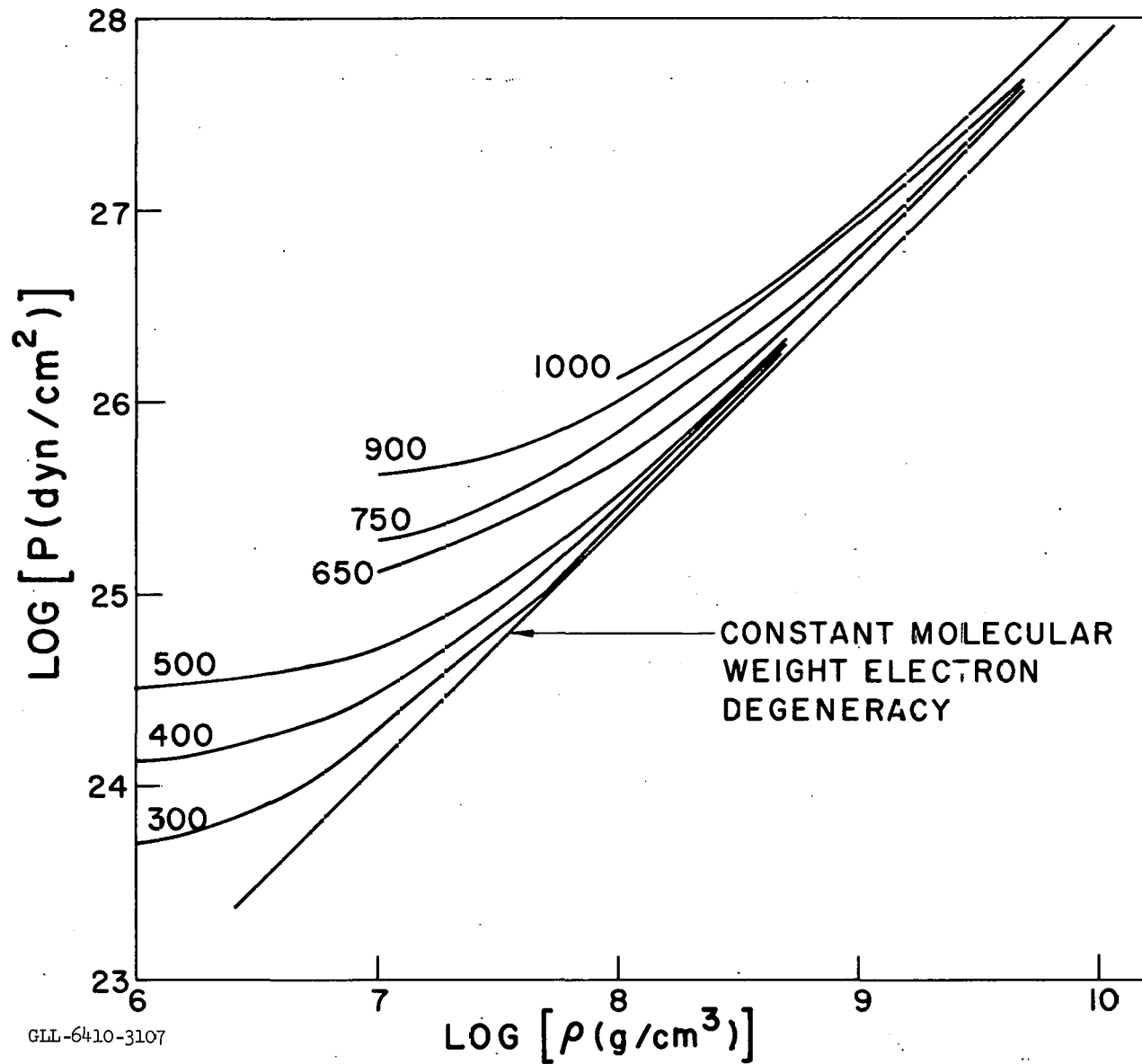


Fig. 8. Pressure vs density for the constant molecular weight Fe-He and He-n, p equation of state. At low temperature the curves asymptotically approach the cold electron degeneracy pressure.

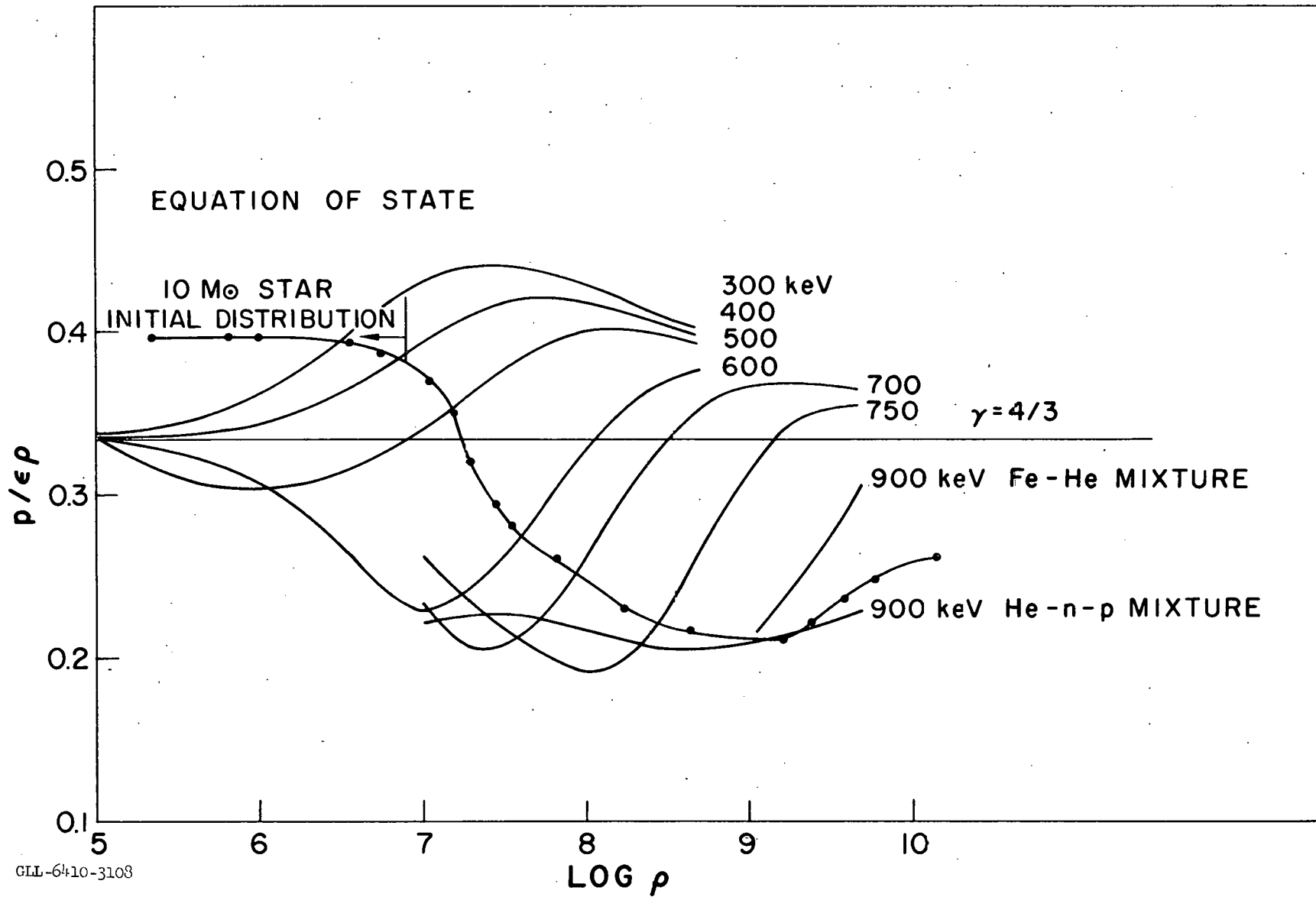
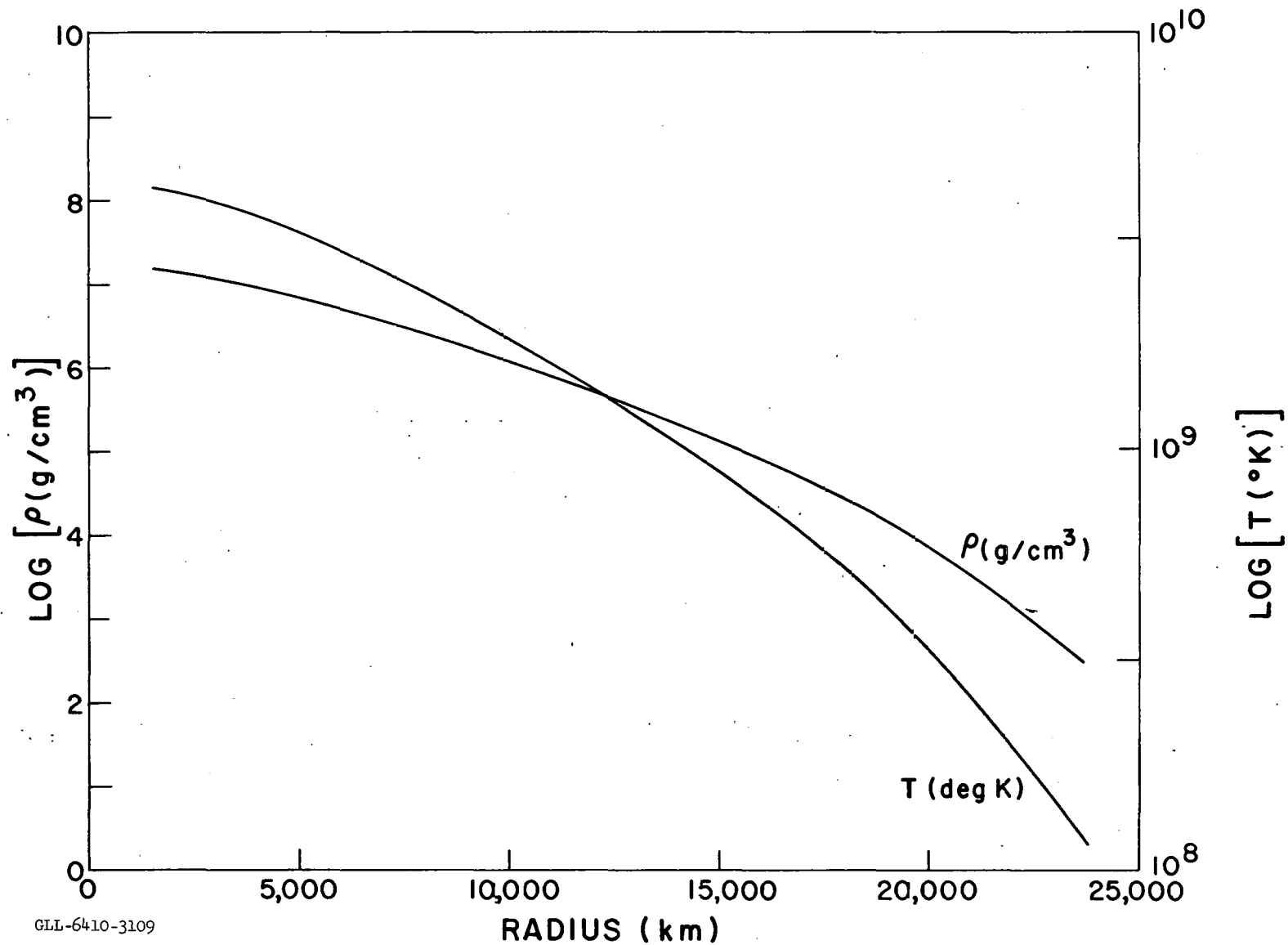


Fig. 9. $p/\epsilon\rho$ vs log density for the Fe-He and He-n,p equation of state. The value $p/\epsilon\rho < 1/3$ leads to gravitational instability and corresponds to temperature-density conditions of thermal nuclear decomposition.



GLL-6410-3109

Fig. 10. Log density and log temperature for the initial distribution of the 10 M \odot polytrope of index 3. The initial central density and temperature were chosen to meet the two conditions of equilibrium and initial Fe-He thermal decomposition.

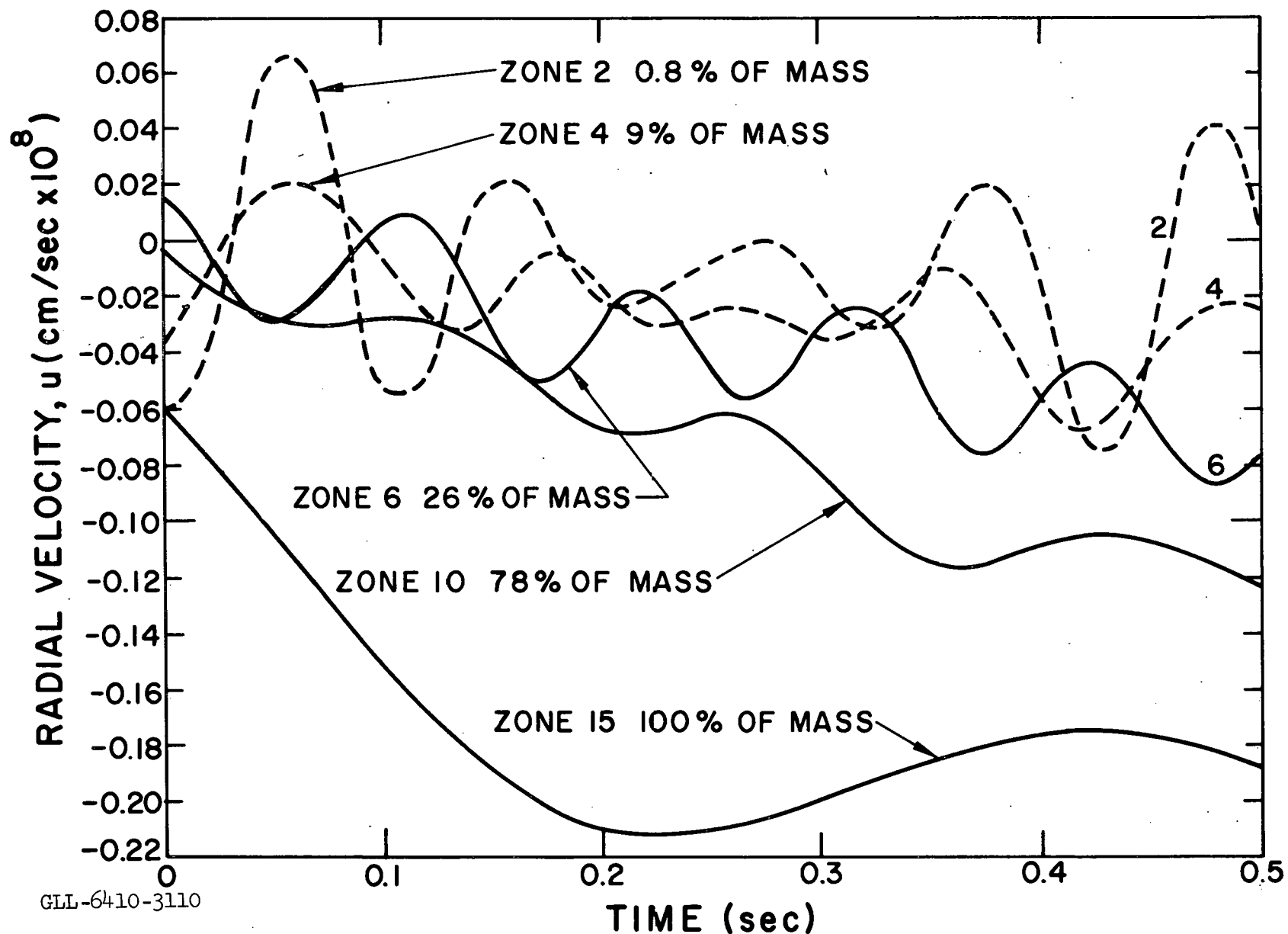


Fig. 11. The velocity vs time oscillations of the zone boundaries represent sonic disturbances around the equilibrium condition. The kinetic energy of these oscillations is about 10^{-4} of the internal energy and so is small.

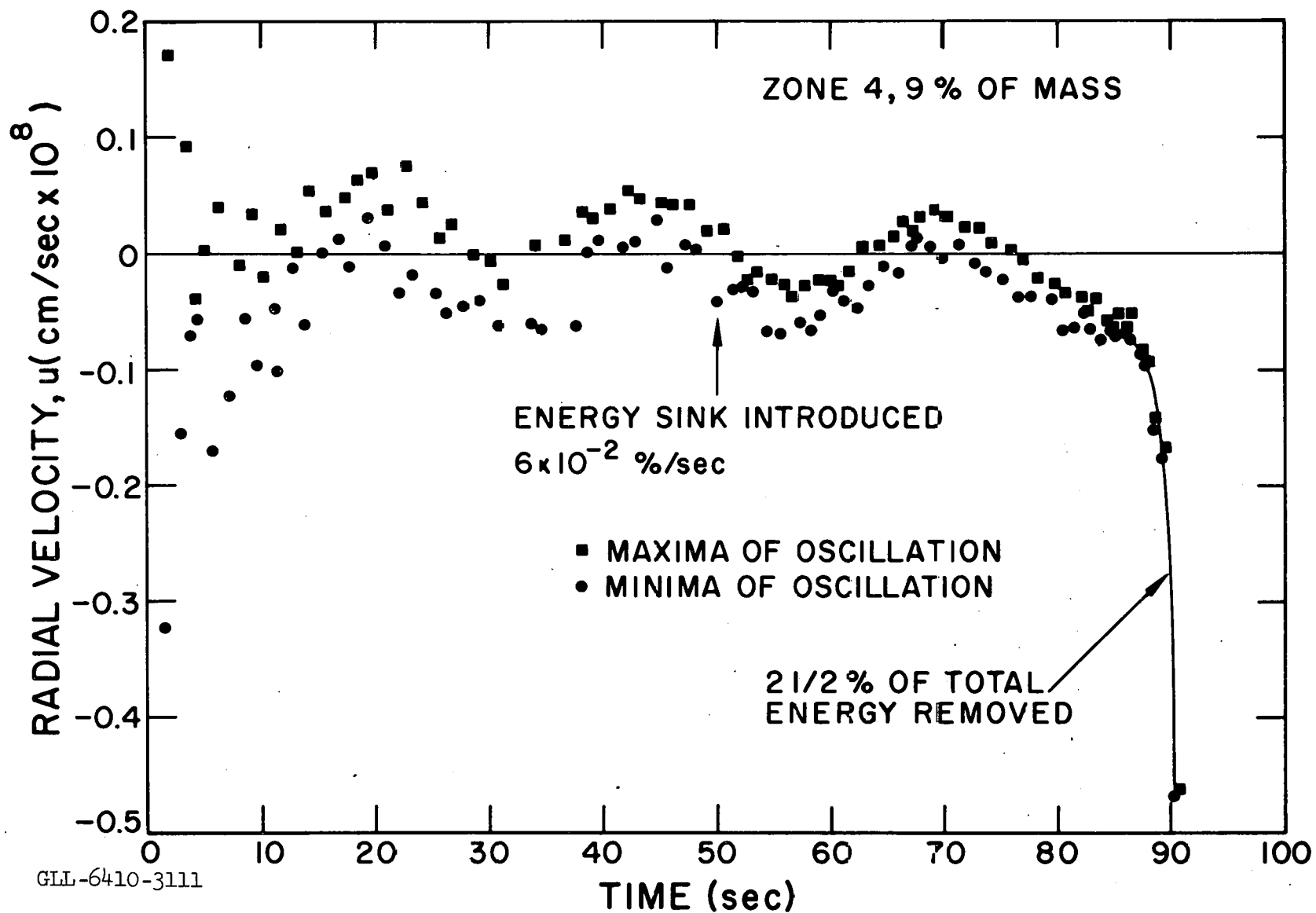


Fig. 12. The circles and squares represent the many maxima and minima of the oscillations of an inner zone before and after the introduction of a slow artificial heat sink of 6×10^{-2} %/sec of initial internal energy. This heat sink has removed 2-1/2% of the total energy at time of unstable collapse.

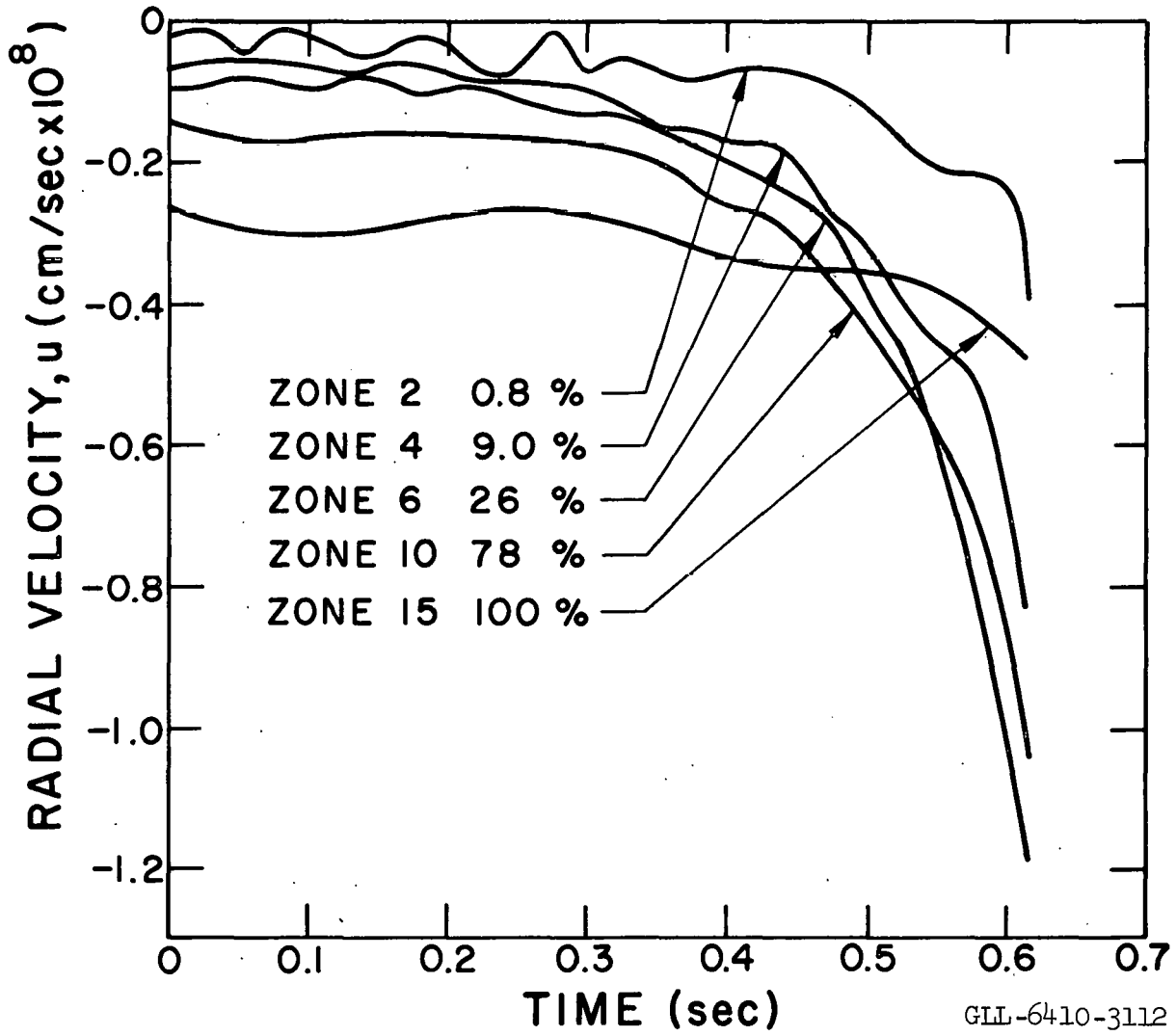


Fig. 13. Velocity history of zones at start of collapse. The ordering of the zones in radius is consecutive, but is partially random in velocity space.

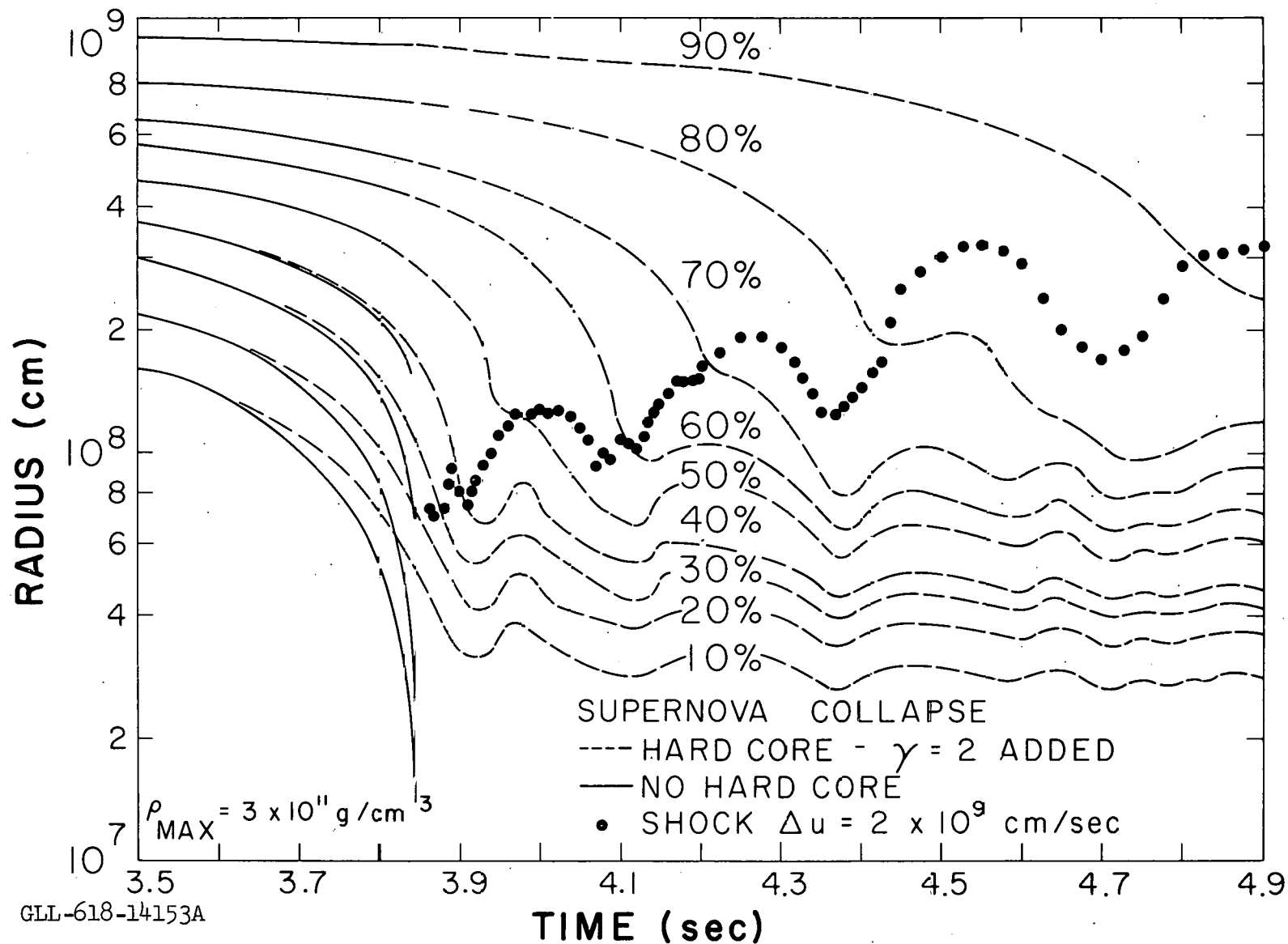


Fig. 14. Radius vs time history during instability collapse of a 10 M \odot supernova star. The solid curves describe the case with no hard-core while the dashed curves show the effect of introducing an initial gas of $\gamma = 2$ and fractional energy of 2×10^{-3} . The generation of a shock wave is indicated by the circles showing the emergence of the shock into the outer stellar zones.

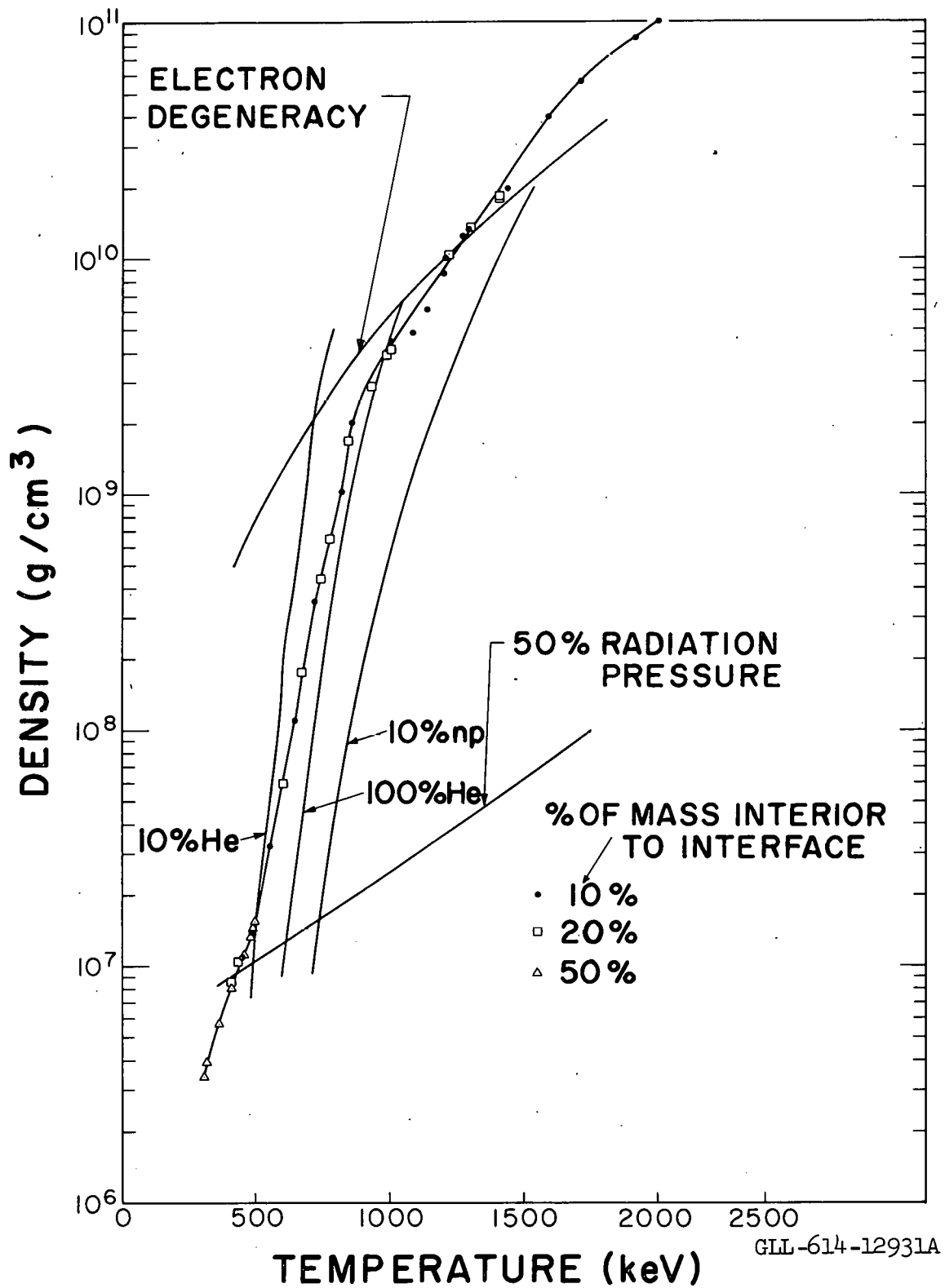
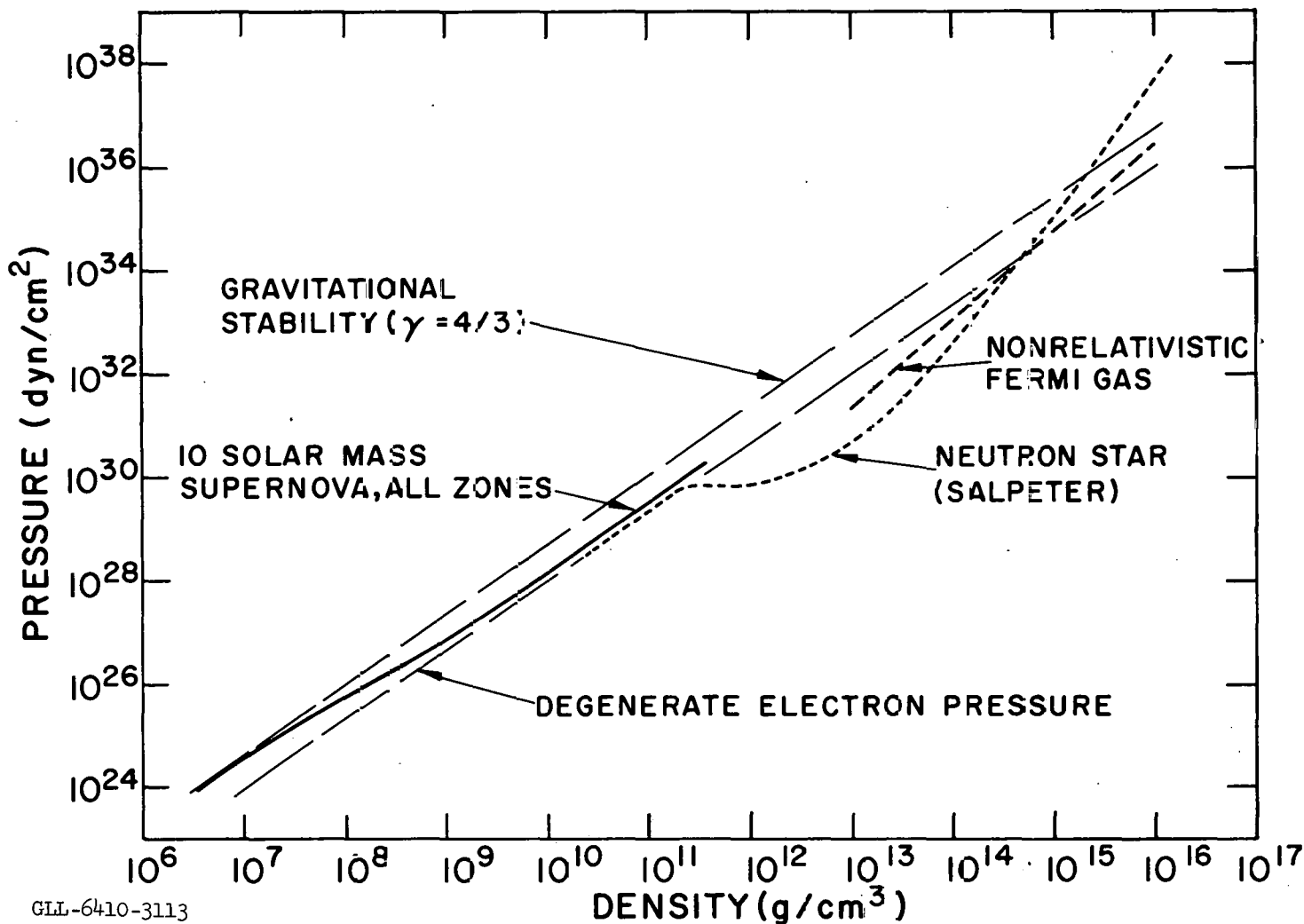
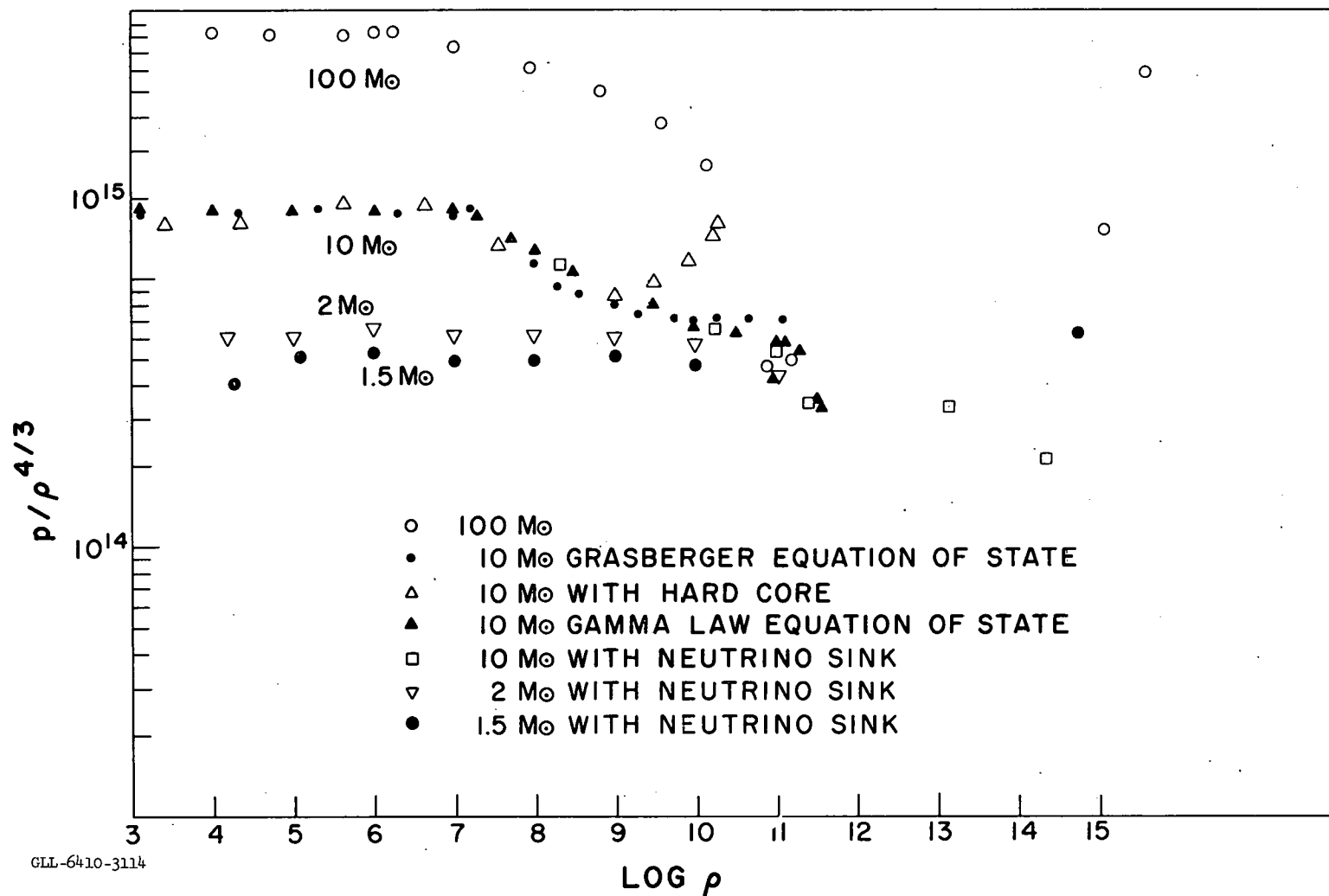


Fig. 15. The equation of state of stellar material for a supernova of 10 M_{\odot} . All zones of the initial star and subsequently during implosion fall along the same adiabat.



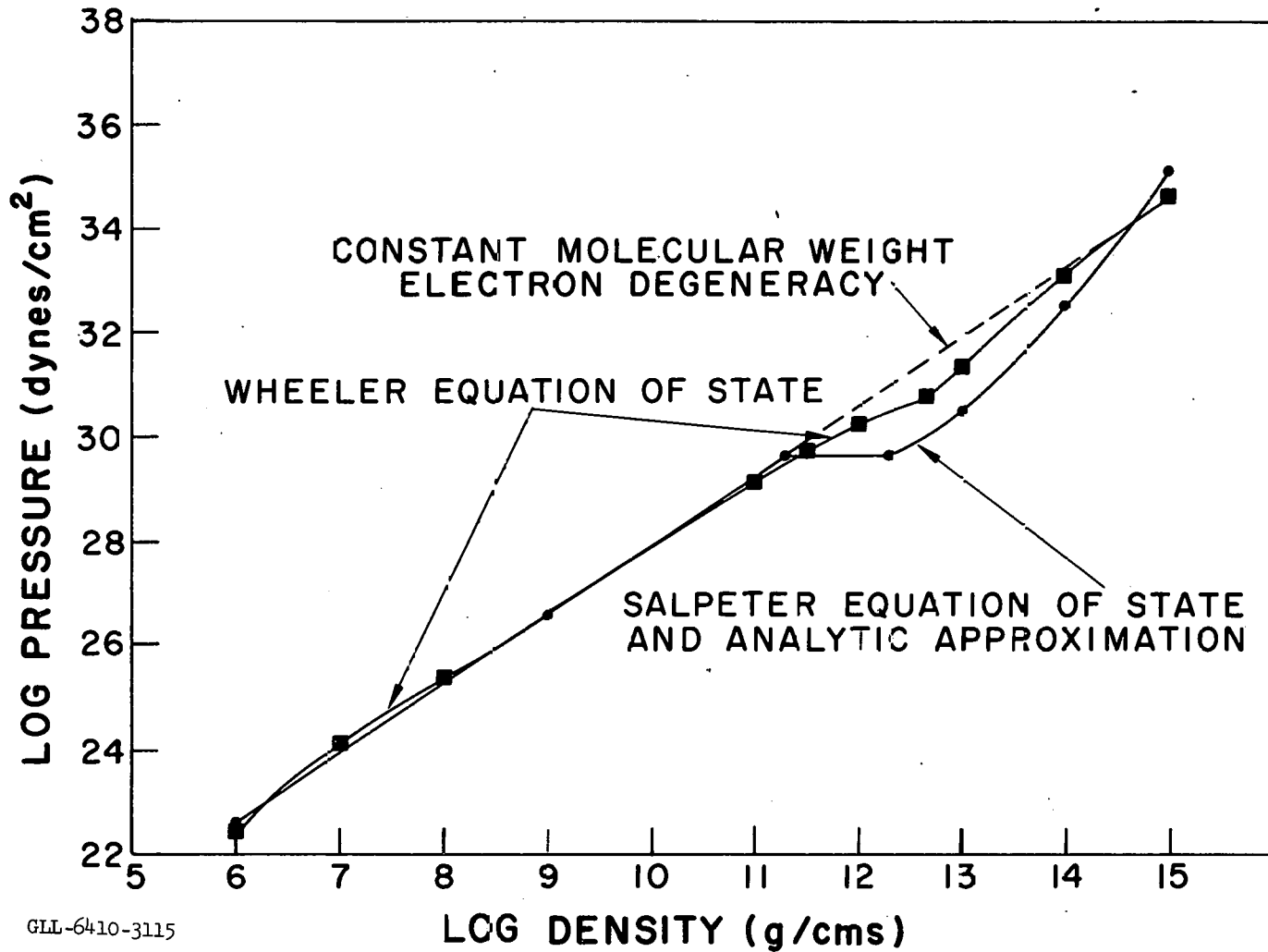
GLL-6410-3113

Fig. 16. The heavy solid curve represents the pressure and density of the initial and imploding zones of the supernova star with no hard core. The heavy dashed curve shows the effect of the core ($\gamma = 2$) extending up to the gravitational stability curve ($\gamma = 4/3$ extension of the initial star). The dotted curve represents the cold neutron star equation of state of Salpeter with the degenerate electron and nucleon pressure curves included. It is expected that the final bounce will occur when the neutron star pressure equals the gravitational stability pressure at 2×10^{15} g/cm³.



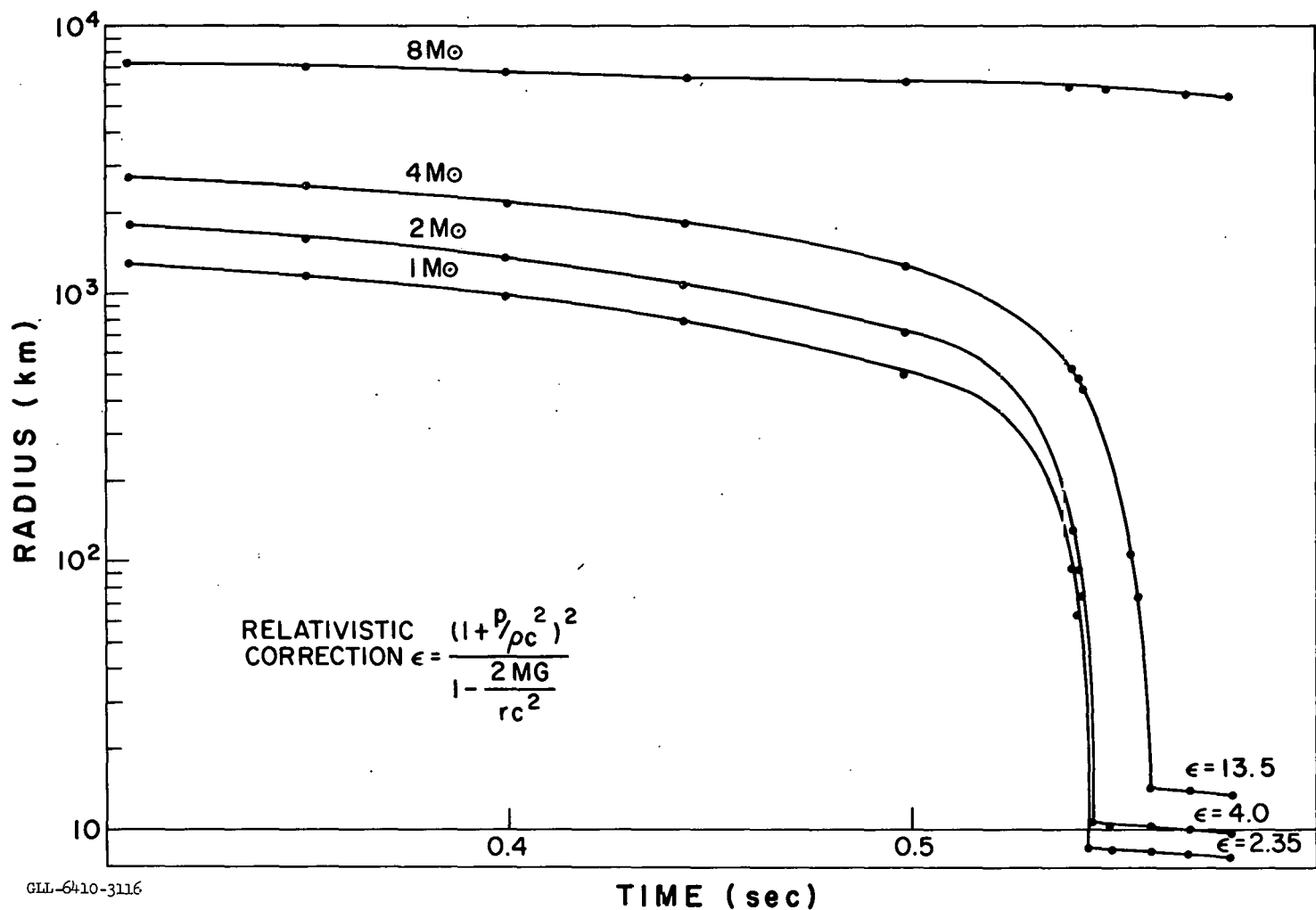
GLL-6410-3114

Fig. 17. $p/\rho^{4/3}$ vs log density. Pressure is in dyn/cm^2 and density in g/cm^3 . The equilibrium pressure density condition is indicated by a constant value of $p/\rho^{4/3}$ for each initial polytrope mass. During subsequent collapse the large decrease in $p/\rho^{4/3}$ can be associated with the minimum supportable core mass. A larger mass must be evolved to give dynamical collapse, and the bounce occurs when $p/\rho^{4/3}$ becomes large enough due to a change in equation of state to support the free falling core.



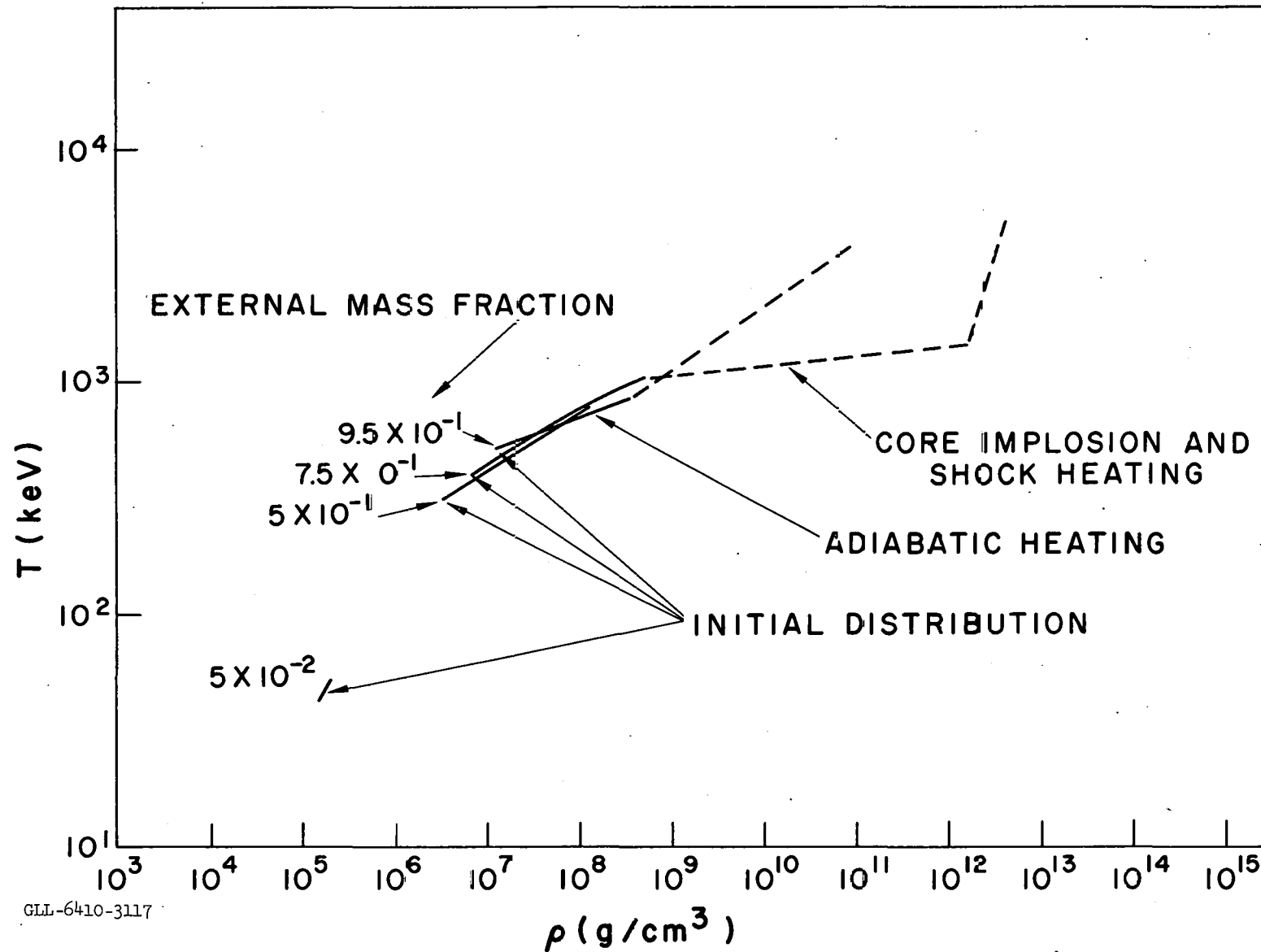
GLL-6410-3115

Fig. 18. Pressure vs density for the three equations of state — Wheeler, Salpeter, and analytic approximation used in the computations. In the density region $5 \times 10^{10} \leq \rho \leq 2 \times 10^{11}$ g/cm³ the Wheeler curve is slightly lower, indicating the formation of neutron-rich nuclei. This would have the effect of initiating the final core collapse at a slightly lower density. The higher value of pressure of the Wheeler curve in the region $2 \times 10^{11} \leq \rho \leq 2 \times 10^{12}$ g/cm³ is due to a revised estimate of nuclear binding and has the effect of reducing the core free-fall energy.



GLL-6410-3116

Fig. 19. Radius vs time for 10 M \odot supernova using neutrino emission showing the collapse with no reflected shock. The parameter ϵ gives the general relativistic correction to the static pressure gradient for each mass addition to the collapsing core. The direction of this correction is in the direction of increasing difficulty for energy emission so that an explosion becomes less likely. The initial equilibrium test and start of instability have been suppressed (20 sec).



GLL-6410-3117

Fig. 20. Temperature vs density for a $10 M_{\odot}$ supernova with neutrino emission. The initial distribution is indicated and during collapse all zones follow the same adiabat until the neutrino emission cools them to $T \approx 0$.

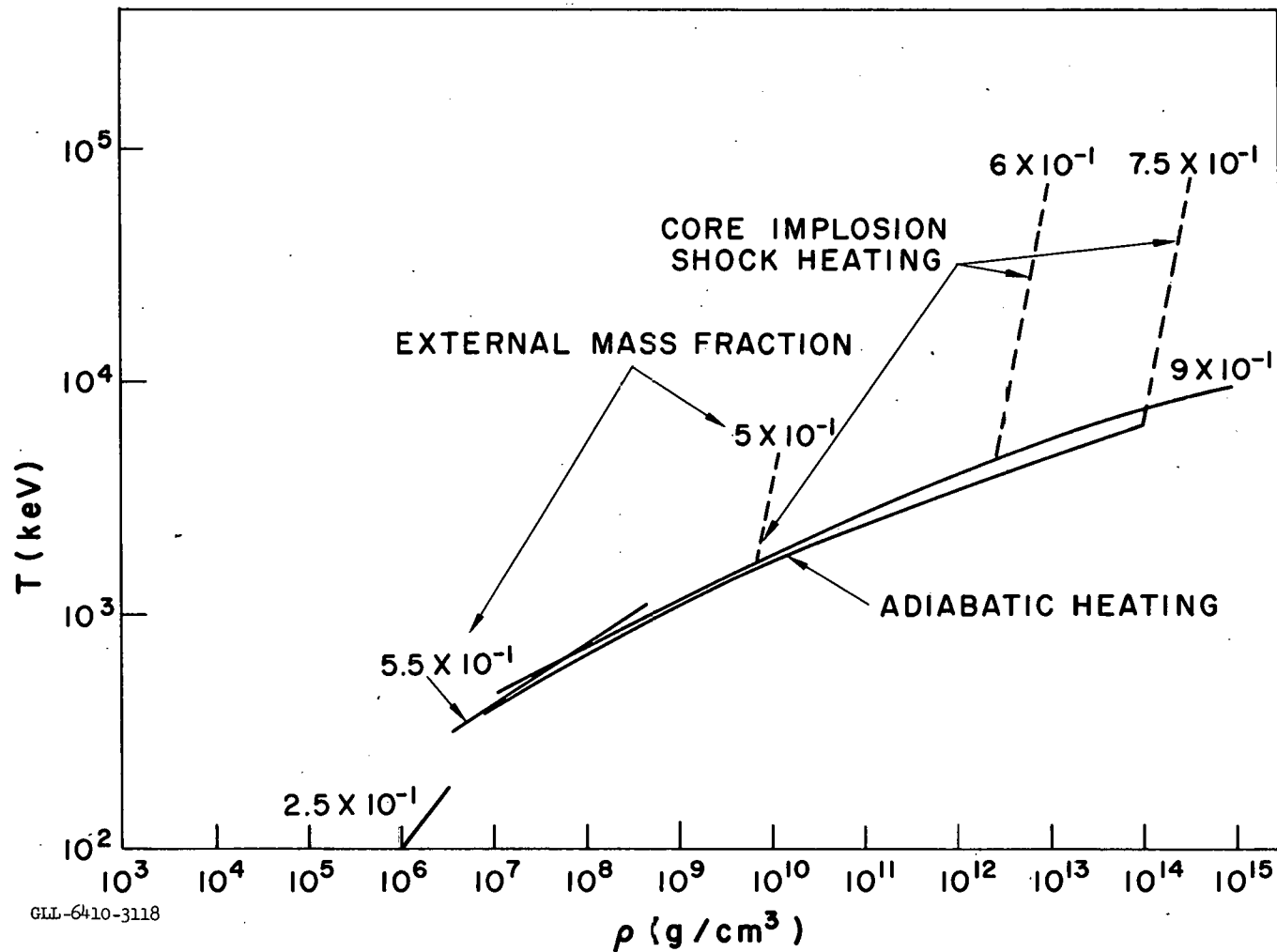
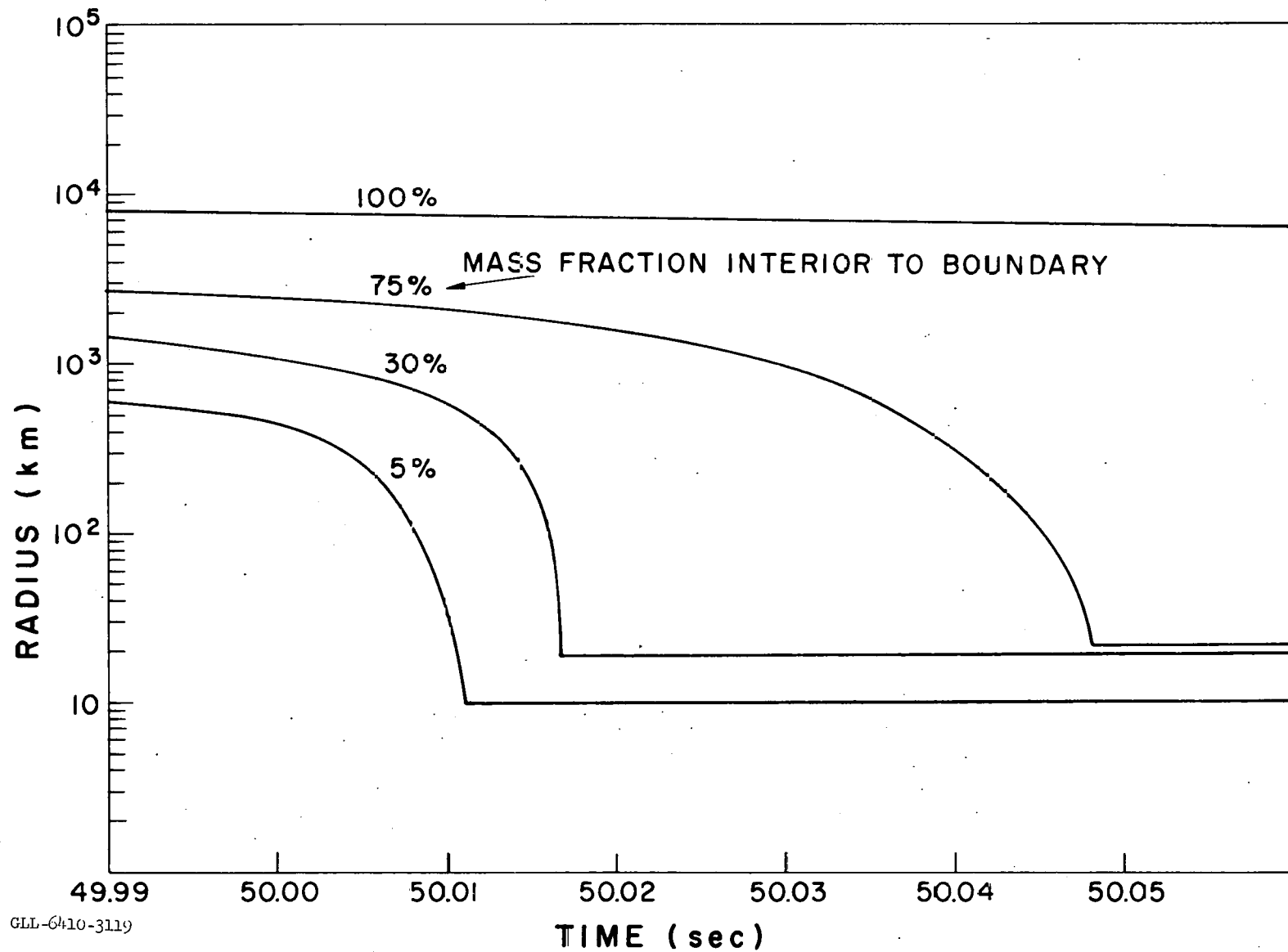


Fig. 21. Temperature vs density $10 M_{\odot}$ supernova with no neutrino emission. The resulting high core temperature is formed both by adiabatic heating and later by shock heating of matter falling onto the equilibrium core. The temperature is artificially high due to neglecting other leptonic thermal degrees of freedom in the equation of state.



GLL-6410-3119

Fig. 22. Radius vs time for $100 M_{\odot}$ supernova with neutrino emission only. The behavior is the same as the $10 M_{\odot}$ core and shows no indication of explosion.

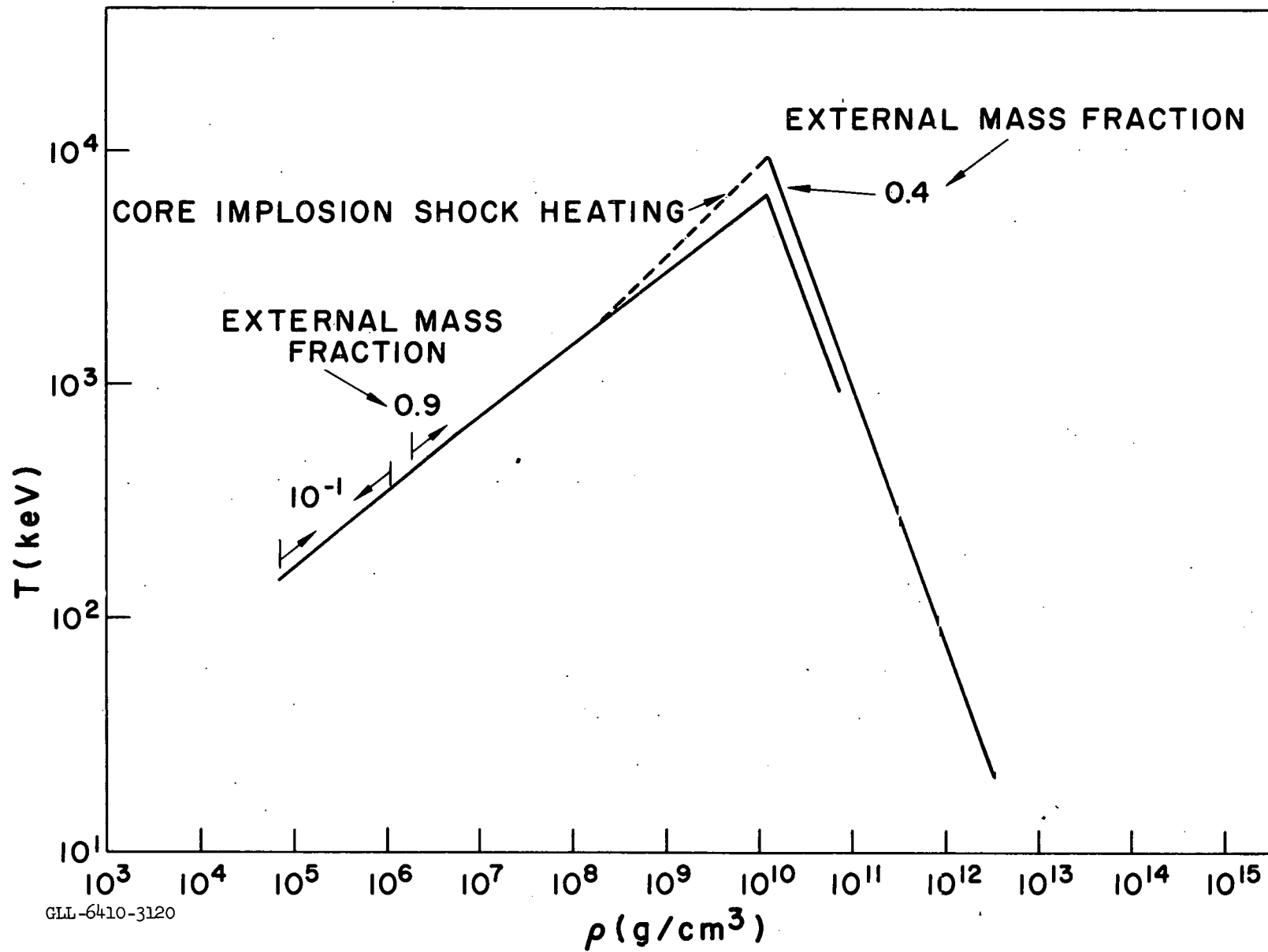


Fig. 23. Temperature vs density for 100 M_{\odot} supernova with neutrino emission only.

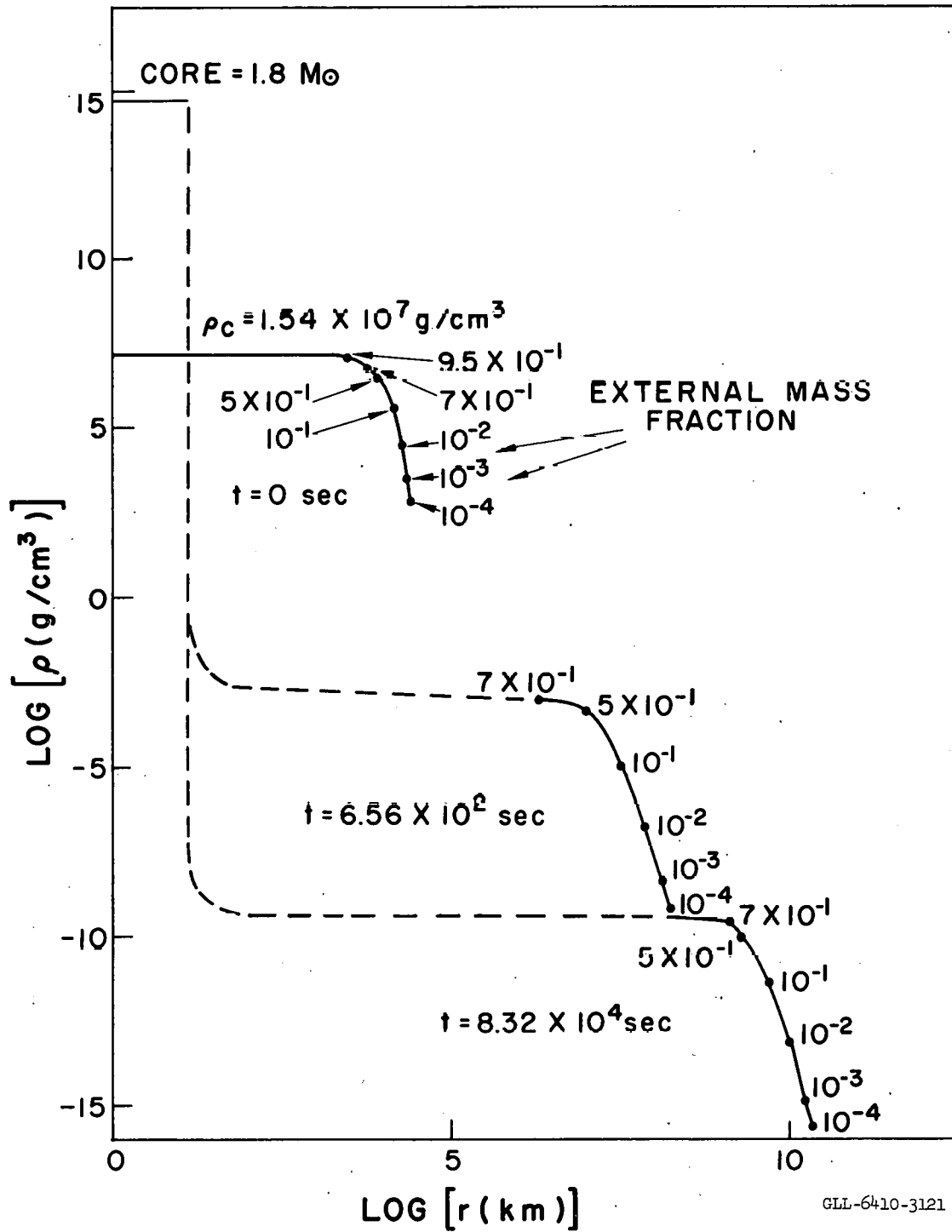


Fig. 24. 10 M_⊙ supernova log density versus log radius for initial conditions as well as various times during the explosion caused by neutrino deposition.

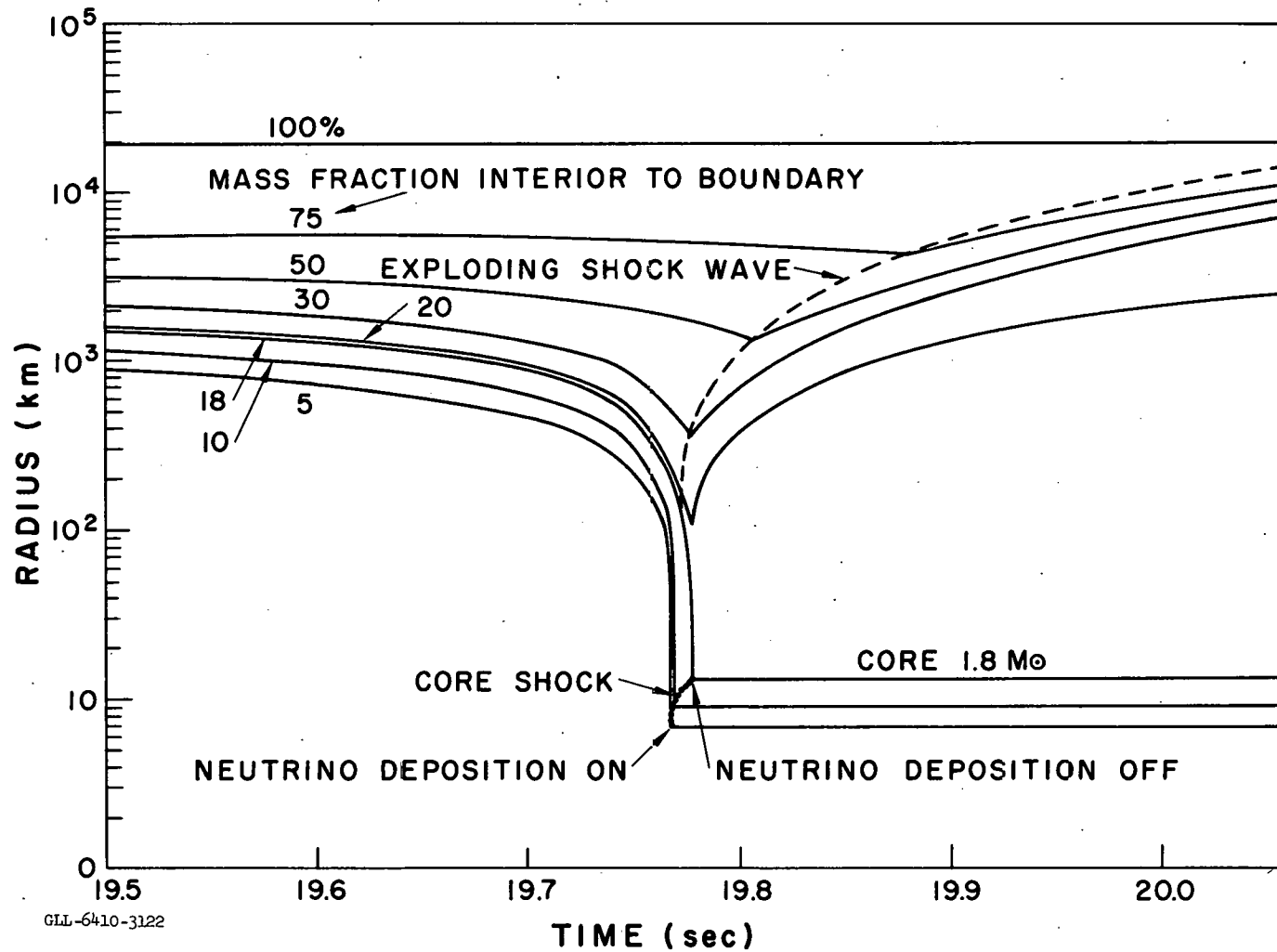
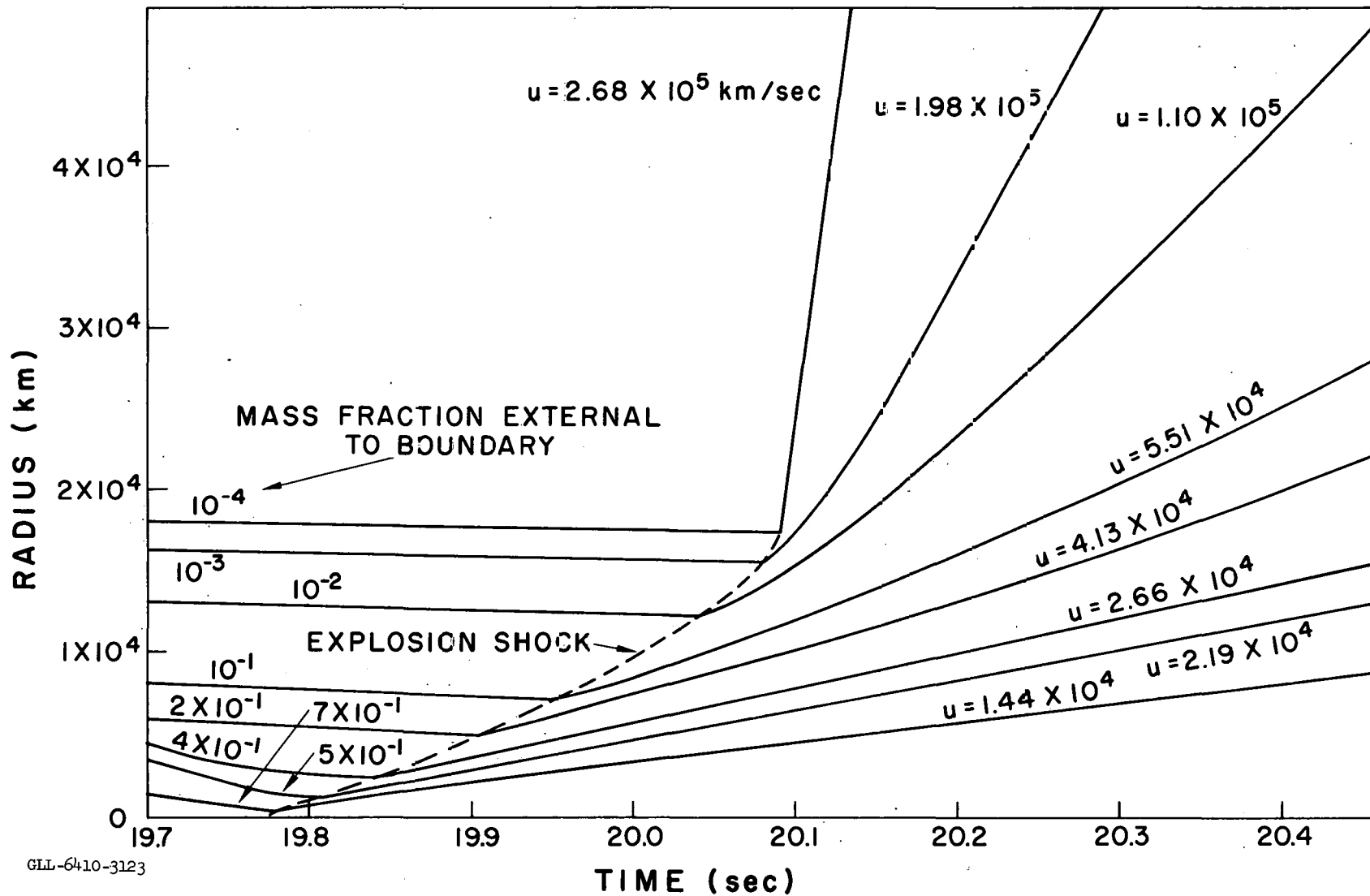
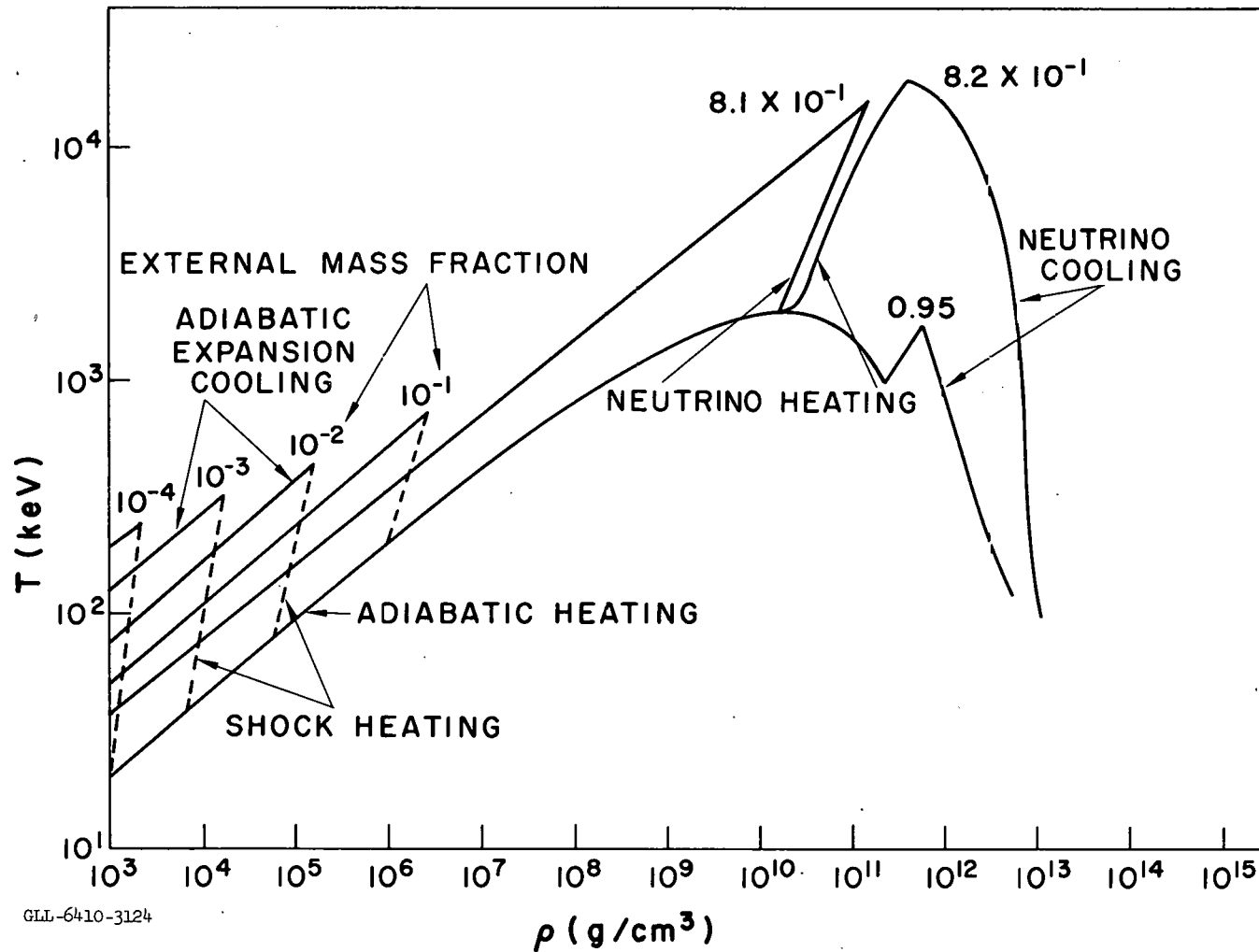


Fig. 25. Radius vs time for 10 M_⊙ supernova with neutrino deposition. During the initial collapse the neutrino energy is assumed lost from the star, but at the time of formation of a core shock wave (heavy dots) a fraction of the neutrino energy is deposited in the envelope. The deposition ceases when the explosion terminates the imploding shock wave on the core.



GLL-6410-3123

Fig. 26. $10 M_{\odot}$ supernova radius vs time. The linear plot shows the increasing velocity of the outward explosion shock wave reaching the relativistic limit for 10^{-4} mass fraction.



GLL-6410-3124

Fig. 27. $10 M_{\odot}$ supernova temperature vs density with neutrino deposition. The lower line of slope $4/3$ corresponds to the initial adiabatic compression during implosion. The innermost zones cool by neutrino emission; the intermediate zones heat by neutrino deposition; and the outermost zones are shock heated. The expanding matter then cools adiabatically.

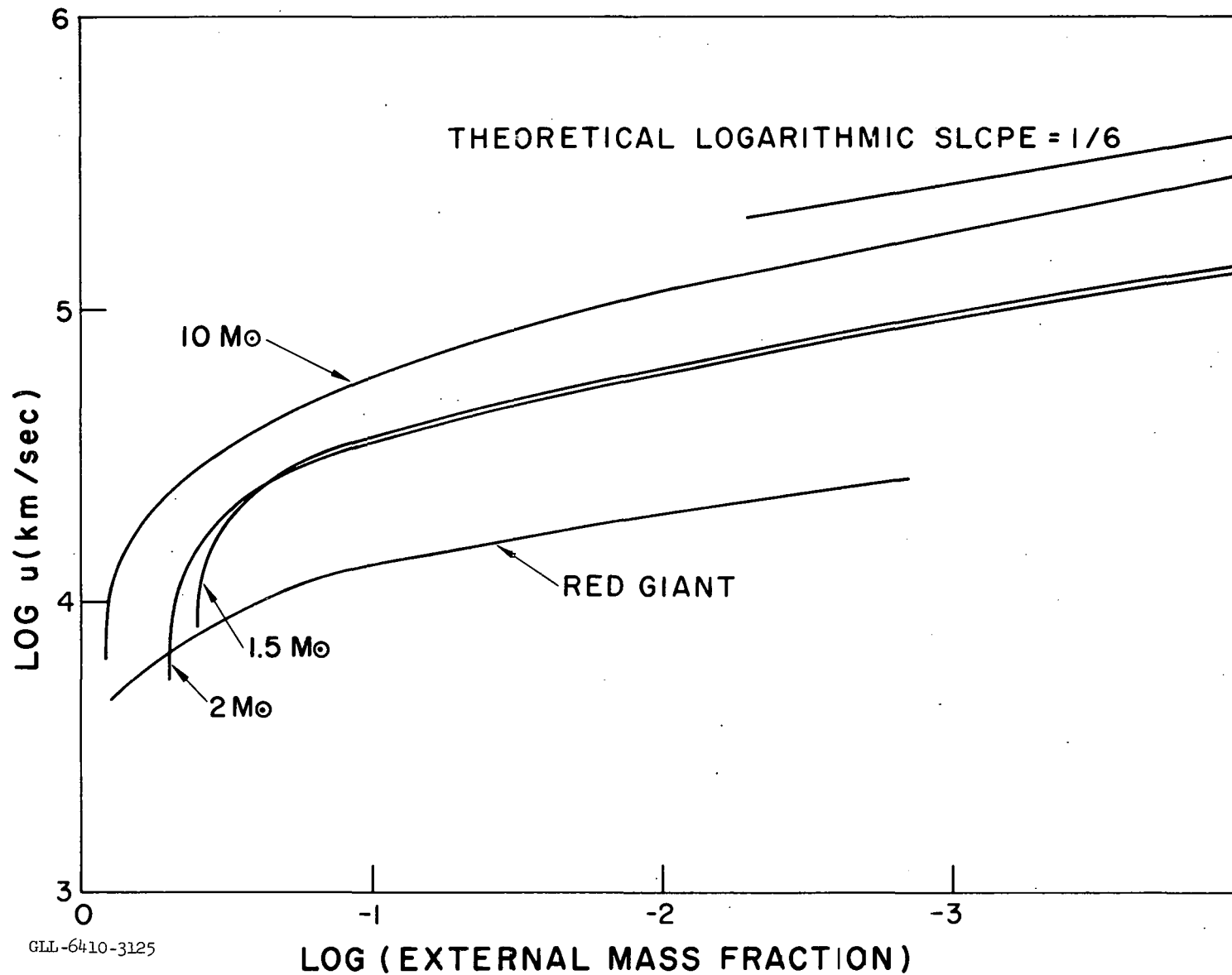


Fig. 28. Log expansion velocity vs log mass fraction for supernova envelopes of 10, 2, and 1.5 M_⊙ polytropic 3 initial stars and a red giant. The logarithmic slope corresponds to the theoretical value of 1/6.

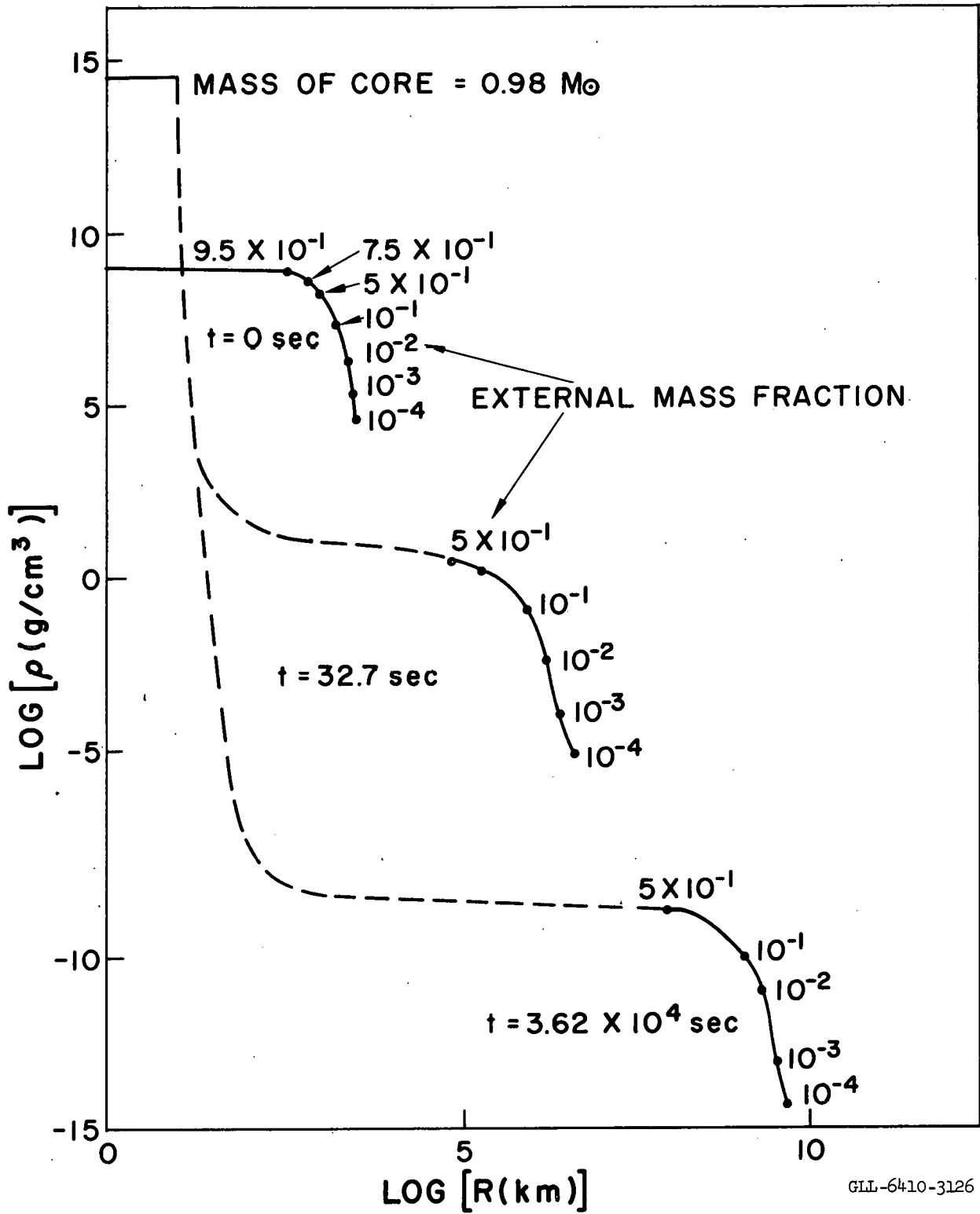
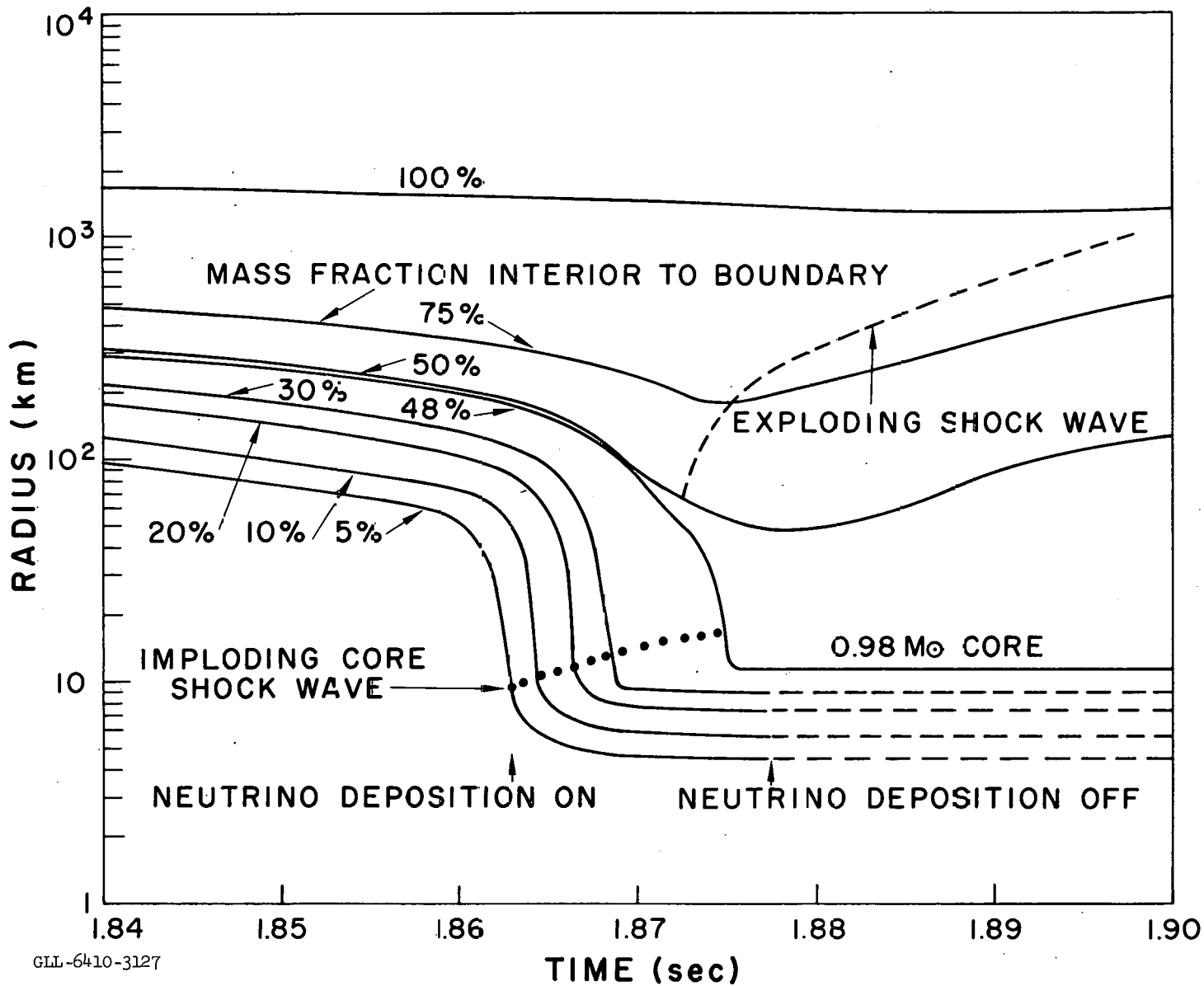
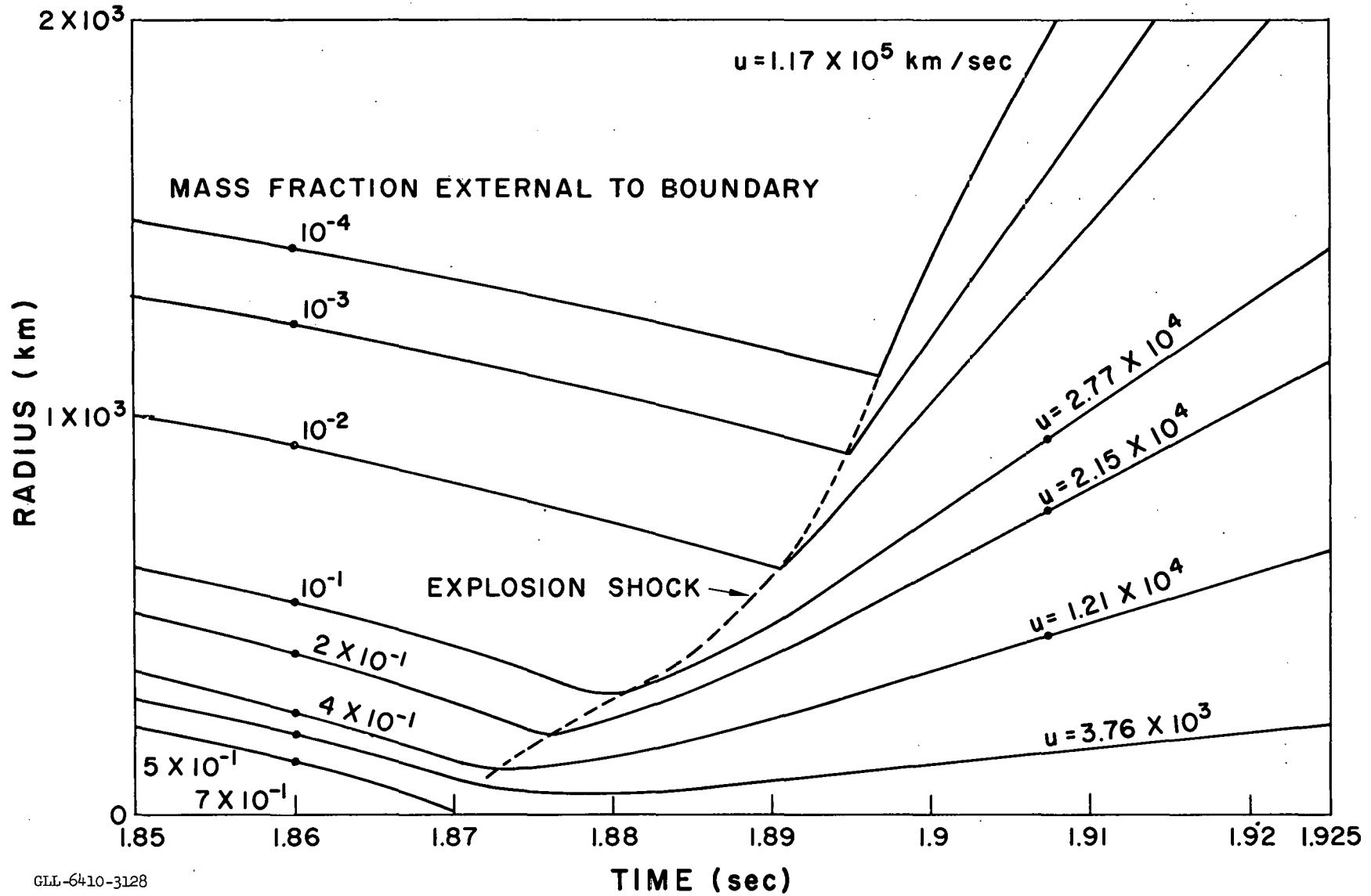


Fig. 29. 2 M_{\odot} supernova log density vs log radius.



GLL-6410-3127

Fig. 30. 2 M_⊙ supernova radius vs time with neutrino deposition. The instability occurs due to neutrino emission and nucleon binding in the equation of state with $\rho > 2 \times 10^{11}$ g/cm³.



GLL-6410-3128

Fig. 31. $2 M_{\odot}$ supernova radius vs time with neutrino deposition.

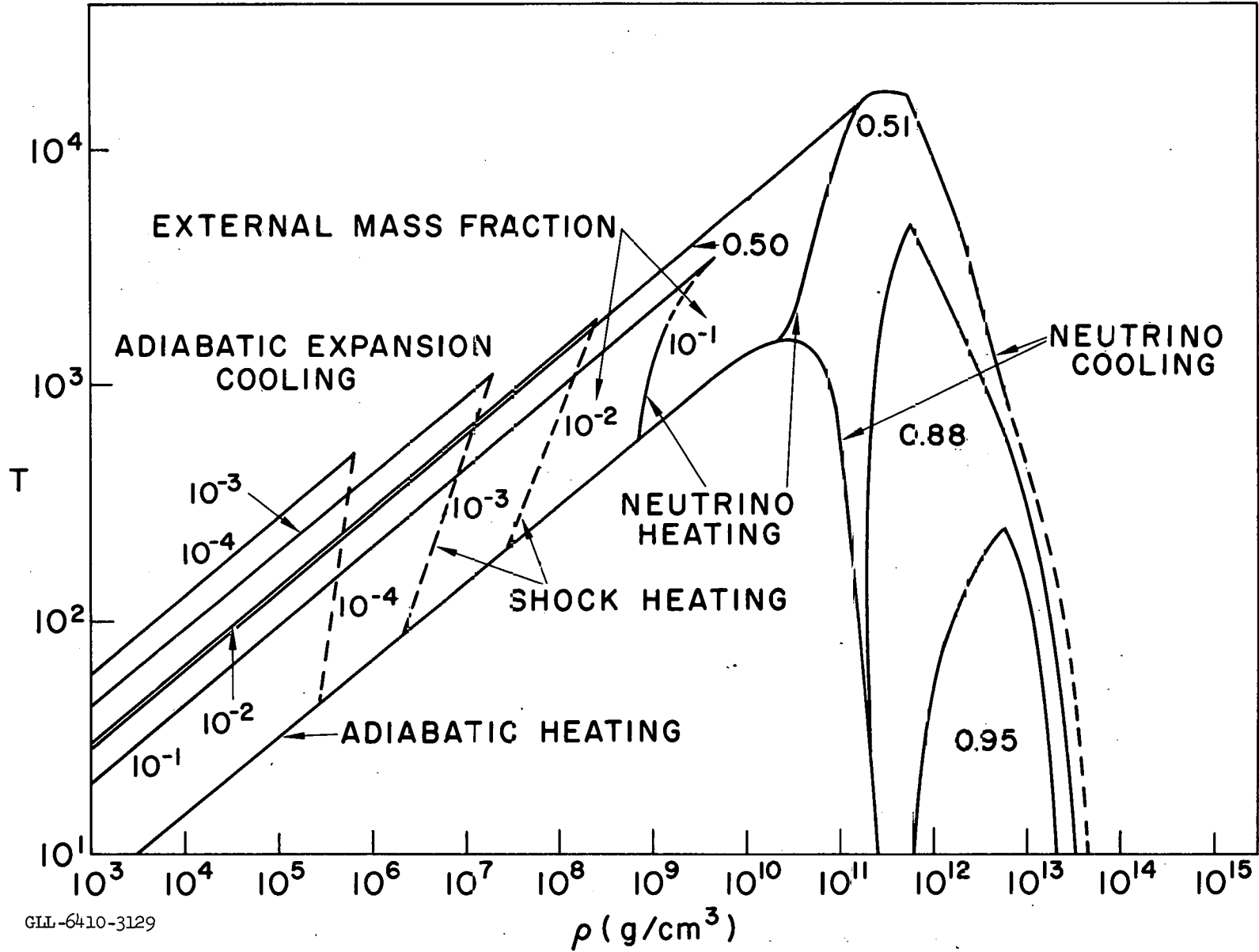


Fig. 32. $2 M_{\odot}$ supernova temperature vs density with neutrino deposition.

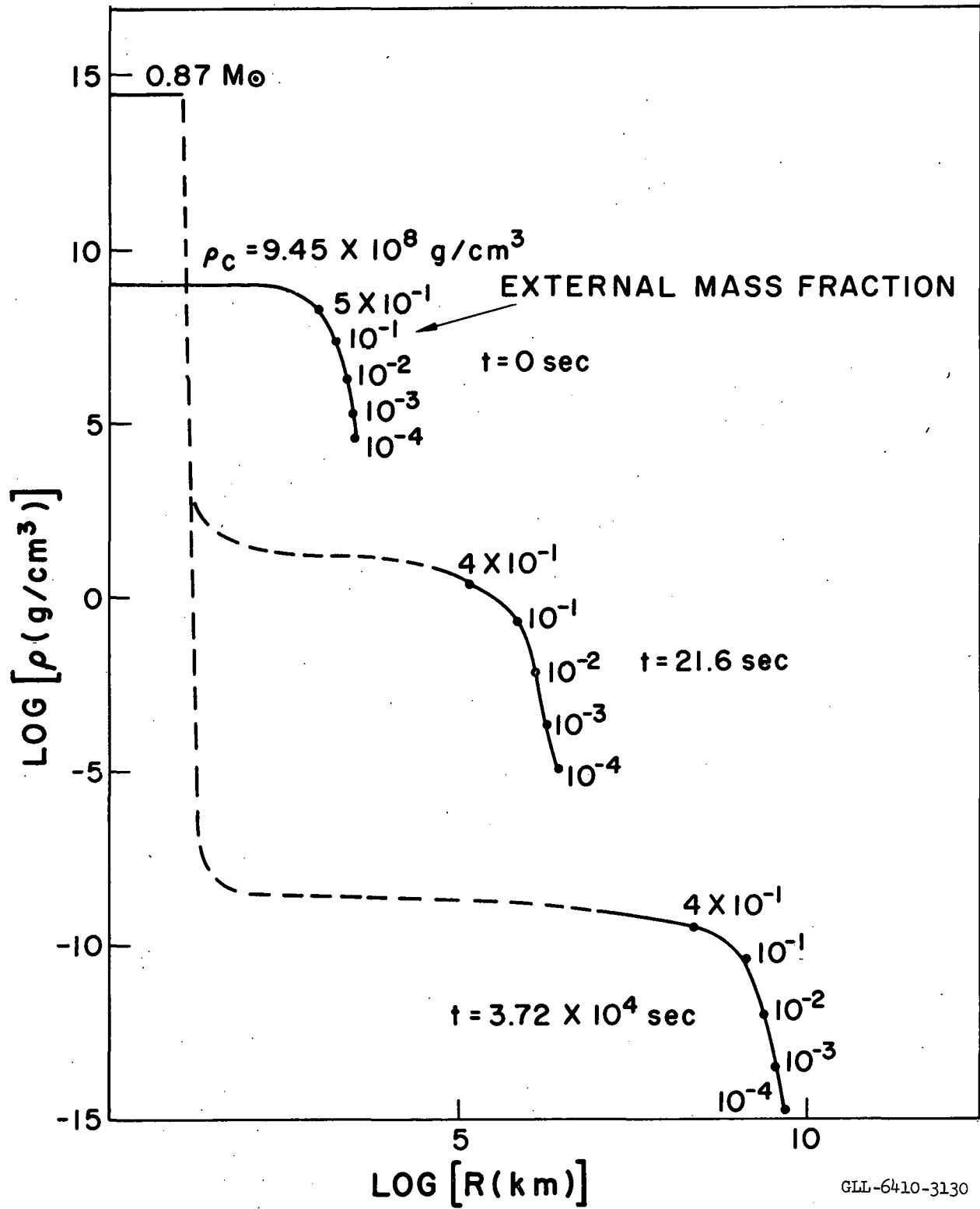
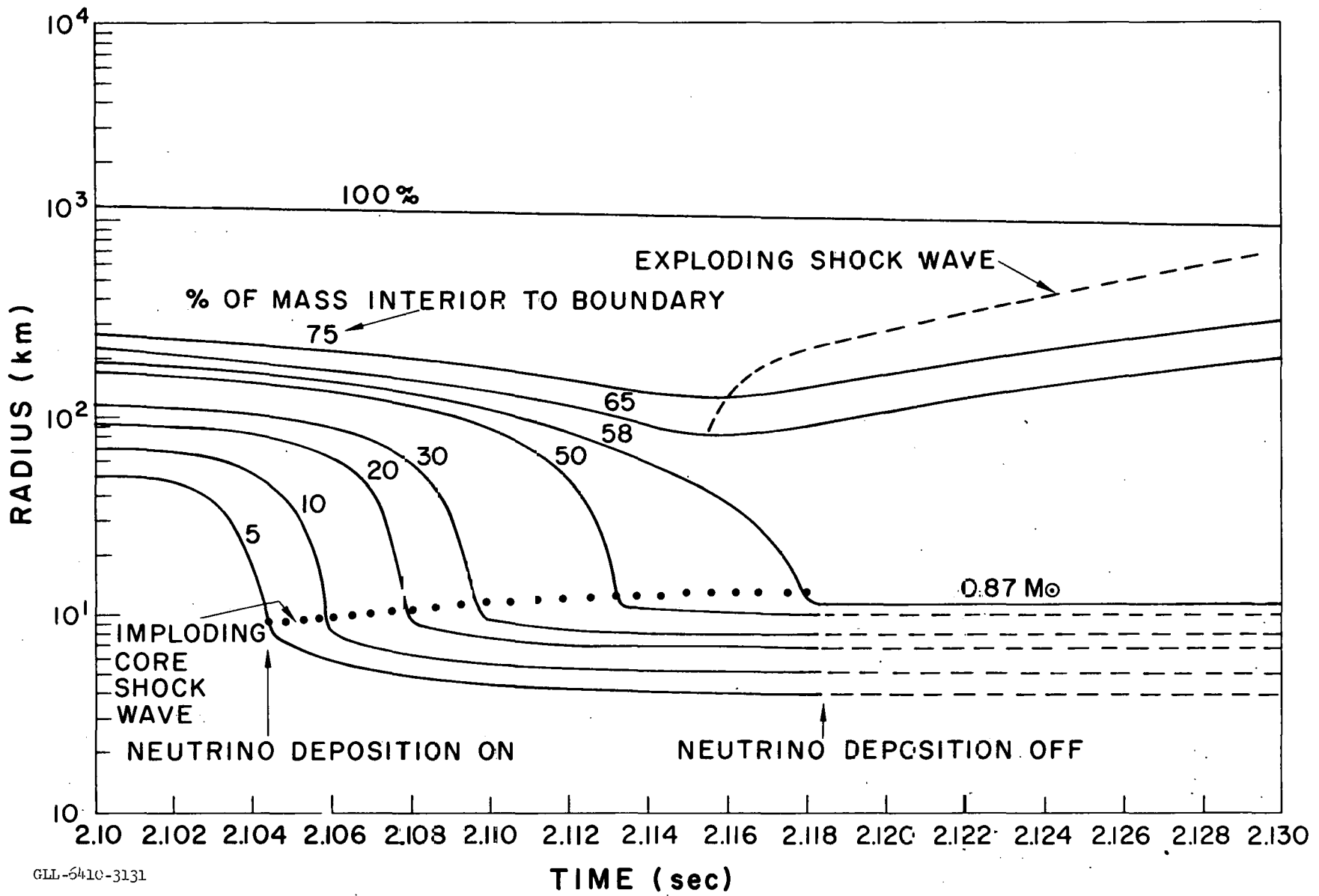
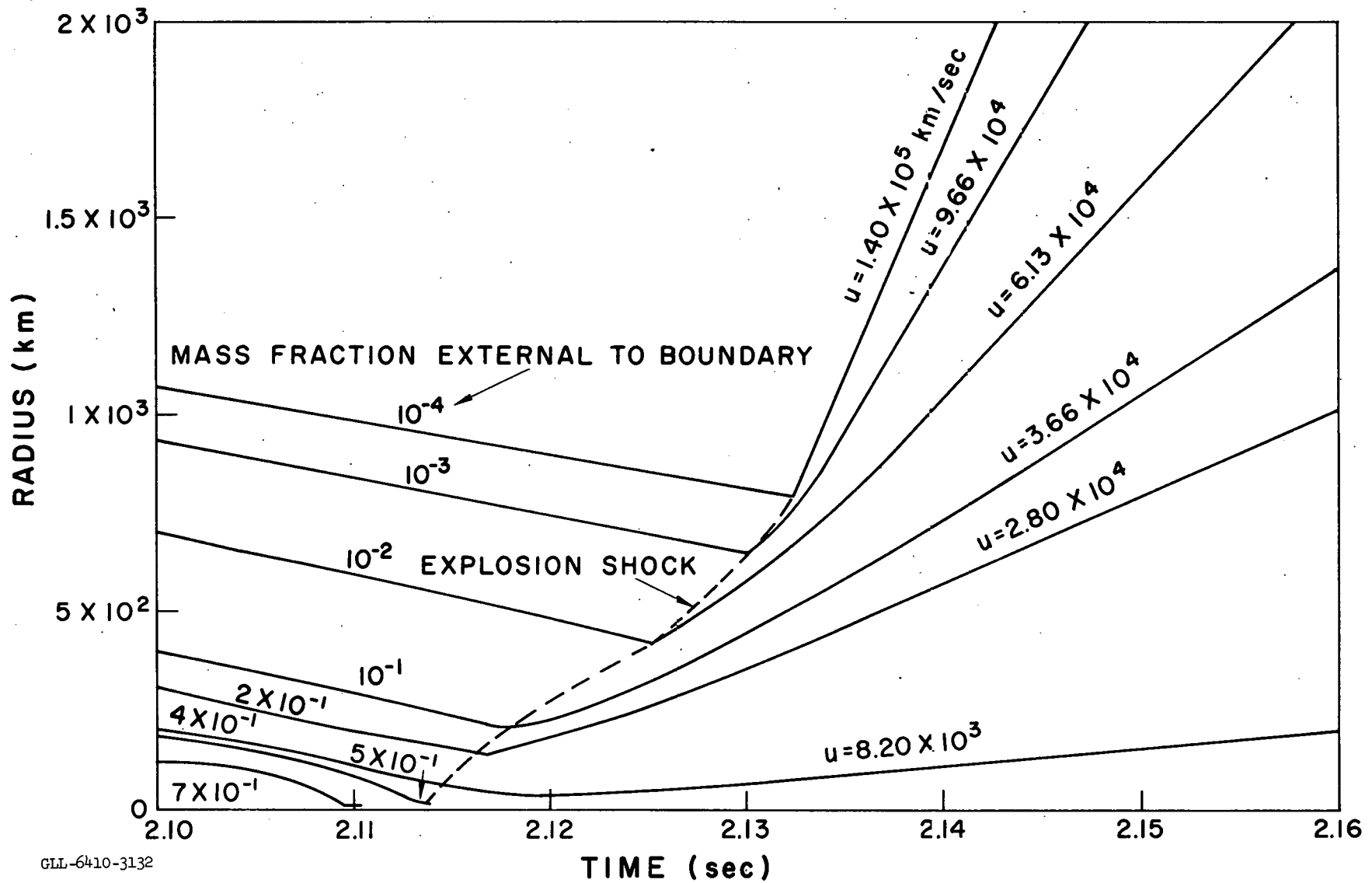


Fig. 33. 1.5 M_⊙ supernova log density vs log radius.



GLL-5410-3131

Fig. 34. 1.5 M_{\odot} supernova radius vs time with neutrino deposition.



GLL-6410-3132

Fig. 35. 1.5 M \odot supernova radius vs time with neutrino deposition.

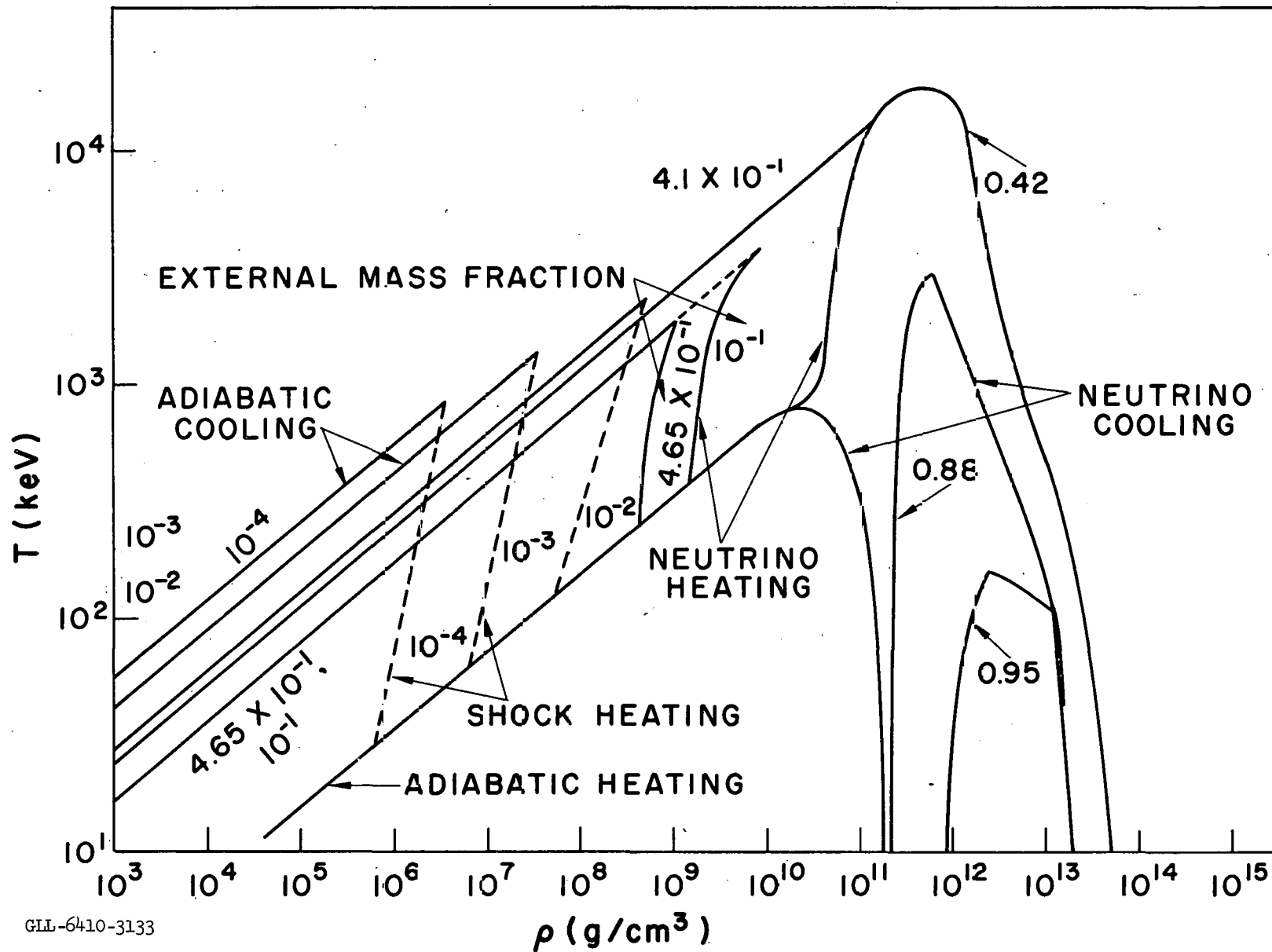


Fig. 36. 1.5 M \odot supernova temperature vs density with neutrino deposition.

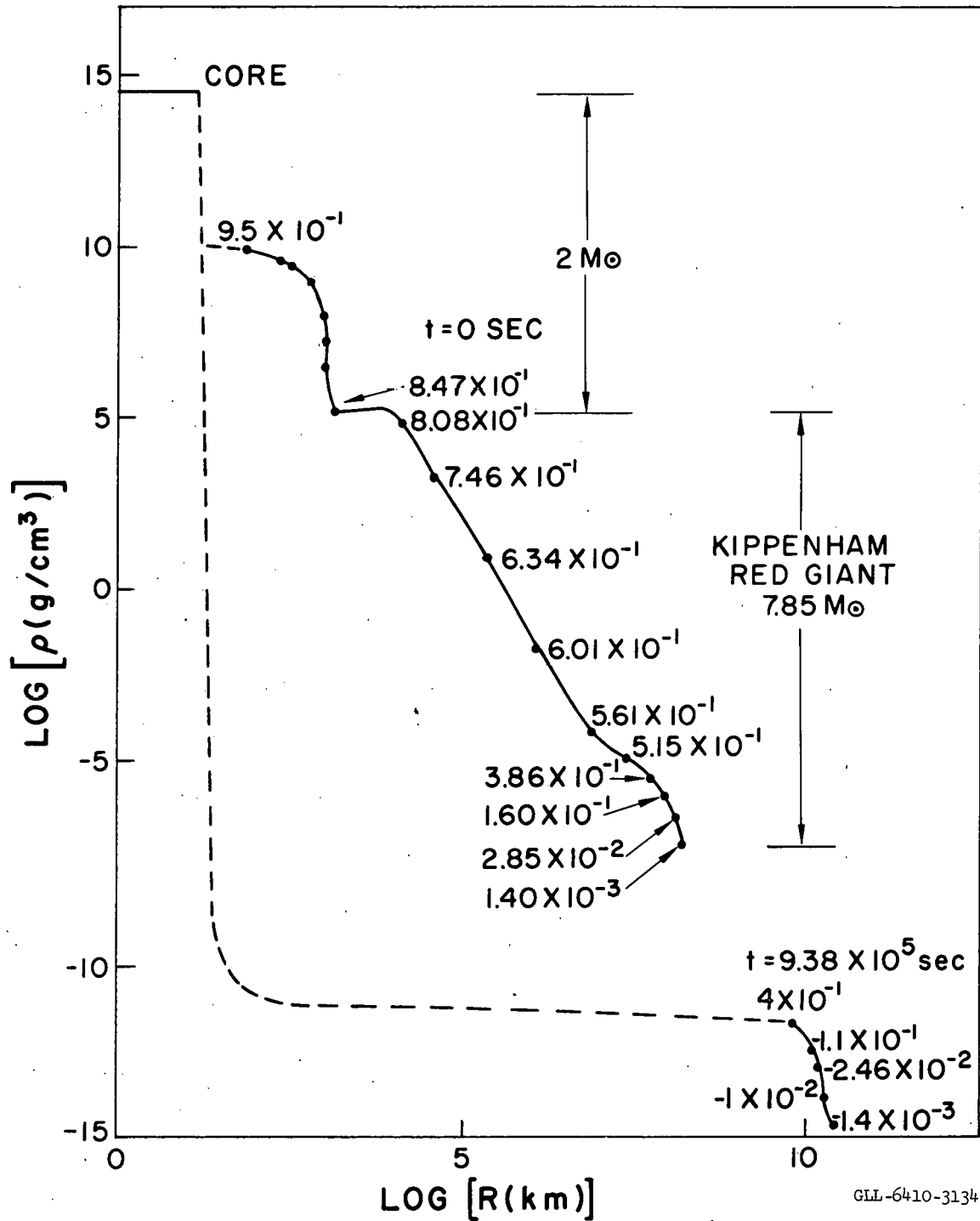


Fig. 37. Red giant structure log density vs log radius. The envelope has been "tacked" on to the 2 M_⊙ supernova at the time of explosion, giving 9.5 M_⊙ total.

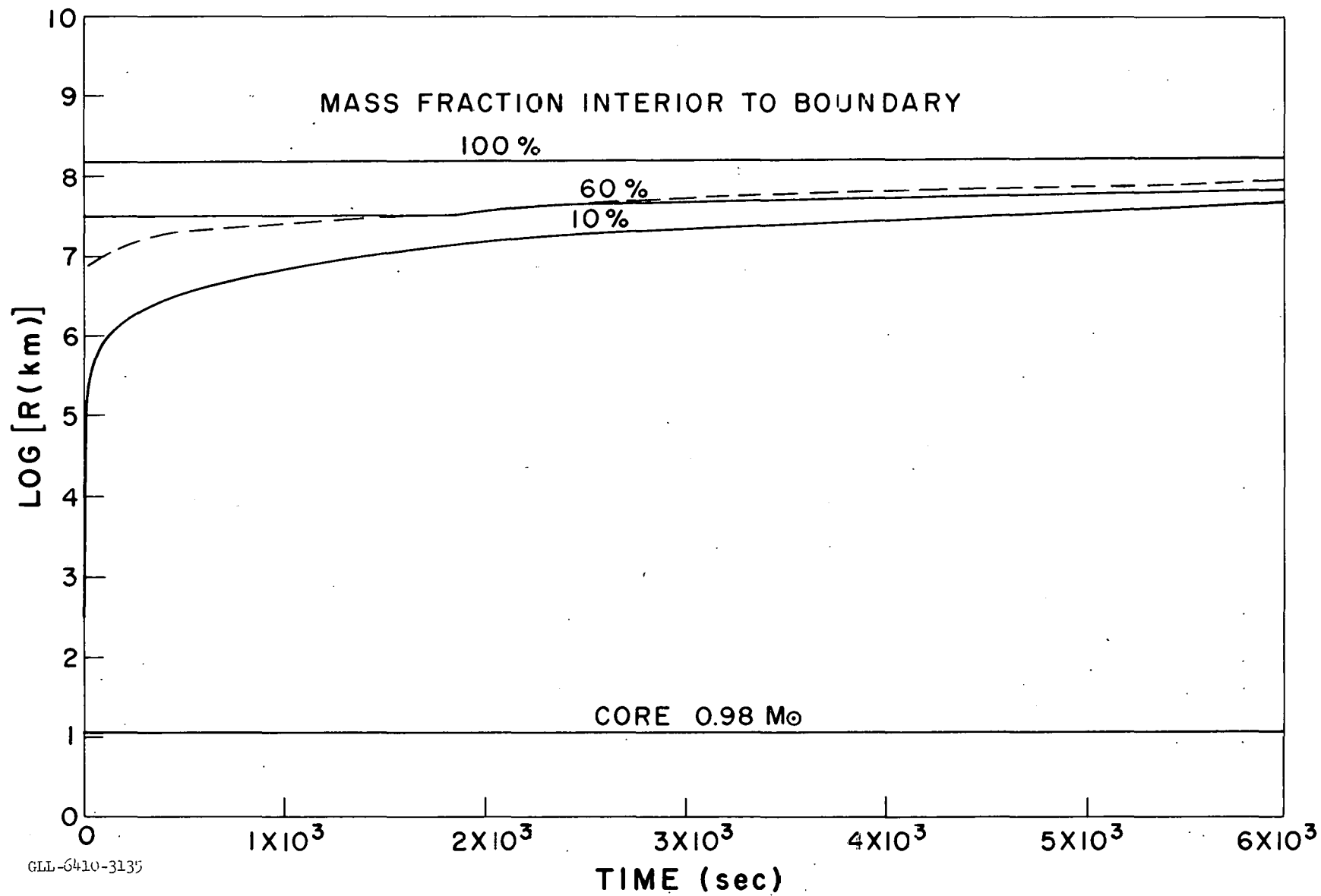


Fig. 38. Log radius vs time for explosion of 2 M_{\odot} polytrope with red giant envelope.

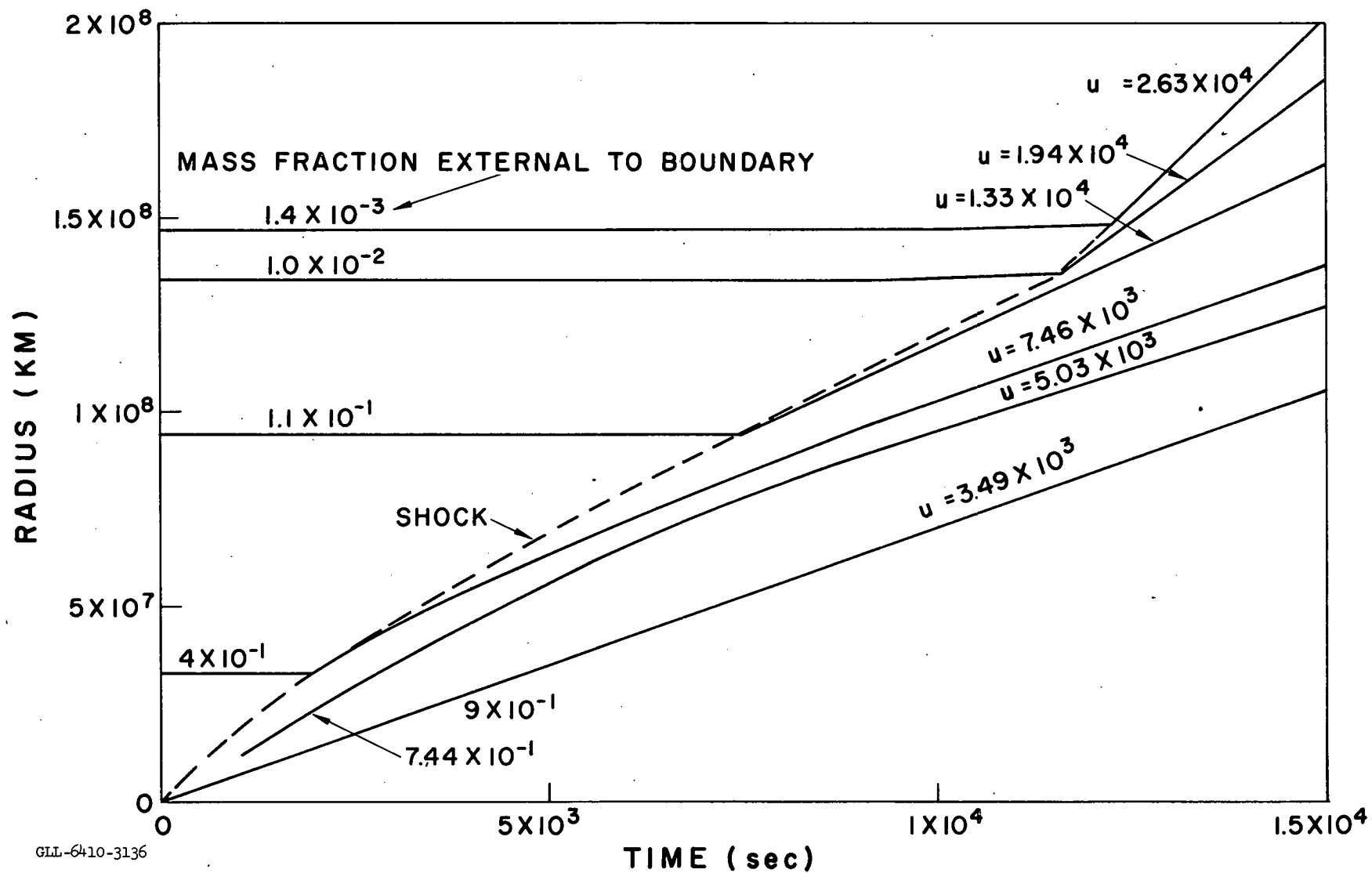


Fig. 39. Radius vs time for red giant explosion. The lower velocities are due to the additional mass of this envelope with which the exploding $2 M_{\odot}$ core collides.

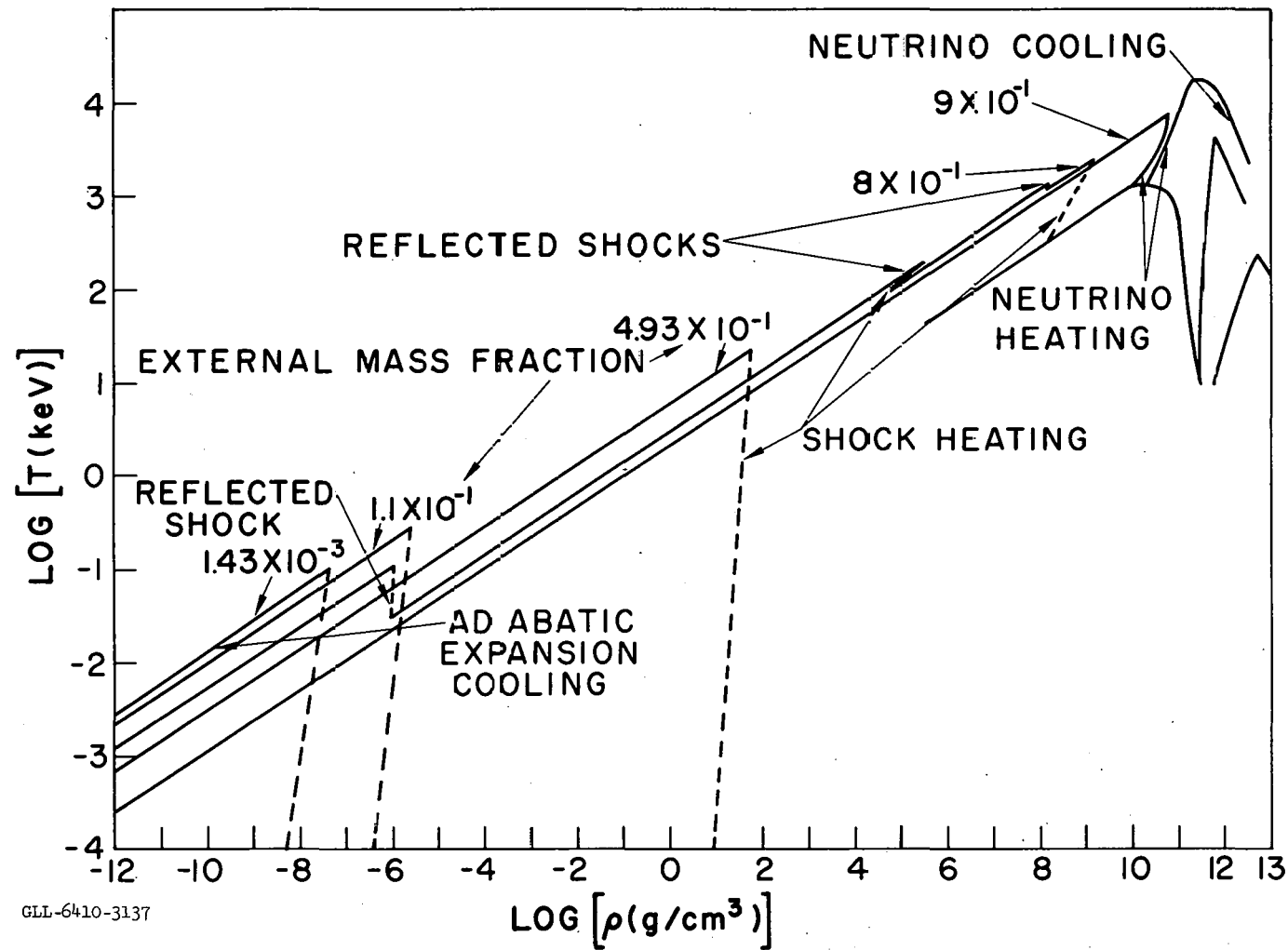


Fig. 40. Red giant structure log temperature vs log density. The initial temperature of the envelope was set to zero. Within the time of the 2 M \odot core instability there is negligible motion of the envelope and the subsequent heating is large compared to any initial temperature.

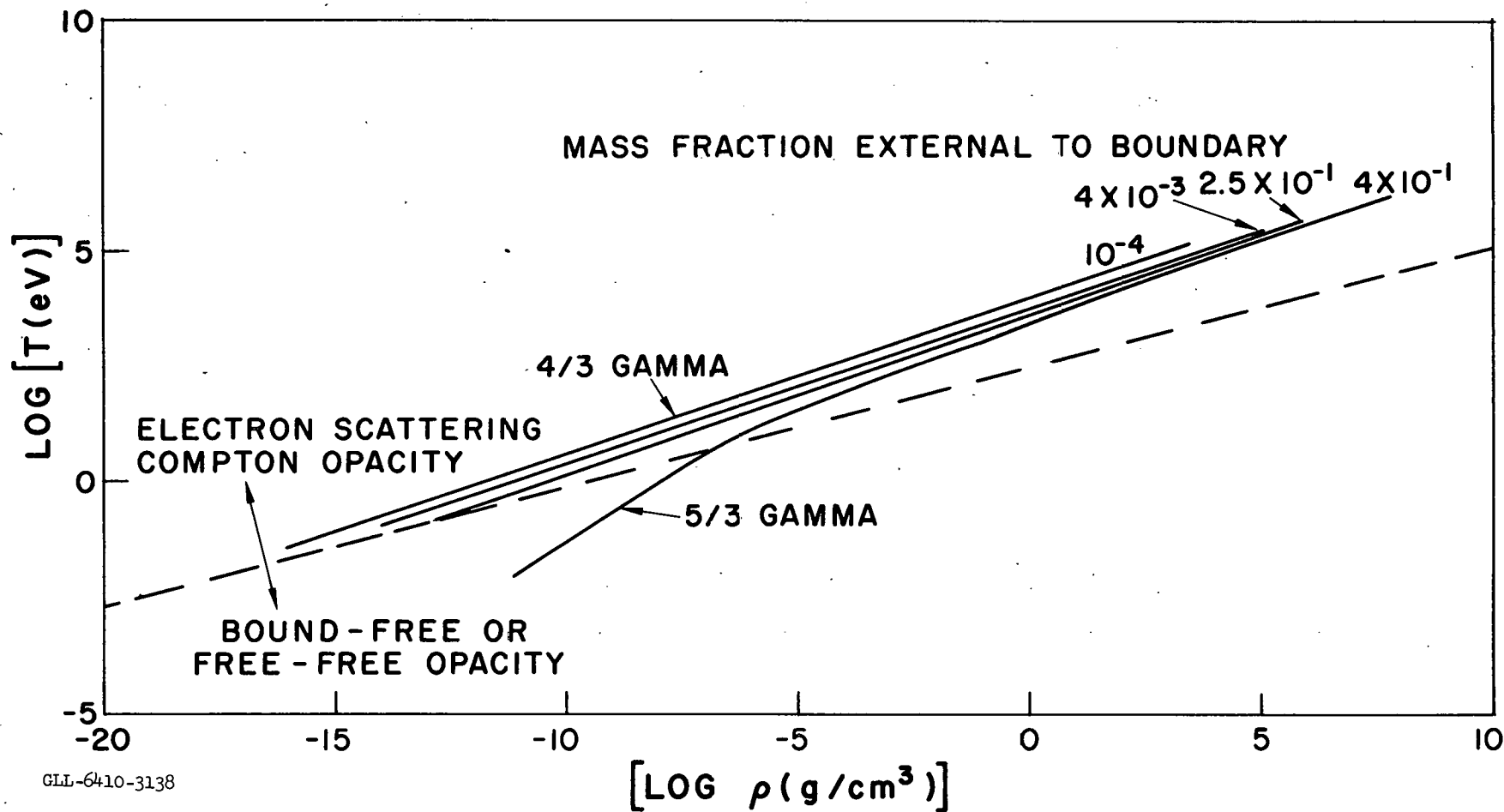
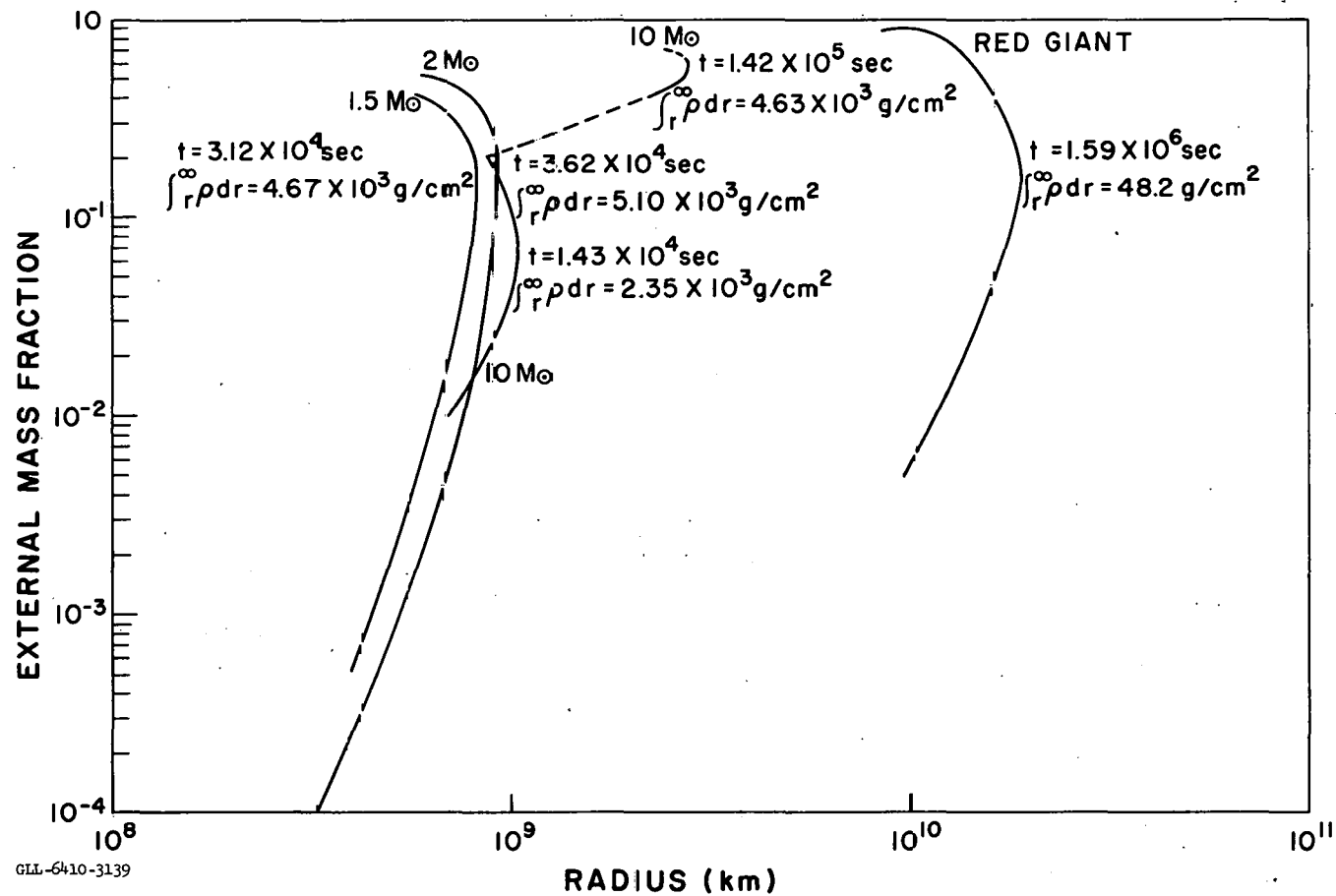


Fig. 41. Log temperature vs log density envelope expansion of $10 M_{\odot}$ star. The outer zones expand on the expected $\gamma = 4/3$ adiabat and the inner zones shift from $\gamma = 4/3$ to $\gamma = 5/3$ when $\beta = 1$. The dashed line represents the division between (bound-free or free-free) and Compton opacity. The opacity of the expanding matter is dominantly Compton.



GLL-6410-3139

Fig. 42. Radius vs mass fraction for the 10^4 deg zone. (The radius at which adiabatic cooling reduces the temperature to 10^4 deg.) The quantity $\int_r^\infty \rho dr$ is given for each star (1.5, 2, and 10 M_⊙ and red giant) at maximum radius.

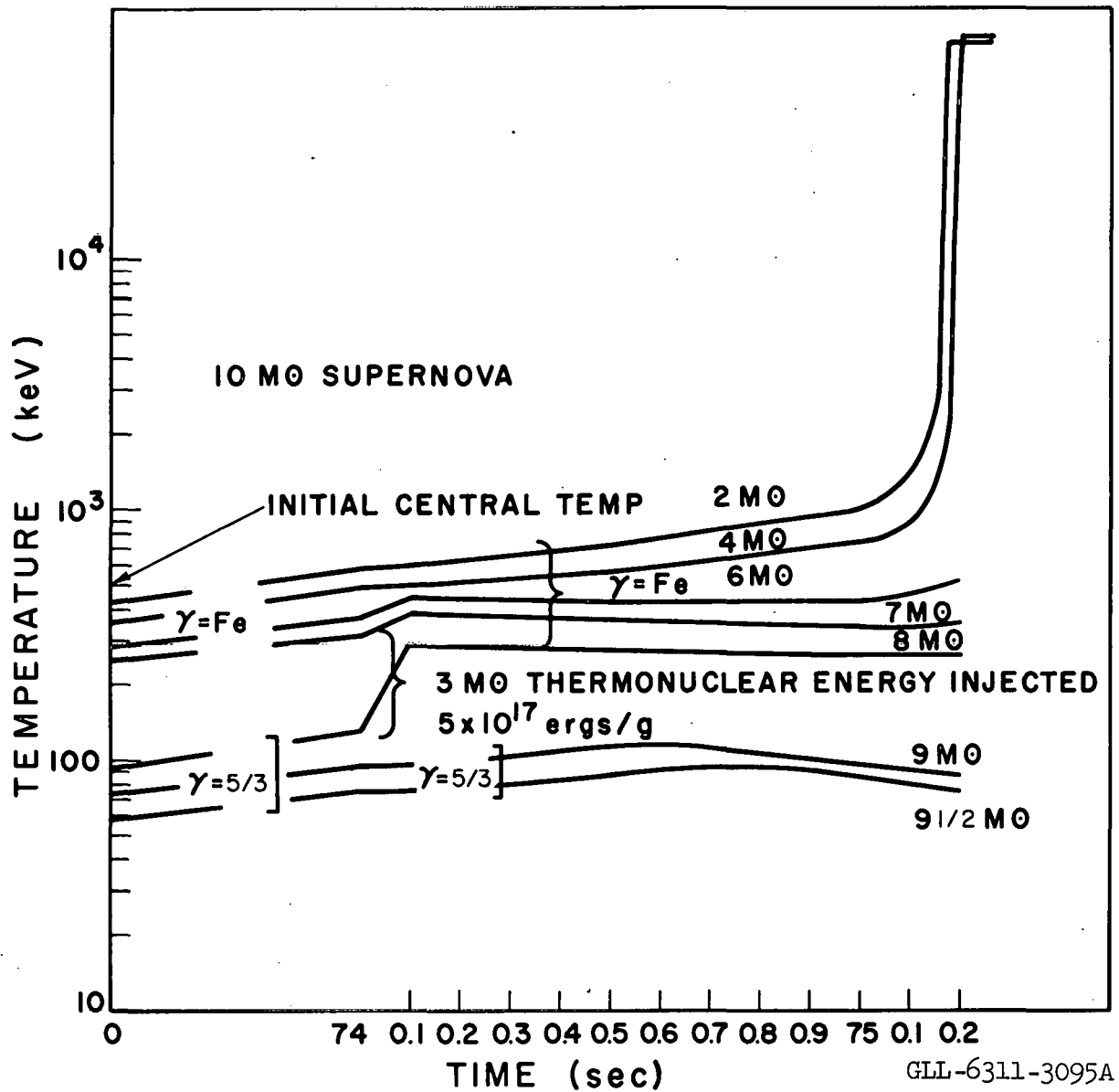


Fig. 43. Temperature vs time for the 10 M_⊙ simulated thermonuclear detonation. The slow initial rise in temperature corresponds to the initial instability. The sudden increase in temperature for the 3 M_⊙ in the envelope corresponds to the mock detonation with the deposition of 5×10^{17} ergs/g. The subsequent implosion proceeds unaffected by the detonation.

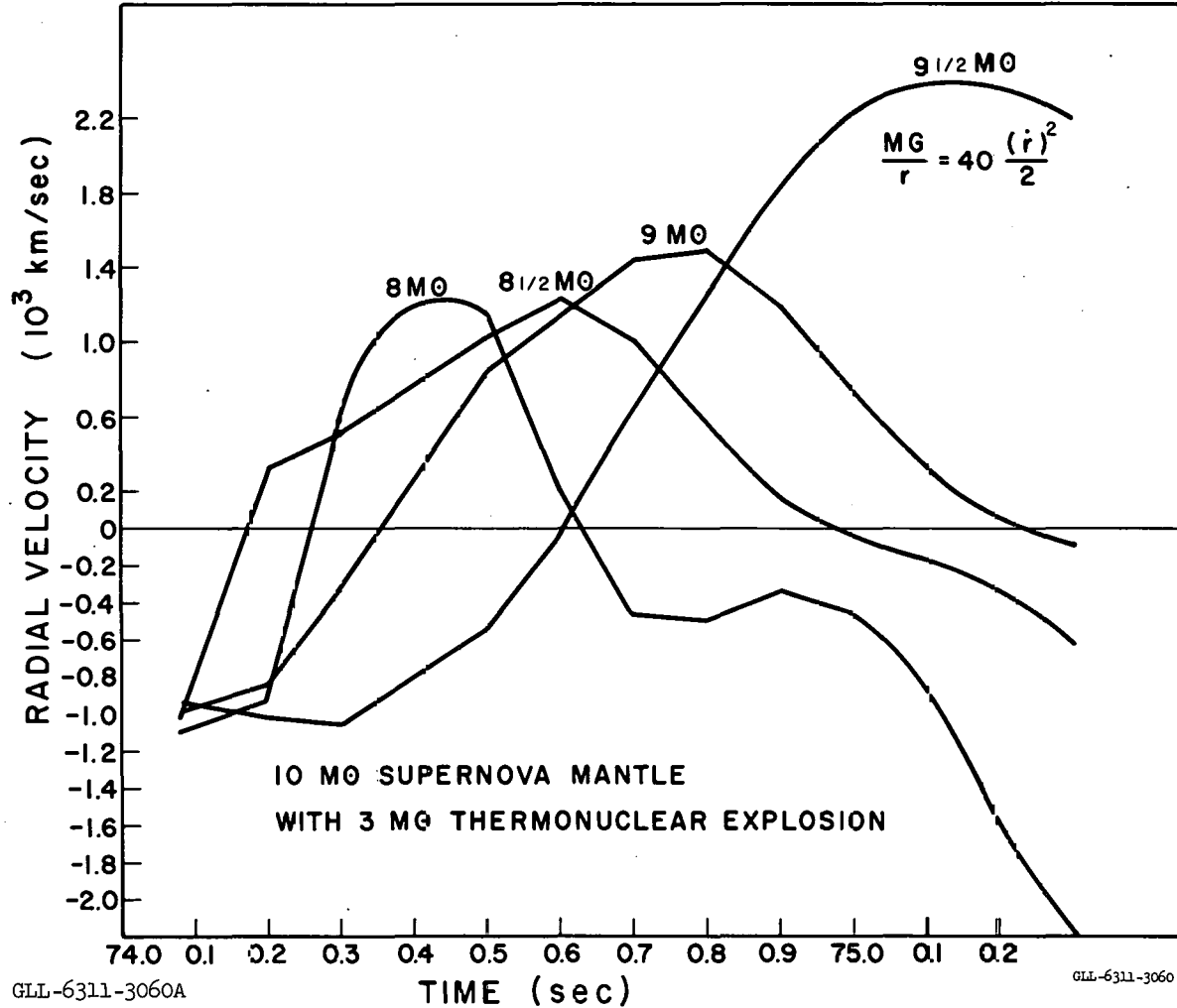


Fig. 44. Velocity vs time for the outer zones of the 10 M_⊙ thermonuclear detonation. The reversal in velocity from negative to positive and returning to negative corresponds to (1) initial radial implosion, (2) detonation outward shock, and then (3) reimplosion from the core rarefaction. The kinetic energy of these zones is shown to be one-fortieth of their gravitational potential.

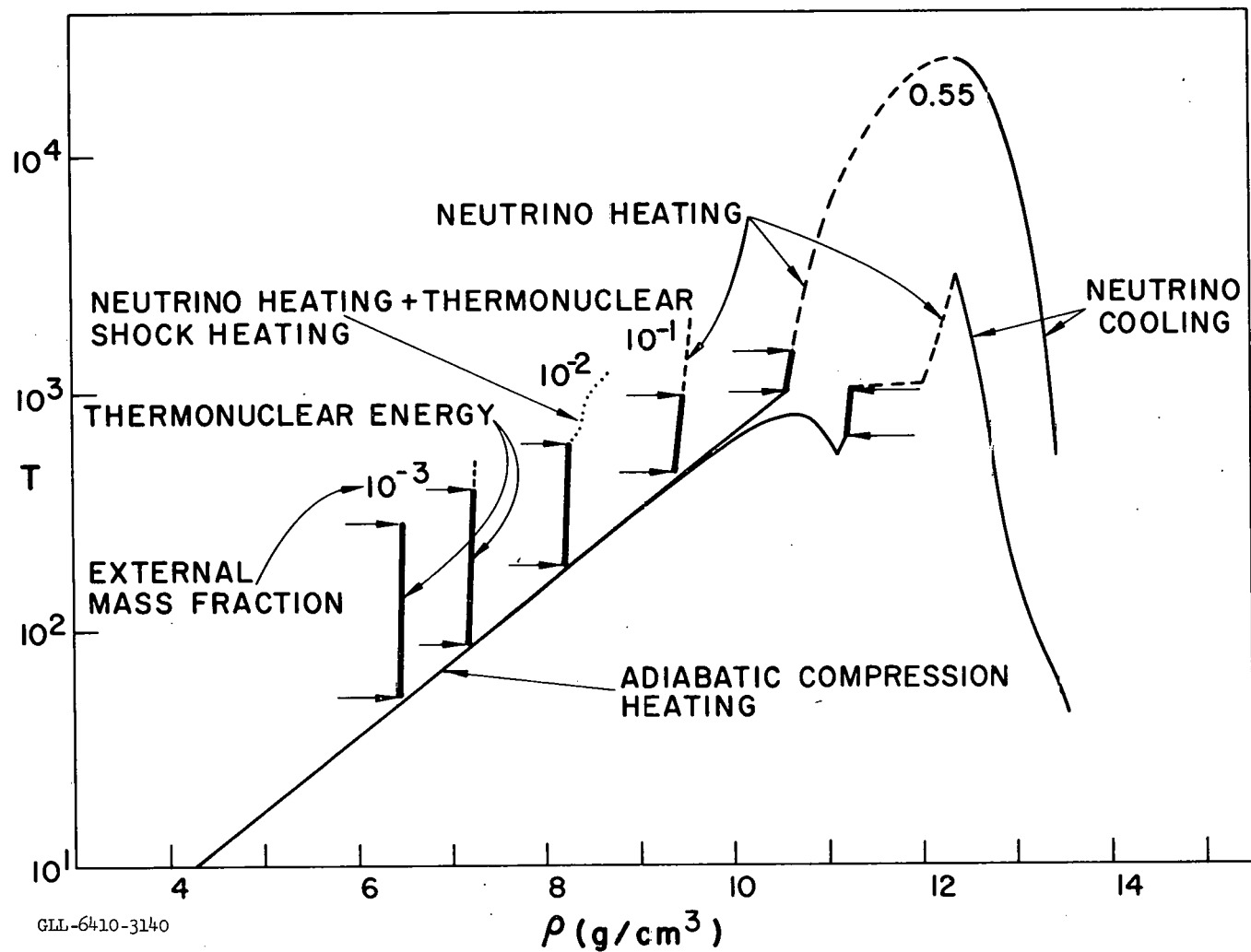


Fig. 45. Temperature vs density for the 1.5 M \odot thermonuclear detonation. The detonation was exaggerated by depositing 5×10^{17} ergs/g throughout the entire star at the time when the central density was 2×10^{11} g/cm³. The neutrino loss rate was reduced to one-tenth the previous value (Fig. 36) and the subsequent explosion by neutrino deposition behaved similarly to the nonthermonuclear case with the exception that the remaining core mass was 0.68 M \odot vs 0.87 M \odot nonthermonuclear.

LEGAL NOTICE

This report was prepared as an account of Government sponsored work. Neither the United States, nor the Commission, nor any person acting on behalf of the Commission:

A. Makes any warranty or representation, expressed or implied, with respect to the accuracy, completeness, or usefulness of the information contained in this report, or that the use of any information, apparatus, method, or process disclosed in this report may not infringe privately owned rights; or

B. Assumes any liabilities with respect to the use of, or for damages resulting from the use of any information, apparatus, method or process disclosed in this report.

As used in the above, "person acting on behalf of the Commission" includes any employee or contractor of the commission, or employee of such contractor, to the extent that such employee or contractor of the Commission, or employee of such contractor prepares, disseminates, or provides access to, any information pursuant to his employment or contract with the Commission, or his employment with such contractor.

*Do not
refer*